DEVELOPMENT OF ELECTROSPUN FIBROUS STRUCTURES FROM CELLULOSE ACETATE FOR WATER PURIFICATION

Yirong Zhang

Department of Food Science and Agricultural Chemistry

McGill University, Montreal

March 2024

A thesis submitted to McGill University in partial fulfillment of the requirements of the degree of Doctor in Philosophy

Abstract

Electrospun fibers have been proven to be effective aqueous contaminant removers owing to their large specific surface area, high porosity, and easy modification. To date, electrospinning has been successfully employed to fabricate numerous combinations of polymers and fillers into ultrafine fibers for water purification. Cellulose acetate (CA), a biodegradable polymer, is increasingly used to produce consumer products (over 600,000 metric tons per year) including cigarette filters, textiles, photographic films, and plastic. However, most of the CA wastes are landfilled, discarded, or incinerated, resulting in intensified greenhouse gas emissions and loss of useful materials. Recycling CA wastes into electrospun adsorbents not only alleviates their impacts on the environment but also produces value-added products. Humic acid (HA) is a natural organic compound that exerts pressure on aquatic environments and water-based engineering systems. The presence of HA in the water system, especially in potable water not only generates unfavorable taste but also induces complexation effects with heavy metal ions and active interactions with Cl_2 used in the water treatment process, giving rise to carcinogenic and reproductive issue-related organochlorines as a disinfection by-product. Herein, HA is selected as an illustrative contaminant, and guided by the intermolecular interaction study, CA and chitosan (CS) derived from wastes materials were recycled to prepare an efficient electrospun adsorbent with abundant amino and methyl groups for HA removal. The results revealed that all the CA/CS fibrous membranes showed high adsorption capacities (> 152 mg/g) towards HA at pH 4. Especially, the CA/CS 1:1 sample had a uniform fibrous morphology, which led to the highest tensile strength and adsorption capacity of 184.72 mg/g. To further optimize the properties and efficacy of the electrospun adsorbent, a core-sheath structured CA-based adsorbent incorporated by CS and cellulose nanocrystals (CNCs) was constructed. All the CS/CA/CNCs fibers with core-sheath structures exhibited smaller diameters, greater homogeneity, and significantly improved mechanical strength

compared to the uniaxial fibers. The removal efficacy was also improved as evidenced by the comparable adsorption capacity toward HA obtained from the CS/CA/CNCs fibers with a lower mass proportion of CS incorporated. Additionally, photoactive agents were introduced into the CA/CS adsorbent to facilitate continuous and synergistic removal of contaminants via photooxidation and adsorption. The results indicated that TiO_2 was uniformly fixed in the electrospun CA/CS fibers, which extended the removal process and facilitated the continuous removal of HA after 60 minutes upon the saturation of the adsorbent. The generated CA electrospun membrane residues were finally collected and utilized to assemble 3D fibrous aerogels for oil/water separations. The hydrophobic aerogels exhibited superior absorption capacities towards diversified oils and organic solvents with good reusability. In general, the results showed that the electrospun fibrous structures derived from CA are promising adsorbents for water purification.

Résumé

Les fibres électrofilées se sont avérées efficaces pour éliminer les contaminants aqueux en raison de leur grande surface spécifique, de leur porosité élevée et de leur facilité de modification. À ce jour, l'électrofilage a été utilisé avec succès pour fabriquer de nombreuses combinaisons de polymères et de charges en fibres ultrafines pour la purification de l'eau. L'acétate de cellulose (CA), un polymère biodégradable, est de plus en plus utilisé pour produire des produits de consommation (plus de 600 000 tonnes par an), notamment des filtres à cigarettes, des textiles, des films photographiques et du plastique. Cependant, la plupart des déchets de CA sont mis en décharge, jetés ou incinérés, ce qui entraîne une augmentation des émissions de gaz à effet de serre et la perte de matériaux utiles. Le recyclage des déchets d'CA en adsorbants électrofilés permet non seulement d'atténuer leur impact sur l'environnement, mais aussi de fabriquer des produits à valeur ajoutée. L'acide humique (HA) est un composé organique naturel qui exerce une pression sur les environnements aquatiques et les systèmes d'ingénierie basés sur l'eau. La présence d'HA dans le système d'eau, en particulier dans l'eau potable, ne génère pas seulement un goût désagréable, mais induit également des effets de complexation avec les ions de métaux lourds et des interactions actives avec le Cl_2 utilisé dans le processus de traitement de l'eau, donnant lieu à des organochlorés cancérigènes et liés à des problèmes de reproduction en tant que sous-produits de désinfection. Ici, l'HA est choisi comme contaminant illustratif, et guidé par l'étude de l'interaction intermoléculaire, le CA et le chitosane (CS) dérivés de déchets ont été recyclés pour préparer un adsorbant électrofilé efficace avec des groupes amino et méthyle abondants pour l'élimination de l'HA. Les résultats ont révélé que toutes les membranes fibreuses CA/CS présentaient des capacités d'adsorption élevées (> 152 mg/g) vis-à-vis de l'HA à pH 4. En particulier, l'échantillon CA/CS 1:1 présentait une morphologie fibreuse uniforme, ce qui a conduit à la résistance à la traction la plus élevée et à la capacité d'adsorption la plus importante de 184.72

mg/g. Afin d'optimiser davantage les propriétés et l'efficacité de l'adsorbant électrofilé, un adsorbant à base de CA structuré en cœur et en gaine et incorporant des CS et des nanocristaux de cellulose (CNCs) a été construit. Toutes les fibres CS/CA/CNCs avec des structures cœur-gaine présentaient des diamètres plus petits, une plus grande homogénéité et une résistance mécanique considérablement améliorée par rapport aux fibres uniaxiales. L'efficacité de l'élimination a également été améliorée, comme le montre la capacité d'adsorption comparable de l'HA obtenue à partir des fibres CS/CA/CNCs avec une proportion de masse plus faible de CS incorporé. En outre, des agents photoactifs ont été introduits dans l'adsorbant CA/CS pour faciliter l'élimination continue et synergique des contaminants par photo-oxydation et adsorption. Les résultats ont indiqué que le TiO_2 était uniformément fixé dans les fibres CA/CS électrofilées, ce qui a prolongé le processus d'élimination et facilité l'élimination continue de l'HA après 60 minutes à la saturation de l'adsorbant. Les résidus de membrane CA électrofilée générés ont finalement été collectés et utilisés pour assembler des aérogels fibreux 3D pour la séparation huile/eau. Les aérogels hydrophobes ont présenté des capacités d'absorption supérieures vis-à-vis d'huiles et de solvants organiques diversifiés, avec une bonne réutilisation. En général, les résultats ont montré que les structures fibreuses électrofilées dérivées de l'CA sont des adsorbants prometteurs pour la purification de l'eau.

Acknowledgement

I would like to express my gratitude to my supervisor, Dr. Yixiang Wang, for his guidance and support throughout this research. His feedback has been pivotal in shaping both this work and my growth as a researcher. His encouragement and faith in my abilities have been a guiding light during the most challenging times of my research. His commitment to pursuing knowledge and his unwavering belief in the importance of meticulous work and rigorous analysis have not only shaped my academic development but have also instilled in me the ethos of what it truly means to be a researcher.

I would like to extend my sincere appreciation to all the professors and administrative staff in the Department of Food Science and Agricultural Chemistry at McGill University for their efforts and dedication to maintaining an environment conducive to academic and personal growth. Especially, thanks to all my supervisory committee members: Dr. V. Yaylayan, Dr. Stéphane Bayen, Dr. Saji George, Dr. Benjamin K. Simpson, Dr. Zhiming Qi, Dr. Ashraf Ismail, and Dr. Marie-Josée Dumont, for their valuable insights and constructive feedback.

I am also very grateful to my labmates and colleagues. The collaborative environment and intellectual exchanges we shared have greatly enriched my research experience. Thank you for the stimulating discussions, the comments, and the many laughs we shared. The countless hours we spent conducting experiments and sharing even the smallest progress, made this journey worthwhile. I realize how valuable these moments have been to me and cherish the memories we have created and the bonds we have formed.

Lastly, I would like to express my deepest gratitude to my husband, my parents, and my parents-in-law. Thanks to my husband for believing in me, supporting me, and always being there for me. His love, patience, and unwavering support have been my stronghold. A big thanks to my parents for their guidance and unconditional love which shaped me into the person I am today. Their belief in my potential and their constant encouragement have been the foundation upon which I have built my aspirations. Thanks to my parents-in-law whose lives have been the most profound examples of resilience, hard work and the greatest source of inspiration and motivation throughout my life. Their kindness, understanding, and encouragement have been a source of comfort and strength in my journey.

Contribution of Authors

Parts of this research have been presented at national and international conferences and submitted for publication in journals. The contributions of the authors are as follows:

Yirong Zhang is the Ph.D. candidate who planned and conducted the experiments, collected and analyzed data, and completed all manuscript drafting.

Dr. Yixiang Wang is the supervisor who guided the research and had direct advisory input into the work as it progressed, and all the manuscripts were submitted after his review and edition.

Dr. Cunzhi Zhang was the co-author and contributed to the original draft preparation and writing in Chapter 2.

Dr. Fen Wang was the co-author and contributed to the experimental work, manuscript preparation, and review in Chapter 3 and Chapter 4.

List of Publications

Yirong Zhang and Yixiang Wang. Construction of three-dimensional aerogels from electrospun cellulose fibers as highly efficient and reusable oil absorbents. *Separation and Purification Technology*, 2024, 353 (Part C), 128604. DOI: 10.1016/j.seppur.2024.128604

Yirong Zhang and Yixiang Wang. One-step electrospinning of cellulose acetate/chitosan/TiO_2 fibrous membranes: efficient humic acid removal by synergistic adsorption and photocatalysis. *Cellulose*. DOI: 10.1007/s10570-024-06034-0

Yirong Zhang and Yixiang Wang. Electrospun cellulose acetate/ chitosan fibers for humic acid removal: improved efficiency and robustness with a core-sheath design. *Nanomaterials*, 2022, 12(8), 1284. DOI: 10.3390/nano12081284

Yirong Zhang, Fen Wang, and Yixiang Wang. Electrospun cellulose acetate/chitosan fibers for humic acid removal: construction guided by intermolecular interaction study. *ACS Applied Polymer Materials*, 2021, 3(10), 5022-5029. DOI: 10.1021/acsapm.1c00778

Yirong Zhang, Cunzhi Zhang, and Yixiang Wang. Recent progress in cellulose-based electrospun nanofibers as multifunctional materials. *Nanoscale Advances*, 2021, 3(21), 6040-6047. DOI: 10.1039/D1NA00508A

Yirong Zhang, Fen Wang, and Yixiang Wang. Recent developments of electrospun nanofibrous materials as novel adsorbents for water treatment. *Materials Today Communications*, 2021, 27: 102272. DOI: 10.1016/j.mtcomm.2021.102272

Fen Wang[†], Yirong Zhang[†], and Yixiang Wang. Recycling of waste cotton sheets into three-dimensional biodegradable carriers for removal of methylene blue. *ACS Omega*, 2021, 6(50), 34314-34326 (co-first author). DOI: 10.1021/acsomega.1c04019

Contribution to Original Knowledge

1. Development of efficient electrospun fibrous adsorbents from CA and CS that are largely available as biomass wastes for HA removal.
2. Demonstration of the feasibility of fabricating highly effective adsorbents guided by intermolecular interaction mechanisms study.
3. Demonstration of the importance of rational design in the preparation of cost-effective functional adsorbents through co-axial electrospinning.
4. Development of electrospun core-sheath fibers with superior performance from biomass wastes for efficient HA removal.
5. Demonstration of the continuous and efficient removal of HA via the synergistic effects of photooxidation and adsorption.
6. Development of reusable 3D hydrophobic aerogels with electrospun CA fibers as building blocks for diversified oils and organic solvents removal.

Table of Content

List of Figures

List of Tables

Chapter 1. Introduction

1.1. General Introduction

Electrospinning is a facile and efficient method for preparing fibers with various diameters, which have a large specific surface area, good interconnectivity, and structural stability. Meanwhile owing to the random arrangement of fibers prepared by electrospinning, a large number of isotropic pores evenly distribute among fibers (Xue et al., 2019; Zhang et al., 2021). These characteristics make electrospun fibers useful in a wide range of applications, including filtration & adsorption materials, "smart" materials, catalytic materials, and so on (C. Chen et al., 2020; Han et al., 2019; Lee et al., 2020; Sun et al., 2021; Yan et al., 2021). However, the existing fibers fabricated by electrospinning are usually based on non-degradable polymers, which may cause environmental issues after disposal.

Cellulose, the most naturally abundant polymer on the earth, possesses many attractive properties, such as biocompatibility, environmental friendliness, and inexhaustible renewability (Xia et al., 2021). A wide variety of cellulose derivatives have been developed taking advantage of the reactive, numerous, and regularly arranged hydroxyl groups along cellulose chains. The transformations are carried out by simple reactions between functional substituents and active hydroxyls of cellulose (Beaumont et al., 2021). Cellulose derivatives own unique features from both cellulose and modified functional groups, including good solubility, processability, and flexibility (Li et al., 2021; O'Dea et al., 2020). The combination of electrospinning technology and cellulose (and its derivatives) provides a feasible approach to produce structured porous materials with desirable properties. Meanwhile, it enables value-added applications of cellulose and its derivatives which are derived from the natural resources or even biomass wastes.

Cellulose acetate (CA) is one of the most used cellulose derivatives for the production of electrospun fibers because CA can achieve continuous and controllable electrospinning in several

conventional solvents, such as acetic acid (Olaru et al., 2019), acetone/DMAC solvent (Liu et al., 2020), and acetone/DMF/water (Chen et al., 2020), and the obtained CA fibers can be easily hydrolyzed into cellulose fibers. On the other hand, CA is increasingly used to produce consumer products (over 600,000 metric tons per year) including cigarette filters, textiles, photographic films, and plastic. However, most of the CA wastes are landfilled, discarded, or incinerated, resulting in intensified greenhouse gas emissions and loss of useful materials. Recycling CA wastes into electrospun adsorbents not only alleviates their impacts on the environment but also produces value-added products.

Humic acid (HA) is a natural organic compound that originates from the decomposition of dead animals and plants. Nevertheless, ubiquitous amounts of HA present in surface water, ocean water, and upload streams, especially in potable water, remain a critical concern associated with organoleptic issues, environmental problems, and even health risks. Accumulation of HA in the water body gives rise to unfavorable taste, color, and odor (Liu et al., 2014). Schmitt et al. demonstrated that HA facilitated the movement of metal ions in aqua systems (Schmitt et al., 2003), while an adverse effect of HA on the removal of organohalides and nitroaromatic contaminants was concluded by Klausen et al. (Klausen et al., 2003). Additionally, Cl_2 used in water treatment reacts actively with the functional groups (hydroxyl groups, carbonyl groups, carboxyl groups etc.) of HA, giving rise to carcinogenic and reproductive issue-related organochlorines as a disinfection by-product (Khodadadi et al., 2019). Herein, HA is selected as an illustrative contaminant, and based on the above considerations, we explored and developed the CA-derived electrospun functional fibrous structures as promising candidates for water purification.

1.2. Hypotheses

Based on the above considerations, the four hypotheses were raised as follows:

1. It is feasible to use an intermolecular interaction study to guide the design of an efficient CA-based adsorbent for the removal of HA.
2. The core-sheath structured CA fibers with the incorporation of chitosan (CS) and cellulose nanocrystals (CNCs) will enable higher mechanical strength and removal efficiency.
3. The synergistic effects of adsorption and photo-degradation will improve the overall removal efficiency.
4. The electrospun CA fibers can be utilized as building blocks for constructing 3D aerogels for oil/water separation.

1.3. Objectives

The hypotheses therefore lead to the main objective of this thesis study: to develop electrospun fibers from CA for water treatment. The specific objectives of the study are:

1. To first prepare an effective electrospun fibrous adsorbent from CA and CS guided by the intermolecular interaction study for HA removal.
2. To construct core-sheath structured CA/CS fibers by incorporating CNCs for enhanced mechanical properties and removal efficiency toward HA.
3. To incorporate photoactive agents into the electrospun CA/CS matrix to improve the removal efficiency through synergistic effects of photooxidation and adsorption.
4. To develop a hydrophobic 3D fibrous aerogel from electrospun CA fibers for oil/water separation.

Chapter 2. A review of recent progress in cellulose-based electrospun nanofibers as multifunctional materials

2.1. Abstract

Cellulose, the most abundant natural polymer, has good biocompatibility, biodegradability, and non-toxicity, which make it and its derivatives promising candidates for the fabrication of multifunctional materials, while maintaining sustainability and environmental friendliness. The combination of electrospinning technology and cellulose (and its derivatives) provides a feasible approach to produce nanostructured porous materials with promising functionalities, flexibility, renewability and biodegradability. At the same time, it enables value-added applications of cellulose and its derivatives that are derived from nature or even biomass wastes. This review summarizes and discusses the latest progress in cellulose-based electrospun nanofibers, including their construction methods and conditions, various available raw materials, and applications in multiple areas (water treatment, biomaterials, sensors, electro-conductive materials, active packaging, and so on), which are followed by the conclusion and prospects associated with future opportunities and challenges in this active research area.

2.2. Introduction

Electrospinning is a facile and efficient method for preparing fibers with nano-scaled diameters, which have a large specific surface area, good interconnectivity, and structural stability. Meanwhile owing to the random arrangement of nanofibers prepared by electrospinning, a large number of isotropic pores evenly distribute among fibers.[1,2] These characteristics make electrospun nanofibers useful in a wide range of applications, including filtration & adsorption materials, “smart” materials, catalytic materials, and so on.[3–7] However, the existing nanofibers fabricated by electrospinning are usually based on non-degradable polymers, which may cause environmental issues after disposal.

As the most abundant biodegradable polymer on the earth, cellulose possesses many fascinating properties, such as biocompatibility, environmental friendliness, and inexhaustible renewability.[8] Taking advantage of the reactive, numerous, and regularly arranged hydroxyl groups along cellulose chains, a wide variety of cellulose derivatives have been developed by simple reactions between functional substituents and active hydroxyls.[9] The derivatives possess interesting properties inherited from both cellulose and modified functional groups, including good solubility and processability, excellent flexibility, high mechanical strength, and so on.[10,11] Hence, the combination of electrospinning technology and cellulose (and its derivatives) provides a feasible approach to produce nanostructured porous materials with desirable properties. At the same time, it enables value-added applications of cellulose and its derivatives that are derived from nature or even biomass wastes.

Overviewing the research work published in last 3 years (2018–2021), various electrospun nanofibers have been successfully prepared from cellulose and cellulose derivatives in different solvent systems.[12–17] These nanofibers demonstrated promising applications in the fields of filtration, tissue engineering and biomedical engineering.[18–22] According to SciFinder, 17 literature reviews with the keywords “cellulose” and “electrospin” have been published during 2018–2021. It is certain that this is an active research area. However, all these reviews focus on either a single compound (*e.g.*, cellulose acetate and nanocellulose)/single solvent system (*e.g.*, ionic liquids) or a single application (*e.g.*, supercapacitors, adsorbents, and wound healing materials). Therefore, this review will provide the researchers with a holistic view of recently reported cellulose-based electrospun nanofibers, including their raw materials (cellulose, cellulose derivatives, and nanocellulose), construction methods (electrospinning solvents and conditions), and applications (water treatment, biomaterials, sensors, electro-conductive materials, active packaging, *etc.*).

2.3. Cellulose-based electrospun nanofiber construction

Cellulose can be directly electrospun into nanofibers, but the process is limited by the poor solubility of cellulose in most commonly used solvents. Therefore, many research studies reported the electrospinning of cellulose derivatives. For different raw materials, optimized electrospinning conditions are essential for the successful fabrication of nanofibers. Typical examples of cellulose-based electrospun nanofibers and their production conditions published in the last three years are summarized in Table 2.1.

Table 2.1. Typical cellulose-based electrospun nanofibers and their production conditions.

Raw materials	Solvents	Electrospinning conditions (concentrations, flow rates, voltages, receiving distances)	Refs
Wood pulp cellulose	DMAc/LiCl	3 wt%; 1 mL/h; 15 kV; 15 cm	[23]
Bacterial cellulose	TFA	2~5 wt%; 0.5 mL/h; 20 kV; 20 cm	[24]
Cellulose acetate	Acetic acid	19 wt%; 0.75 mL/h; 20 kV; 15 cm	[25]
Cellulose acetate	Acetone/DMF	5 wt%; 35 μL/min; 16 kV; 10 cm	[26]
Cellulose acetate	Acetone/DMAc	16 wt%; 0.3 mL/h; 11 kV; 15 cm	[13]
Hydroxypropyl methylcellulose	Ethanol	1~6 wt%; 0.5~1 mL/h; 10 kV;15 cm	[27]
Ethyl(hydroxyethyl) Cellulose	DMF	5 wt%; 0.01~3.0 mL/h; 7~14 kV; 10~20 cm	[28]
Ethyl(hydroxyethyl) cellulose	THF	1 wt%; 0.2 mL/h; 27 kV; 15 cm	[29]
Ethyl cellulose	Ethanol	2 wt%; 0.3 mL/h; 10~13 kV; 13 cm	[30]
Aldehyde cellulose	Water	7.5 wt%; 0.01 mL/min 10 kV; 20 cm	[31]
PVA/CNCs	Water	7 wt%; 0.5 mL/h; 22 kV; 10 cm	[32]
PLA/CNCs	$CHCl_3$/DMF	10 wt%; 16 kV; 15 cm	[33]
PVDF/CNCs	Acetone/DMF	12 wt%; 0.02 mL/min; 12 kV; 18 cm	[34]
PAN/CNFs	DMF	1~10 wt%; 15 μL/min; 20 kV; 20 cm	[35]

Note: PVA, poly(vinyl alcohol); CNCs, cellulose nanocrystals; PLA, poly(lactic acid); PVDF, polyvinylidene difluoride; PAN, poly(acrylonitrile); CNFs, cellulose nanofibrils; DMAc, dimethylacetamide; TFA, trifluoroacetic acid; DMF, N,N-dimethylformamide; THF, tetrahydrofuran.

2.3.1. Electrospinning of cellulose

The most effective way is to directly convert cellulose into nanofibers; however, raw materials have to be dissolved or melted for electrospinning. Although several cellulose solvent systems

have been developed, such as ionic liquids,[36] *N*-methylmorpholine-*N*-oxide (NMMO),[37] LiCl/DMAc,[38] tetra(*n*-butyl)ammonium hydroxide/dimethyl sulfoxide (TBAH/DMSO),[39] alkali/urea aqueous solution,[40] and sulphuric acid solution,[41] most of them are not suitable for electrospinning due to their high boiling point or high salt concentration. LiCl/DMAc has been proved as an effective solvent, and recent research focused on improving the current process and looking for new solvent systems. Shu *et al.*[23] reported that wood pulp cellulose nanofibers were successfully prepared by the design of a new electrospinning receiving device and optimization of process parameters in a LiCl/DMAc dissolution system (Figure 2.1). Compared to using a sink as the receiver, a novel drum-type receiving device was able to deal with high boiling-point solvents and obtain nanofibers with uniform diameters. The diameters of the resultant nanofibers were in the range of 200–550 nm; the porosity of the nanofiber mat was 76.5%; and there was no LiCl residue in the nanofibers. The breaking strength of the nanofibers could reach 148.2 cN. T. Jayani *et al.*[24] developed a new approach to electrospin bacterial cellulose in a TFA/PVA solvent system. Without the addition of PVA as a co-solvent, only beaded particles were collected, and there was no nanofiber formation, irrespective of the solution concentration, voltage, and flow rate. Continuous nanofibers were formed due to the excellent spinnability of PVA and the hydrogen bonding interactions between PVA and bacterial cellulose, which exhibited an average breaking strength of 448 g F, breaking elongation of 10%, surface area of 4.248 $m^2 g^{-1}$, average pore volume of 0.005 $cm^3 g^{-1}$, and pore diameter of 1.72 nm.

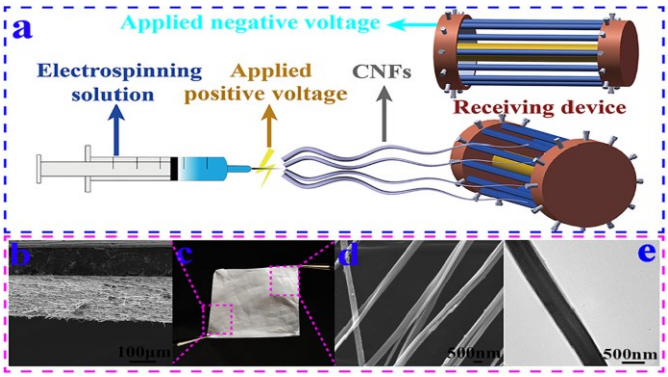

Figure 2.1. (a) Improved electrospinning receiving device. (b) SEM image of cross section of cellulose nanofiber mat. (c) Photo of a piece of cellulose nanofiber mat. (d) SEM image of CNFs. (e) TEM image of CNFs. (Reprinted with permission[23], Elsevier publishing).

2.3.2. Electrospinning of cellulose derivatives

Compared to the poor solubility of cellulose, cellulose derivatives have greatly improved solubility in many organic and inorganic solvents due to changes in the structure of cellulose. Cellulose acetate (CA) is one of the most commonly used cellulose derivatives for the production of electrospun nanofibers because CA can achieve continuous and controllable electrospinning in several conventional solvents, such as acetic acid,[25] acetone/DMAC solvent,[13] and acetone/DMF/water,[26] and the obtained CA nanofibers can be easily hydrolysed into cellulose nanofibers. The utilization of other cellulose derivatives has also been reported recently. For example, Silva *et al.*[27] produced electrospun nanofibers from hydroxypropyl methylcellulose (HPMC) with different molecular weights. High molecular weight HPMC formed beaded fibers at a concentration of 1% (w/v) and smooth fibers when the concentrations were between 1.5 and 2.25% (w/v). However, HPMC with a low molecular weight could not form nanofibers but just particles. Electrospun nanofibers were also fabricated from ethyl cellulose and modified ethyl

cellulose in DMF, THF, ethanol solutions for fluorescent materials, drug carriers, and food preservation, respectively, since ethyl cellulose has high versatility, biocompatibility, and excellent mechanical properties.[28–30] At the same time, it was noticed that some water-soluble cellulose derivatives were employed for electrospinning in order to avoid the use of unfavourable organic solvents. Zhang *et al.*[31] prepared water-soluble aldehyde cellulose by periodate oxidation, which was capable of forming nanofibers with a smooth surface and uniform size. The nanofiber diameters decreased from 833 nm to 303 nm with the increase of the oxidation degree from 34% to 91%. The prepared fibrous mats showed a moderate wet mechanical strength of around 1 MPa, and were able to absorb water equal to 30 times their own weight. These aldehyde cellulose nanofibers were particularly designed for biomedical fields, such as wound healing and tissue regeneration, and displayed a Murine L929 fibroblast cell viability of higher than 90%, suggesting good biocompatibility. However, their water-solubility limited the applications in high humidity or water environments.

2.3.3. Electrospinning of nanocellulose

Generally, the term "nanocellulose" encompasses rigid, rod-shaped cellulose nanocrystals (CNCs) and flexible, fiber-like cellulose nanofibrils (CNFs).[42] Nanocellulose is distinguished by high mechanical strength, structurally configurable chemistry, a high aspect ratio, and biodegradability and has been applied as a sustainable "green" filler in many industrial applications.[43] Due to its nanoscale dimensions, nanocellulose can be easily incorporated into electrospun nanofibers by dispersing in spinning solutions rather than dissolving, so as to maintain the nanostructure and special features. It is worth noting that nanocellulose can be modified to be dispersed in different organic and inorganic solutions. Recently, nanocellulose has been combined with various

polymers (*i.e.*, PLA,[33] PVDF,[34] and PAN[35]) to prepare composite nanofibers. For example, Zhang *et al.*[32] fabricated electrospun PVA/CNC nanofibers for the filtration of particulate matter. The addition of nanocellulose might increase the diameter of nanofibers by interfering with the interactions of the original matrix[44] or reduce the nanofiber diameter by increasing the charge density of electrospinning solution.[32]

2.4. Cellulose-based electrospun nanofiber applications

2.4.1. Water treatment

With the rapid development of urbanization and industrialization, wastewater discharge from various sources (agricultural wastes, biomedical industry, food industry, petroleum industry, manufacturing industry, *etc.*) poses a significant threat to the sustainability of the ecosystem and human health. Cellulose and its derivatives are widely involved in the treatment of contaminated water in the form of electrospun nanofibers, not only due to their intrinsic nanostructures but also owing to their active functional groups and subsequently good surface chemistry. For example, Phan *et al.*[45] reported electrospun chitosan/cellulose nanofibers for the effective adsorption of heavy metal ions, where arsenic(V), lead(II), and copper(II) were chosen as representatives. It was illustrated that the hydrogen bonding in the structure of cellulose contributed to the high water stability of nanofibers, hindering the swelling behavior of chitosan in water to enable high adsorption capacity.

CA can be easily dissolved in conventional solvents, making it attractive as a carrier for loading other polymers and functional fillers with desired properties. Therefore, CA was of great significance in the field of water treatment in the last three years. For example, to tackle the aggregation issue of hydroxyapatite nanoparticles (a mineral fixator), Hamad *et al.*[46] impregnated

them into the CA matrix through the electrospinning technique. Hydroxyapatite particles with concentrations of up to 3 wt/v% could be well dispersed in the spinning solution, enabling the improvement of the mechanical strength and adsorption performance of nanofibers. The strong hydrogen bonding interactions between the nanoparticles and CA matrix also contributed to the composite integrity and stability during the adsorption process. Other modifications of electrospun CA nanofibers, such as the addition of thiol groups,[47] citric acid,[48] and polyvinylamine,[13] have also been applied for the removal of Cu(II), Cr(VI), and organoarsenic contaminants, respectively. Photocatalysts such as ZnO[49] and metal–organic frameworks[50] are another group of functional fillers that are usually incorporated into electrospun nanofibers for degrading organic contaminants like effluent dye molecules. Besides the most widely used CA, cellulose acetate butyrate was also employed as a low-cost and accessible bearer for the immobilization of photocatalysts, which could provide a smooth and uniform membrane with an average fiber diameter of 1 μm for growing ZnO nanocrystals.[49]

The release of petroleum hydrocarbons from oil spills has serious environmental impacts on marine ecosystems. Cellulose has been electrospun into nanofibers for the application of oil/water separation, delivering extraordinary separation efficiencies of up to 99.5% for the emulsion of vacuum pump oil and water.[51] A water film was generated immediately on the surface of the electrospun cellulose membrane owing to the existence of hydroxyl groups, while the oil droplets were extruded by the membrane due to their relatively larger diameters compared to the porous fiber network (Figure 2.2). Electrospun cellulose nanofibers are usually obtained by deacetylating CA fibers.[52,53] The incorporation of CNCs into a PVDF nanofibrous membrane also contributed to the oil/water separation by forming convex and concave structures on the nanofiber surface.[34] The 4 wt% CNC/PVDF membrane showed the highest flux of water-in-toluene emulsion

(5842 L m^{-2} h^{-1}) and separation efficiency (97%), which were due to the larger water contact angle along with the increased roughness, higher porosity, and larger average pore sizes. However, the water contact angle started to drop when the amount of CNCs increased to 6 wt%, owing to the presence of a high number of hydrophilic hydroxyl groups.

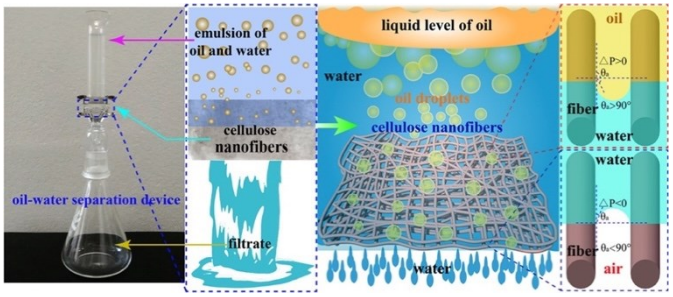

Figure 2.2. Illustration of the oil–water separation process and mechanisms by using electrospun cellulose nanofibers (reprinted with permission,[51] Elsevier publishing).

2.4.2. Biomaterials

Electrospun nanofibers from cellulose and their derivatives have been widely used in the fields of biomedical materials and tissue engineering. For example, the requirements for wound healing materials such as biocompatibility, oxygen permeability, water absorption, and non-toxicity can be fulfilled by electrospun cellulose-based fabrics. Electrospun CA/collagen nanofibers were incorporated with latex (L) from *C. Procera* (medicinal plant) for wound healing, and it was found that CA played an important role in restricting the swelling behaviour and strengthening the fabrics.[54] Similar electrospun CA nanofibers loaded with gelatin and Zataria multiflora (antibacterial plant) could absorb accumulated wound exudates and exhibited good wound healing capacity and antibacterial properties.[55] A considerably smaller wound area on the burned upper back of rats was observed compared to the commercial gauze treatment after 22 days (Figure 2.3). Moreover, electrospun ethyl cellulose[56] and cellulose diacetate[57] nanofibers with antibacterial

properties were prepared by doping with silver sulfadiazine and protoporphyrin, respectively. The former showed good inhibition activities against *Bacillus* (9.71 ± 1.15 mm) and *E. coli* (12.46 ± 1.31 mm),[56] while the protoporphyrin IX-embedded cellulose diacetate membranes exhibited 99.8% reduction in Gram-positive *S. aureus* after illumination.[57]

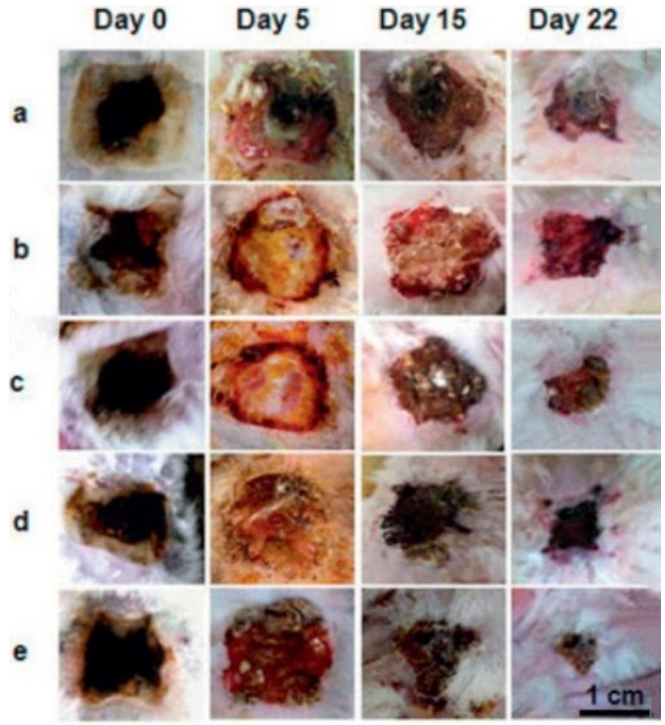

Figure 2.3. Representative images of the burn wound healing process treated with (a) commercial gauze, (b) drug-free nanofiber CA/Gel = 100 : 0, (c) drug-free nanofiber CA/Gel = 50 : 50, (d) drug-loaded nanofiber CA/Gel = 100 : 0, and (e) drug-loaded nanofiber CA/Gel = 50 : 50 (reprinted with permission,[55] Elsevier publishing).

Bioactive compounds have also been loaded into electrospun cellulose-based nanofibers to increase their stability in harsh environments and controlled release at the destinations where they are typically absorbed. Recently, flufenamic acid (an anti-inflammatory drug) was encapsulated in electrospun carboxymethyl cellulose/PVA nanofibers for prolonged drug release.[58] Covalent bonds

between the amine groups of the drug and the carboxyl groups of carboxymethyl cellulose were established to extend the biological half-life of the drug. Electrospun CNC/polycaprolactone nanofibers for the release of tetracycline were reported by Hivechi *et al.*[59] The presence of CNCs resulted in improved mechanical strength, degradability, and controlled release. The nanofibers were broken in the second week, and the number of broken fibers increased when the CNC content was up to 1 wt%.

2.4.3. Sensors

Electrospun nanofibers have a large surface area to volume ratio and excellent pore-interconnectivity, which are particularly important for initiating the signalling pathways for targeted compound detection in a short period of time. Moreover, compared to free nanoparticles, electrospun nonwoven fabrics have fewer safety issues owing to the immobilization of responsive compounds on the fibers, and better handling properties enabling easy application in various devices. Ethyl(hydroxyethyl)cellulose (EHEC) was functionalized by anchoring 4-(2-(pyridine-4-yl)vinyl)phenol (PBM) and 4-[4-(dimethylamino)styryl]pyridine, and then mixed with poly(methyl methacrylate) (PMMA) to prepare electrospun nanofibers for the detection of CN^- in water.[60] EHEC endowed the entire matrix with high hydrophilicity even at a low concentration (PMMA/EHEC 20 : 1 wt/wt), so as to have a high water retention capacity for application in fluorogenic optical devices and achieve the detection and quantification limits of 2.15×10^{-5} and 7.17×10^{-5} mol L^{-1}, respectively.

More research work was based on electrospun CA matrices. For instance, core–shell ferrous nanoparticles functionalized with Rhodamine B were embedded into electrospun CA nanofibers for gas ammonia sensing.[61] It was revealed that the encapsulation of γ-Fe_2O_3/SiO_2/Rhodamine B

nanoparticles impeded the release of fluorescent molecules to a significant extent and ensured the stability of sensing materials. Moreover, the good spinnability of CA enabled the loading of a high amount of sensing elements, and the large surface-to-volume ratio of CA nanofibers contributed to a high sensitivity in the response concentration range of 200 ppm to 12 750 ppm and a quick response time (30 s). Jia *et al.*[62] exploited electrospun CA-based ratiometric fluorescent materials for monitoring the freshness of seafood through ammonia sensing (Figure 2.4). The fluorescent unit, protoporphyrin IX, was covalently bonded to CA, which secured food safety by preventing migration. An instant fluorescent color-response (<1 s) of the prepared nanofibrous membrane to a drop of ammonia (concentration as low as 5.0 ppm) was demonstrated. Similar approaches were applied to synthesize CA-based nanofiber sensors for detecting mercury(II) and lead(II) ions, hydrogen chloride vapors, and gas ammonia.[63,64] All of them exhibited fast detection of targeted substances.

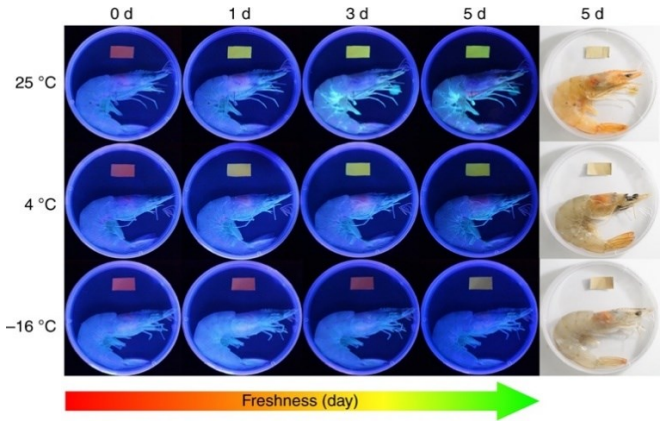

Figure 2.4. Electrospun cellulose acetate-based ratiometric fluorescent material with red initial fluorescence for monitoring the freshness of shrimps stored under different conditions (reprinted with permission,[62] Springer Nature publishing).

2.4.4. Electro-conductive materials

A flexible support material with a three-dimensional porous structure is essential for developing conducting electrodes. Wu *et al.*[65] reported electrospun polyindole/carbon nanotube/bacterial cellulose electrodes for energy storage devices. Its outstanding specific capacitance was ascribed to the three-dimensional hierarchical network formed by bacterial cellulose and polyindole for effective charge transfer. An electrospun polyacrylonitrile/cellulose nanofibril electrode carbon material has been developed[35] and displayed improved mechanical strength and electrical conductivity compared to a neat polyacrylonitrile membrane. Cellulose nanofibrils also accelerated the stabilization process by reducing the required energy for nitrile-based cleavage in the carbonization reaction.

An interesting and novel study was reported by Lyu *et al.*,[66] who utilized the porous structure of electrospun CA fabrics to construct moisture-induced electricity generators. The hydroxyl and carbonyl groups of CA dissociated and formed negatively charged surfaces when the nanofibers were exposed to moisture. Due to the accumulation of moisture on one side of the fabrics, an imbalanced distribution of protons occurred, and streaming potential was generated consequently (Figure 2.5c). The potential was primarily impacted by the porosity and average pore size of electrospun nanofabrics that could be tuned by varying the annealing time. The generation of electricity in response to the change of the moisture content is shown in Figure 2.5a and 2.5b. Water molecules moved along the 3D nanochannels with charged surfaces, generating a voltage output of up to 0.3 V and a short-circuit current density of 80 nA cm^{-2}.

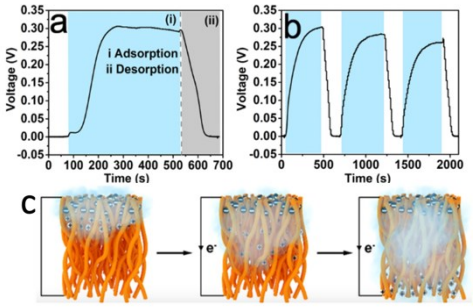

Figure 2.5. (a) Electricity generation as a function of moisture change based on the CA nanofiber with an annealing time of 5 min. The two shaded areas correspond to the (i) adsorption (blue zone) and (ii) desorption (grey zone) of moisture. (b) Electricity generation based on the CA nanofiber with an annealing time of 5 min in response to the change of RH (ΔRH = 85%). (c) Illustration of electrospun cellulose acetate nanofibers exposed to the moist flow (reprinted with permission,[66] ACS publishing).

2.4.5. Active packaging

Cellulose and many of its derivatives, such as CMC, CA, ethyl cellulose, *etc.*, have been regarded as safe food substances according to the U.S. Department of Agriculture and considered as food additives by the FDA regulations. Therefore, they are promising raw materials for the preparation of advanced food packaging. Zaitoon *et al.*[67] fabricated electrospun ethyl cellulose/poly(ethylene oxide) hybrid nanofibers encapsulated with ethyl formate for the preservation of strawberries (Figure 2.6). The efficacy was confirmed visually, where the strawberries treated with 2 mg ethyl formate released from electrospun nanofibers were not spoiled for up to 10 days, and the untreated strawberries showed microbial growth on day 8. Nevertheless, the stability of the prepared nanofibers was not good at 100% relative humidity, which might limit its applications under high moisture conditions. Niu *et al.*[68] incorporated cinnamaldehyde essential oil (CEO) into electrospun zein/ethyl cellulose nanofibers for improved water resistance of food. Hydrogen bonds formed between the hydroxyl groups of ethyl cellulose and the amino groups of zein thus reduced the

presence of free hydrophilic groups and improved the water-resistance remarkably, resulting in the controlled release of CEO during the storage period of fresh produce for achieving a prolonged shelf-life. At the same time, Yi *et al.*[69] constructed electrospun anthraquinone-2-carboxylic acid grafted silk fibroin (G-SF)/CA nanofibers with antibacterial activity against *E. coli*, where CA contributed to the handling properties and the reinforcement of tensile strength from 34.52 cN mm^{-2} to 88.92 cN mm^{-2}.

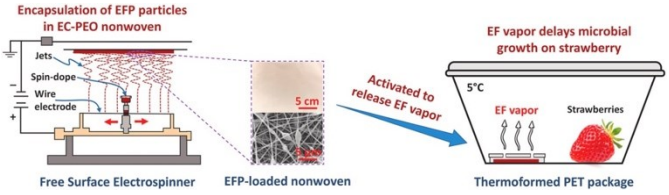

Figure 2.6. Ethyl formate-encapsulated electrospun ethyl cellulose/poly(ethylene oxide) nanofibers for strawberry preservation (reprinted with permission,[67] Elsevier publishing).

2.4.6. Other applications

Based on the unique structure and properties of electrospun cellulose-based nanofibers, some other applications have been proposed in recent years. An interesting study was reported by Knapczyk-Korczak *et al.*, who fabricated electrospun CA/polystyrene nanofibers for the collection of water from fog (Figure 2.7).[70] Due to the hydrophobicity of the CA/polystyrene matrix, water vapor was repelled from the fiber surface. The existence of CA reduced the roughness and contact angle of nanofibers, allowing an easier and free drainage pathway. Also, CA was proved to strengthen the entire matrix, which is a prominent property of water collectors.

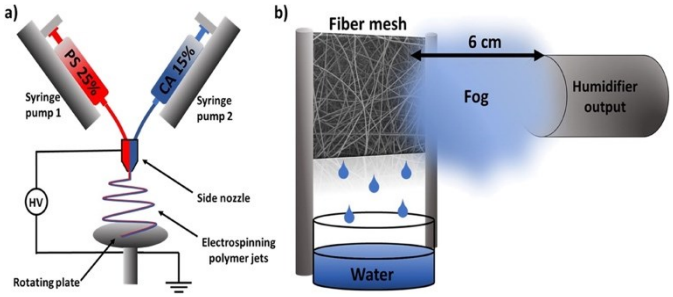

Figure 2.7. Schematic diagrams of electrospun cellulose acetate/polystyrene nanofibers for water harvesting (reprinted with permission,[70] ACS publishing).

Electrospun cellulose nanofibers have played a role in energy conservation, such as dye-sensitized solar cells[71] and solar thermal applications.[72] Electrospun CA and deacetylated CA nanofibers were used as electrolyte membranes in dye-sensitized solar cells, which showed higher open circuit voltages (780 ± 10 mV and 780 ± 10 mV) compared to the reference cell (771 ± 9 mV).[71] It was attributed to the more uniform distribution of the electrolyte within the electrospun membranes in contact with the electrode interface. At the same time, electrospun CA nanofibers loaded with thermal conductive cadmium selenide nanoparticles displayed high solar-thermal conversion potential and efficiency, which reached 40 °C under 1 sun (100 mW cm^{-2}) illumination.[72]

Besides water treatment, electrospun nanofibers were also applied for air purification.[73] With the aim of toluene (volatile organic compound) adsorption, CNCs were filled in electrospun polyamide 6 nanofibers to improve adsorption efficiency and mechanical strength, owing to their high hydrophilicity, large active surface area, and crystalline structure.[74] In the meantime, electrospun PAN-based activated carbon and PVA nanofibers incorporated with CNCs were used for the adsorption of cyclohexane[75] and filtration of particular matter.[32,76] It was worth noting that various other functional fillers, such as silica nanoparticles,[77] silica zeolites,[78] iron oxide nanoparticles,[79] and $Ti_3C_2T_x$ (metal carbide),[80] were doped in cellulose-based nanofibers for

desalination, adsorption of ammonia vapor, tunable saturation magnetization, and electromagnetic interference shielding, respectively.

2.5. Conclusion and future prospects

Recent progress in cellulose-based electrospun nanofiber production and applications is summarized. In one aspect, research work focused on exploring new cellulose solvents and cellulose derivatives that are suitable for electrospinning and improving electrospinning apparatus for better fiber quality; in another, various applications in water treatment, biomaterials, sensors, electro-conductive materials, active packaging, and so on have been proposed to make full use of these renewable, biodegradable and nontoxic nanofibrous networks with a large surface area and interconnected porous structure. Different forms of cellulose (wood pulp, nanocellulose, *etc.*) and derivatives (CA, hydroxypropyl methylcellulose, carboxymethyl cellulose, azido-cellulose, aldehyde cellulose, ethyl cellulose, *etc.*) have been employed as raw materials for electrospinning. However, the optimized electrospinning conditions of all these materials have relatively low polymer concentrations in spinning solutions and low flow rates during spinning, resulting in low productivity. Therefore, future research on new solvents and cellulose derivatives is still required to address these issues and improve productivity. It is worth noting that the electrospinning technology improved largely in the past 15 years; for example, advanced electrospinning apparatuses allow the production of nanofabrics with multiple structures (aligned, multi-layered, composite, *etc.*). However, current research work mainly focuses on the formulations and electrospinning conditions of nanofibers, and not many novel structures have been reported. Hence, the rational design of electrospun nanofibers with better performance is expected in future research, which should be based on the understanding of the structure–property relationship and linked tightly with the targeted application.

2.6. References

1. J. Xue, T. Wu, Y. Dai and Y. Xia, *Chem Rev*, 2019, **119**, 5298-5415.
2. Y. Zhang, F. Wang and Y. Wang, *Materials Today Communications*, 2021, **27**.
3. S. Lee, S. Franklin, F. A. Hassani, T. Yokota, M. O. G. Nayeem, Y. Wang, R. Leib, G. Cheng, D. W. Franklin and T. Someya, *Science*, 2020, **370**, 966-970.
4. X. Sun, L. Bai, J. Li, L. Huang, H. Sun and X. Gao, *Carbon*, 2021, **182**, 11-22.
5. J. Yan, Y. Wang, Y. Zhang, S. Xia, J. Yu and B. Ding, *Adv Mater*, 2021, **33**, e2007525.
6. K. S. Han, S. Lee, M. Kim, P. Park, M. H. Lee and J. Nah, *Advanced Functional Materials*, 2019, **29**.
7. C. Chen, W. Zhang, H. Zhu, B.-G. Li, Y. Lu and S. Zhu, *Nano Research*, 2020, **14**, 1465-1470.
8. Q. Xia, C. Chen, Y. Yao, J. Li, S. He, Y. Zhou, T. Li, X. Pan, Y. Yao and L. Hu, *Nature Sustainability*, 2021, DOI: 10.1038/s41893-021-00702-w.
9. M. Beaumont, P. Jusner, N. Gierlinger, A. W. T. King, A. Potthast, O. J. Rojas and T. Rosenau, *Nat Commun*, 2021, **12**, 2513.
10. M. C. Li, Q. Wu, R. J. Moon, M. A. Hubbe and M. J. Bortner, *Adv Mater*, 2021, **33**, e2006052.
11. R. M. O'Dea, J. A. Willie and T. H. Epps, *ACS Macro Letters*, 2020, **9**, 476-493.
12. S. R. Djafari Petroudy, S. Arjmand Kahagh and E. Vatankhah, *Carbohydr Polym*, 2021, **251**, 117087.
13. K. Liu, Z. Huang, J. Dai, Y. Jiang, G. Yang, Y. Liu, C. Lin, Y. Lv and M. Liu, *Chemical Engineering Journal*, 2020, **382**.
14. Q. Cao, M. Zhu, J. Chen, Y. Song, Y. Li and J. Zhou, *ACS Appl Mater Interfaces*, 2020, **12**, 1210-1221.
15. T. Pirzada, Z. Ashrafi, W. Xie and S. A. Khan, *Advanced Functional Materials*, 2019, **30**.
16. S. Hell, K. Ohkawa, H. Amer, A. Potthast and T. Rosenau, *Nanomaterials (Basel)*, 2020, **10**.
17. X. Miao, J. Lin and F. Bian, *Journal of Bioresources and Bioproducts*, 2020, **5**, 26-36.
18. N. Tang, Y. Li, J. Ge, Y. Si, J. Yu, X. Yin and B. Ding, *ACS Appl Mater Interfaces*, 2020, **12**, 31852-31862.
19. S. Zheng, M. Du, W. Miao, D. Wang, Z. Zhu, Y. Tian and L. Jiang, *Advanced Functional Materials*, 2018, **28**.
20. M. A. Teixeira, M. C. Paiva, M. T. P. Amorim and A. H. P. Felgueiras, *Nanomaterials (Basel)*, 2020, **10**.

21. T. Lu, J. Cui, Q. Qu, Y. Wang, J. Zhang, R. Xiong, W. Ma and C. Huang, *ACS Applied Materials & Interfaces*, 2021, **13**, 23293-23313.

22. M. Zhang, W. Ma, J. Cui, S. Wu, J. Han, Y. Zou and C. Huang, *Journal of Hazardous Materials*, 2020, **383**, 121152.

23. D. Shu, P. Xi, B. Cheng, Y. Wang, L. Yang, X. Wang and X. Yan, *Int J Biol Macromol*, 2020, **162**, 1536-1545.

24. T. Jayani, B. Sanjeev, S. Marimuthu and S. Uthandi, *Carbohydr Polym*, 2020, **250**, 116965.

25. N. Olaru, N. Anghel, P. Pascariu and G. Ailiesei, *Journal of Applied Polymer Science*, 2019, **136**.

26. W. Chen, H. Ma and B. Xing, *Int J Biol Macromol*, 2020, DOI: 10.1016/j.ijbiomac.2020.04.249.

27. P. M. Silva, C. Prieto, J. M. Lagarón, L. M. Pastrana, M. A. Coimbra, A. A. Vicente and M. A. Cerqueira, *Food Hydrocolloids*, 2021, **118**.

28. J. P. Dreyer, R. I. Stock, L. G. Nandi, I. C. Bellettini and V. G. Machado, *Carbohydr Polym*, 2020, **236**, 115991.

29. A. Wali, Y. Zhang, P. Sengupta, Y. Higaki, A. Takahara and M. V. Badiger, *Carbohydr Polym*, 2018, **181**, 175-182.

30. B. Niu, L. Zhan, P. Shao, N. Xiang, P. Sun, H. Chen and H. Gao, *Int J Biol Macromol*, 2020, **142**, 592-599.

31. H. Zhang, Y. Liu, S. Cui, Y. Zhou, J. Hu, J. Ma and Y. Liu, *Cellulose*, 2020, **27**, 8695-8708.

32. Q. Zhang, Q. Li, T. M. Young, D. P. Harper and S. Wang, *ACS Sustainable Chemistry & Engineering*, 2019, **7**, 8706-8714.

33. D. K. Patel, S. D. Dutta, J. Hexiu, K. Ganguly and K. T. Lim, *Int J Biol Macromol*, 2020, **162**, 1429-1441.

34. X. Wang, W. Cheng, D. Wang, X. Ni and G. Han, *Journal of Membrane Science*, 2019, **575**, 71-79.

35. W. Xu, B. Xin and X. Yang, *Cellulose*, 2020, **27**, 3789-3804.

36. B. Araldi da Silva, R. de Sousa Cunha, A. Valério, A. De Noni Junior, D. Hotza and S. Y. Gómez González, *European Polymer Journal*, 2021, **147**.

37. R. Protz, A. Lehmann, J. Ganster and H. P. Fink, *Carbohydr Polym*, 2021, **251**, 117027.

38. J. Garemark, X. Yang, X. Sheng, O. Cheung, L. Sun, L. A. Berglund and Y. Li, *ACS Nano*, 2020, **14**, 7111-7120.

39. X. Chen, X. Chen, X.-M. Cai, S. Huang and F. Wang, *ACS Sustainable Chemistry & Engineering*, 2018, **6**, 2898-2904.

40. H. Tu, M. Zhu, B. Duan and L. Zhang, *Adv Mater*, 2020, DOI: 10.1002/adma.202000682, e2000682.

41. C. Zhou and Y. Wang, *Journal of Applied Polymer Science*, **n/a**, 51255.

42. N. Peng, D. Huang, C. Gong, Y. Wang, J. Zhou and C. Chang, *ACS Nano*, 2020, **14**, 16169-16179.

43. M. E. Pasaoglu and I. Koyuncu, *Chemosphere*, 2021, **269**, 128710.

44. Y. Wang and L. Chen, *ACS Applied Materials & Interfaces*, 2014, **6**, 1709-1718.

45. D.-N. Phan, H. Lee, B. Huang, Y. Mukai and I.-S. Kim, *Cellulose*, 2019, **26**, 1781-1793.

46. A. A. Hamad, M. S. Hassouna, T. I. Shalaby, M. F. Elkady, M. A. Abd Elkawi and H. A. Hamad, *International Journal of Biological Macromolecules*, 2020, **151**, 1299-1313.

47. H. Y. Choi, J. H. Bae, Y. Hasegawa, S. An, I. S. Kim, H. Lee and M. Kim, *Carbohydrate Polymers*, 2020, **234**, 115881.

48. D. Zhang, W. Xu, J. Cai, S.-Y. Cheng and W.-P. Ding, *International Journal of Biological Macromolecules*, 2020, **149**, 459-466.

49. P. Pascariu, N. Olaru, A. Rotaru and A. Airinei, *Nanomaterials*, 2020, **10**, 1873.

50. W. Lu, C. Duan, Y. Zhang, K. Gao, L. Dai, M. Shen, W. Wang, J. Wang and Y. Ni, *Carbohydrate Polymers*, 2021, **258**, 117676.

51. D. Shu, P. Xi, B. Cheng, Y. Wang, L. Yang, X. Wang and X. Yan, *International Journal of Biological Macromolecules*, 2020, **162**, 1536-1545.

52. H. P. Karki, L. Kafle, D. P. Ojha, J. H. Song and H. J. Kim, *Separation and Purification Technology*, 2019, **210**, 913-919.

53. W. Wang, J. Lin, J. Cheng, Z. Cui, J. Si, Q. Wang, X. Peng and L.-S. Turng, *Journal of Hazardous Materials*, 2020, **385**, 121582.

54. G. Ramanathan, L. S. Seleenmary Sobhanadhas, G. F. Sekar Jeyakumar, V. Devi, U. T. Sivagnanam and P. Fardim, *Biomacromolecules*, 2020, **21**, 2512-2524.

55. H. Farahani, A. Barati, M. Arjomandzadegan and E. Vatankhah, *International Journal of Biological Macromolecules*, 2020, **162**, 762-773.

56. S. Ahmadian, M. Ghorbani and F. Mahmoodzadeh, *International Journal of Biological Macromolecules*, 2020, **162**, 1555-1565.

57. T. Wang, H. Ke, S. Chen, J. Wang, W. Yang, X. Cao, J. Liu, Q. Wei, R. A. Ghiladi and Q. Wang, *Materials Science and Engineering: C*, 2021, **118**, 111502.

58. A. Allafchian, H. Hosseini and S. M. Ghoreishi, *International Journal of Biological Macromolecules*, 2020, **163**, 1780-1786.

59. A. Hivechi, S. H. Bahrami and R. A. Siegel, *Materials Science and Engineering: C*, 2019, **94**, 929-937.

60. J. P. Dreyer, R. I. Stock, L. G. Nandi, I. C. Bellettini and V. G. Machado, *Carbohydrate Polymers*, 2020, **236**, 115991.

61. A. Petropoulou, S. Kralj, X. Karagiorgis, I. Savva, E. Loizides, M. Panagi, T. Krasia-Christoforou and C. Riziotis, *Scientific Reports*, 2020, **10**, 367.

62. R. Jia, W. Tian, H. Bai, J. Zhang, S. Wang and J. Zhang, *Nature Communications*, 2019, **10**, 795.

63. S. Ahmadian-Fard-Fini, D. Ghanbari, O. Amiri and M. Salavati-Niasari, *Carbohydrate Polymers*, 2020, **229**, 115428.

64. M. Kim, H. Lee, M. Kim and Y. C. Park, *Nanomaterials*, 2021, **11**, 222.

65. W. Jiajia, D. Zhanwen, X. Ping and C. Zhijiang, *Cellulose*, 2020, **27**, 6353-6366.

66. Q. Lyu, B. Peng, Z. Xie, S. Du, L. Zhang and J. Zhu, *ACS Applied Materials & Interfaces*, 2020, **12**, 57373-57381.

67. A. Zaitoon, L.-T. Lim and C. Scott-Dupree, *Food Hydrocolloids*, 2021, **112**, 106313.

68. B. Niu, L. Zhan, P. Shao, N. Xiang, P. Sun, H. Chen and H. Gao, *International Journal of Biological Macromolecules*, 2020, **142**, 592-599.

69. S. Yi, Y. Wu, Y. Zhang, Y. Zou, F. Dai and Y. Si, *ACS Sustainable Chemistry & Engineering*, 2020, **8**, 16775-16780.

70. J. Knapczyk-Korczak, J. Zhu, D. P. Ura, P. K. Szewczyk, A. Gruszczyński, L. Benker, S. Agarwal and U. Stachewicz, *ACS Sustainable Chemistry & Engineering*, 2021, **9**, 180-188.

71. J. J. Kaschuk, K. Miettunen, M. Borghei, E. Frollini and O. J. Rojas, *Cellulose*, 2019, **26**, 6151-6163.

72. N. Angel, S. N. Vijayaraghavan, F. Yan and L. Kong, *Nanomaterials*, 2020, **10**, 1329.

73. D. Lv, G. Tang, L. Chen, M. Zhang, J. Cui, R. Xiong and C. Huang, *ACS Applied Polymer Materials*, 2020, **2**, 5686-5697.

74. E. Buyukada-Kesici, E. Gezmis-Yavuz, D. Aydin, C. E. Cansoy, K. Alp and D. Y. Koseoglu-Imer, *Materials Science and Engineering: B*, 2021, **264**, 114953.

75. R. Awad, A. Haghighat Mamaghani, Y. Boluk and Z. Hashisho, *Chemical Engineering Journal*, 2021, **410**, 128412.

76. J. Cui, Y. Wang, T. Lu, K. Liu and C. Huang, *Journal of Colloid and Interface Science*, 2021, **597**, 48-55.

77. N. Dizge, E. Shaulsky and V. Karanikola, *Journal of Membrane Science*, 2019, **590**, 117271.

78. A. Ojstršek, D. Fakin, S. Hribernik, T. Fakin, M. Bračič and M. Kurečič, *Carbohydrate Polymers*, 2020, **236**, 116071.

79. G. Papaparaskeva, M. M. Dinev, T. Krasia-Christoforou, R. Turcu, S. A. Porav, F. Balanean and V. Socoliuc, *Nanomaterials*, 2020, **10**, 517.

80. C. Cui, C. Xiang, L. Geng, X. Lai, R. Guo, Y. Zhang, H. Xiao, J. Lan, S. Lin and S. Jiang, *Journal of Alloys and Compounds*, 2019, **788**, 1246-1255.

Connecting Statement to Chapter 3

Recent advances in the development and application of cellulose-based electrospun fibers, emphasizing their role as multifunctional materials, were reviewed in Chapter 2. Building on the comprehensive review of electrospun fibers, Chapter 3 further narrows the focus to the use of electrospun fibers specifically for water treatment.

Chapter 3. A review of recent developments of electrospun nanofibrous materials as novel adsorbents for water treatment

3.1. Abstract

Electrospun nanofibers have shown great potential for removal of contaminants from aqueous solutions owing to their large specific surface area, high porosity, easy modification, and good compatibility with other functional materials. To date, hundreds of polymers have been successfully fabricated into ultrafine nanofibers by electrospinning for adsorption purposes. In this review, the recent progress in electrospun adsorbents is summarized, and special attention is paid to the critical parameters for electrospinning of ultrafine fibers, commonly used polymers and fillers, as well as the adsorption capacities of electrospun nanocomposites for various water contaminants removal. First, various parameters including solution viscosity, polymer molecular weight, applied voltage, tip-to-collector distance, and flow rate for the fabrication of defectless and uniform nanofibers are illustrated. Electrospun fibrous adsorbents are then categorized according to their compositions, such as single polymer adsorbents, polymer composite adsorbents, and filler-added polymeric adsorbents, and their adsorption capacities towards specific contaminants are compared with discussions on the adsorption mechanism. Finally, a conclusion on recent achievements and current challenges is stated, and prospects associated with the applications of electrospun nanofibers in water treatment are provided.

Keywords: Electrospinning, adsorption, nanofibrous material, polymers, water treatment

3.2. Introduction

Nanofibers are fibrous materials with nano-scaled diameters, which have gained tremendous attention along with the study and development of material engineering owing to their promising properties and characteristics in a wide range of applications. Comparing with other fibrous structures, the uniqueness of nanofibers relies not only on their large surface area-to-volume ratio, light-weight, nano-sized diameter, adjustable morphology, and pore distributions, but also on their

high reactivity and biocompatibility [1]. Among various well-studied nanofiber-generating techniques, electrospinning has gained plenty of interest during the past decades and has been widely used to prepare nanofiber mats with various functional properties. The process involves the spinning of polymer solutions under electrostatic force to generate and collect nanofibers with diameters of 40-200nm (Figure 3.1A) [2]. As is widely reported, electrospinning to date is the simplest technique, in terms of the setup and conducting the process, and the most cost-effective method to generate long and uniform nanofibers consistently [3]. Electrospinning of nanofiber has been recognized as an effective strategy in a broad range of fields, including adsorption, filtration, antibacterial textile, tissue engineering, sensor, and drug delivery, attributing to its highly porous structure, large specific surface area, good interconnectivity, and structural stability [4-7].

Nowadays, environmental pollutions provoke more and more attention from the public and tend to be one of the most serious issues faced by human worldwide. Among the threatening pollutions, water contamination is one of the most urgent environmental problems owing to its direct adverse effects on human health and other biological communities [8-11]. Pollutants in water systems are generally grouped into organic (proteins, natural organic matters, dyes, etc.), inorganic (e.g., heavy metals), and acid/base agents [12]. Feasible and practical strategies to ameliorate pollution are in high demand owing to the growing pressure on freshwater exerted by anthropogenic activities. Numerous methods have been reported to remove wastes from the water, including oxidation process, electro-coagulation, photolysis, filtration, and so on [13-18]. Adsorption is especially a promising method for removing contaminants from aqueous environment, which is attributed to the simple operation, cost-effectiveness, and easy regeneration of the adsorbents [19-21].

A broad range of materials have been applied to develop effective adsorbents to date. Nevertheless, their applications are usually impeded by the poor stability and recyclability and the relatively high

cost considering large-scale productions [22]. Electrospun nanofibers have great potential to ameliorate these drawbacks. In one aspect, electrospun nanofibers can be easily functionalized chemically or physically, potentially enhancing the overall stability and mechanical properties; in another, the adjustable diameter, morphology and alignment of electrospun nanofibers offer great flexibility in various applications [12]. Moreover, their high surface-to-volume ratio and porosity are desirable for adsorption, facilitating the interactions between adsorbents and contaminants. Various functional fillers have been incorporated in electrospun nanofibers to improve the chemical and mechanical properties or provide additional binding sites for the targeted contaminants and maximize the adsorption capacity and efficiency.

The development of electrospun polymeric nanofibrous membranes for water treatment has attracted much attention, and more than 200 research papers have been published in last five years. A number of reviews have greatly contributed to our present understanding of this technology (Progress in Polymer Science 2018, 77, 69-94) and the adsorption effect on a certain type of contaminant (Journal of Hazardous Materials 2020, 401, 123608). In this review, we particularly focus on the construction of electrospun adsorbents (electrospinning conditions and fiber compositions). Therefore, 120 recent papers were reviewed to summarize and discuss the effects of crucial parameters, including both polymer solution parameters and ambient parameters, on the electrospinning process, which are the key to obtain defectless fibers and achieve superior adsorptive performance subsequently. These electrospun adsorbents were grouped into several categories comprehensively, and their adsorption capacities towards targeted contaminants were compared. This will guide the design and promote the development of novel electrospun adsorbents with high efficiency for water treatment.

3.3. Parameters for electrospun adsorbent construction

The first version of electrospinning apparatus patented in 1902 consisted of four types of charged spinnerets: conventional, co-axial, air assisting, and rotating heads, and it was stated that liquid droplets were transferred into a fine stream of fibrous fluids under the force of electrical charges [23-24]. Electrospinning was applied to large-scale production of commercial filaments in 1934 [23-25], and in the 1960s, the cone-shaped droplet formation induced by electrostatic force was modeled, which is now known as the Taylor cone (Figure 3.1B). In the mid-1990s, nanotechnology began to attract researchers' attention and interests, and it was gradually realized that nanofibers possess a significant number of promising properties and potential applications. The simplicity and good adaptability of the electrospinning process made it attractive for the preparation of nanofibers. It is crucial to develop the optimal conditions to generate continuous and uniform nanofibers. Critical variables, such as the viscosity and flow rate of polymer solution, the molecular weight of polymer, applied voltage, and nozzle-to-collector distance, were considered when electrospun adsorbents were designed and fabricated.

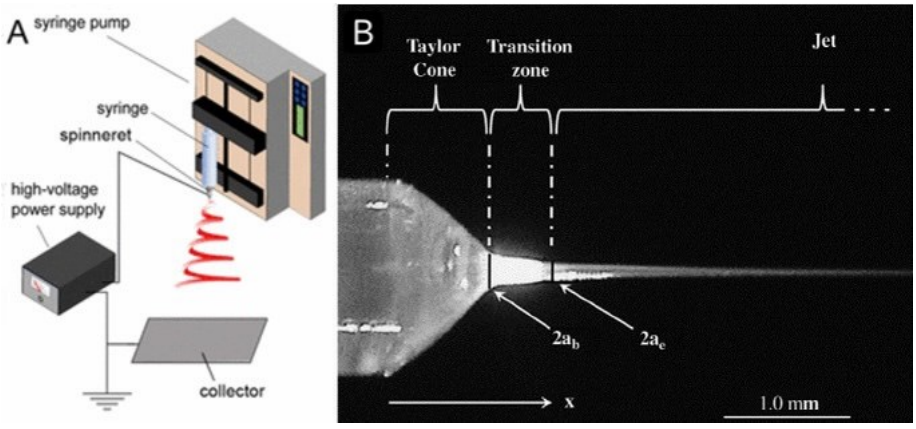

Figure 3.1. A. Schematic display of electrospinning process (reprinted with permission from Ref [26]. Copyright 2017 American Chemical Society.) B. Formation of Taylor cone (reprinted from Ref [27], with permission from Elsevier)

3.3.1. Solution viscosity

The continuity and smoothness of fibers and production of fibers with appropriate diameters are significantly influenced by the viscosity of polymer solution [6], which is positively related to polymer concentration [2]. The increase of concentration usually results in lower solution electrical conductivity and stronger viscous resistance, and thus induces the weaker stretching force along the fibers and the enlargement of fiber diameter during electrospinning. However, beaded fibers and fibers with uneven surfaces are less likely to occur when using a viscous solution [28]. Bassyouni et al. [6] found that the formation of beads and nonhomogeneous fibers was ameliorated by increasing the concentration of polyamide 6 (PA6). The absence of beads was achieved at 15 wt% of PA6. Nevertheless, the solution viscosity may be too high to eject the polymer solution from the Taylor cone. At extremely low viscosity, the polymer solution is unable to form continuous fibers. Therefore, polymer solutions with a viscosity of 50-400 mPa/s are usually used for electrospinning.

3.3.2. Molecular weight

The molecular weight of polymers is a predominant factor influencing solution viscosity, surface tension, and dielectric strength; accordingly, altering the morphology of fibers [30]. The extent of polymer chain entanglement in solution is related to molecular weight [31]. Generally, the viscosity increases when the molecular weight is high, and the polymer solution may achieve the desired level of viscosity even low solution concentration is applied. High molecular weight also contributes to the conquering of surface tension by electrostatic repulsive force and restraining bead formation. It was reported by Gupta et al. [32] that bead formation and occurrence of droplets

were ameliorated when the molecular weight of PMMA was raised from 12.47 to 365.7 kDa, but it also led to larger average fiber diameters.

3.3.3. Applied voltage

Sufficient voltage is demanded to conquer surface tension and viscoelastic forces, so jet velocity is high enough to disperse the polymer solution [33]. Otherwise, the Taylor cone would become unstable and induce the formation of beads. Changing applied voltage has an impact on electric field force when the tip-to-collector distance is fixed. It thus influences the shape of the Taylor cone and the deposition rate of the polymer jet. In general, fiber diameter decreases at high applied voltage since the strengthened electric field force stretches the fiber more. For example, raising the voltage from 15 kV to 25 kV led to decreased mean cellulose nanofiber diameter from 300 nm to 210 nm [34]. Nevertheless, when the voltage exceeded 26 kV (which was the optimal voltage in the study), the fiber diameter increased, and plenty of beads were induced [6]. The instability of fluid caused by the excessive voltage (>35 kV) was also observed in the electrospinning of lignin for pharmaceutical pollutant removal [35].

3.3.4. Tip-to-collector distance

The solvent evaporates during the stretching process between the Taylor Cone and the collector, so an appropriate tip-to-collector distance is essential to ensure the successful evaporation of the solvent and the deposition of dry fibers on the collector. However, the electrostatic force is impaired if the distance is too long. A study on electrospun lignin nanofibers discussed the optimal nozzle-to-collector distance. It was shown that a relatively long distance (20 cm) led to a well-performed dispersion of fibers and a thin nanofibrous mat [35]. Bassyouni et al. fabricated electrospun Fe_3O_4/o-MWCNTs/PA6 hybrid nanofibrous membrane. They found that the reduction

in tip-to-collector distance accounted for the increased electric field force and the formation of beads. In contrast, the weaker electric field was induced by longer distance, and more stretching of fibers with reduced diameters was observed [6].

3.3.5. Flow rate of polymer solution

The flow rate of solutions affects the shape of polymer droplets, ejection velocity, and subsequent fiber formation. As the feeding rate of the solution increases, larger droplets form with reduced surface tension. Therefore, less electrostatic force is required to conquer the surface tension, leading to less stretching and relatively large fiber diameter [6]. Moreover, the formation of beads may occur when the flow rate is high, which is attributed to the lack of sufficient solvent evaporation time before the collection of fibers [2]. It was reported that the average diameter of electrospun chitosan/cellulose acetate/gelatin nanofibers increased from 152.32±41.48 nm to 165.68±54.75 nm when the applied feeding rate rose from 11.67 μL/min to 35 μL/min [36]. Generally, a relatively low flow rate (0.8 to 1.2 ml/h) is desirable to obtain continuous and uniform fibers with small diameters.

3.3.6. Control of parameters in co-axial electrospinning

Fabrication of nanofibers with core/sheath structure is recognized as a prevailing strategy for adsorption applications. Polymer solutions are electrospun through two separate capillaries with a co-axial structure. The rapid fabrication process limits the interaction between polymer chains and inhibits the two entities from mixing together after solidification [37]. Factors affecting the formation and morphology of core/sheath nanofibers include the immiscibility, flow rates, viscosity, and conductivity of both core and sheath solutions. For example, a stable Taylor cone and core/sheath structure could merely be observed when two miscible solutions were used for

electrospinning [38]. To improve the stability and homogeneousness of core/sheath fibers, moisture-sensitive sol-gel precursors are often used. It was proven that the addition of $Ti(OiPr)_4$ to the polymer solutions contributed to the stability of co-axial jets [39]. $Ti(OiPr)_4$ hydrolyzed immediately and condensed into an inorganic gel network in the polyvinylpyrrolidone (PVP) sheath layer. To do so, the viscosity was increased, and the viscoelastic forces were enhanced on the interface of core and sheath layers.

The flow rates of sheath and core solutions have significant impacts on the structure and diameter of fibers. It was found that the coaxially electrospun TiO_2/PVP hollow fibers exhibited larger openings with flow rates of the sheath solution higher than 0.1 ml/h [39]. However, the division of sheath solution from core fluid jet occurred when the inappropriate flow rate ratio was applied [40]. Conductivity is another critical factor for successful co-axial electrospinning. Ma et al. [41] investigated the core-shell structured cellulose acetate/polycaprolactone-chitosan (CA/PCL-CS) nanofibers for Cr (VI) removal. They found that a more explicit interface between core and sheath layers was observed when the conductivity of the core solution increased. The high conductivity led to more vital stretching forces on the core solution under the electrical field, which promoted the diffusion and separation of core polymer molecules from the sheath layer.

3.3.7. Mass production of electrospun nanofibers

The single-nozzle design of electrospinning apparatus is primarily applied at laboratory scale, which is featured as simple and versatile. In order to improve the production rate and subsequently achieve mass production, several electrospinning setups, such as nozzleless and multi-nozzle electrospinning systems, have been developed in recent years [42, 45]. Nozzleless electrospinning is designed to generate nanofibers from a large surface (cylinder, disc, ring, slit, etc.) instead of the

tip of needle, so as to improve the yield of nanofibers. Wang et al. [42] developed a ring-structured spinneret to achieve needleless electrospinning. Multiple rotating rings made from copper wire served as spinnerets to pick up 9% PVA solutions and fabricate considerable amounts of fibers simultaneously. This novel design exhibited a high production rate (up to 9.5 g/h using four rings) of uniform nanofibers with diameters of less than 1μm. Wei et al. [43] extruded polymer melts from an annular slit, which could form multiple jets at the edge of annular spinneret (Figure 3.2). The highest production rate of this electrospinning system reached 4.5 g/h of PAN solution. Niu et al. [44] demonstrated the nozzleless electrospinning using disc and cylinder spinnerets for the fabrication of PVA fibers, and it was concluded that cylinder spinneret was more dependent on the applied voltage and polymer concentration. Multi-nozzle electrospinning has also been reported to improve the productivity and enlarge the deposition area. For example, Varesano et al. [45] investigated different multi-nozzle electrospinning designs with various nozzle numbers (ranging from 2 to 16) and configurations (columns x rows). It was found that the deposition area of fibers was enlarged, and the collector dimension was increased from 20 cm x 25 cm to 50 cm x 50 cm when the nozzle number was more than 6. Moon et al. [46] reported a syringeless electrospinning system by integrating needle-like conductive probes into a rotating cylinder. A polymer reservoir was positioned under the cylinder, and the tips of needles could pick up polymer melts when the cylinder started to rotate. The productivity of this setup was 3.2 g/h of PAN solutions.

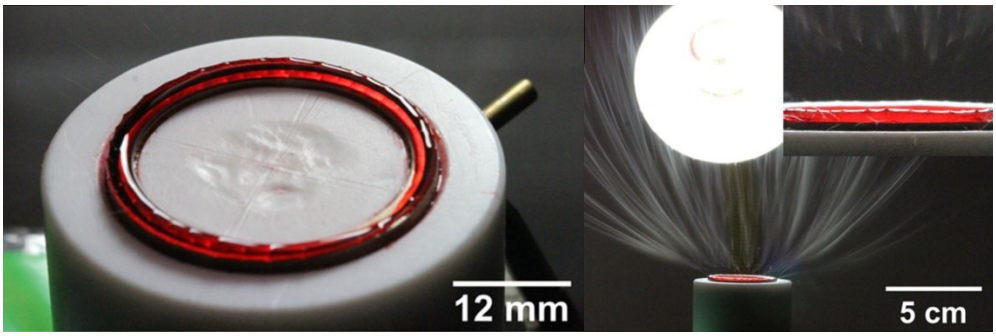

Figure 3.2. Images of annular spinneret electrospinning design (reprinted with permission from Ref [43], Copyright 2019 Elsevier).

3.4. Electrospun adsorbent compositions

Approximately 200 polymers, including natural polymers, synthetic polymers, or a combination of both, have been used in electrospinning for a wide range of applications to date [47]. Both natural and synthetic polymers possess unique characteristics. Natural polymers such as chitosan, protein, cellulose, lignin, and alginate are generally renewable, biodegradable, abundant naturally, and non-toxic, while synthetic polymers, such as polyacrylonitrile (PAN), polyvinyl alcohol (PVA), polyamide-6, poly(methylmethacrylate) (PMMA), and polystyrene (PS), deliver several advantages over natural polymers concerning mechanical properties and chemical strength [2,48,49]. Electrospinning also enables the incorporation of various polymers and functional fillers into a single matrix to deliver applications cost-effectively. Figure 3.3 shows the morphologies of electrospun nanofibers developed from both natural and synthetic polymers in recent years for water treatment.

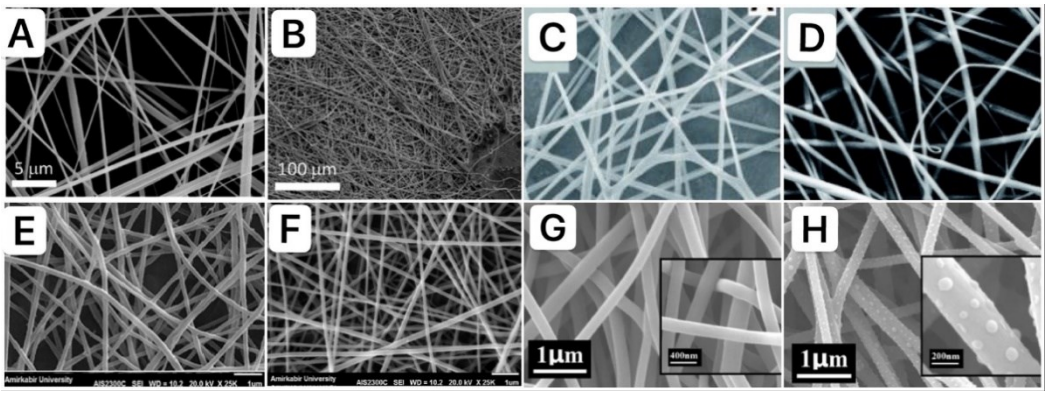

Figure 3.3. SEM images of (A) neat PMMA nanofibers, (B) PMMA- graphene oxide nanofibers, (C) neat PS nanofibers, (D) PS- poly (dibenzo-18-crown-6) nanofibers, (E) neat chitosan nanofibers, (F) chitosan/multi-walled carbon nanotubes/ Fe_3O_4 nanofibers, (G) neat lignin nanofibers, (H) lignin- TiO2

nanofibers (A, B were reprinted with permission from Ref [49], Copyright 2017 RSC Publishing; C, D were reprinted with permission from Ref [50], Copyright 2017 RSC Publishing; E, F were reprinted with permission from Ref [29], Copyright 2016 Elsevier; G, H were reprinted with permission from Ref[51], Copyright 2020 Springer Nature)

3.4.1. Electrospun adsorbents from a single polymer

Polymers are not only utilized as matrix material. Some of them contain a great deal of desired functional groups, offering adsorption sites for efficient pollutant removal. PVA is one of the most common materials used in electrospinning, which is featured to be biodegradable, processable, spinnable, and eco-friendly [52]. To prepare electrospun PVA nanofibers, a concentration varied from 10wt% to 15wt% is suitable to deliver a self-standing fibrous membrane with proper flexibility [53-56]. The solvents are usually deionized water, acetic acid, and ethanol, while Mukhlish et al. used a multi-solvent system mixed with formic acid, acetic acid, and water at a ratio of 1:1:3 (v/v) [57]. PVA has numerous hydroxyl groups capable of adsorbing substances by hydrogen bonding and crosslinking. Nevertheless, water-resistance hinders the performance of PVA-based fibers, which is often alleviated by modifications. Tian et al. fabricated PVA nanofibers that were crosslinked by glutaraldehyde (GA) [52]. The obtained fibers retained their morphology after the adsorption of Cu^{2+} and Pb^{2+} in the aqueous environment. Chitosan, one of the most abundant natural polysaccharides, is capable of effectively absorbing heavy metals and organic compounds through its hydroxyl and amine groups. The adsorption capacity of electrospun chitosan-based nanofibers for Pb^{2+} ions has been investigated, where Haider et al. added K_2CO_3 to the chitosan nanofibrous mat and Li et al. crosslinked chitosan with GA to improve the stability in aqueous system [58-59]. It was worth noting that the addition of K2CO3 raised the stability to 92%, which was higher than that of GA crosslinked chitosan nanofibers (73.8%). The

neutralization of chitosan by K_2CO_3 converted ammonium to amine groups, offering extensive chelating groups, strength, and tension to nanofibers. Alginate, another natural polysaccharide, has also been employed to prepare electrospun adsorbent due to its carboxylic groups [60]. Unlike chitosan, alginate, and PVA, the hydrophobicity of electrospun PS nanofibers ensures excellent stability in an aqueous solution. An insignificant weight loss of PS was observed from its dissolution in certain organic solvents, such as acetonitrile and 1-decanol [61]. In contrast, electrospun nylon 6,6 nanofibers take advantage of their excellent mechanical strength, stability, and self-lubricating feature [62]. Electrospun nylon 6,6 membrane exhibited desirable adsorptive performance for removing Bisphenol A, forming hydrogen bonds between the adsorbate and carbonyl groups of Nylon 6,6 [62]. Electrospun adsorbents prepared from a single polymer and their optimized electrospinning conditions reported in the last five years are listed in Table 3.1.

Table 3.1. Electrospun adsorbents prepared from a single polymer and their optimized electrospinning conditions.

Polymers	**Concentrations**	**Solvents**	**Electrospinning conditions** (voltage, flow rate, tip-to-collector distance)	**Refs**
PVA	6 wt%	Deionized water	20kV, 1.0ml/h, 12cm	[52]
Chitosan	3 wt%	TFA	20kV, 0.5ml/h, 15cm	[59]
Cellulose acetate	19 wt%	Acetic acid/water (9:1, w/w)	20kV, 0.75ml/h, 15cm	[63]
Poly (L-lactic acid)	5 wt%	Chloroform/ N, N-dimethylformamide (9:1, v/v)	20kV, 1ml/h, 15cm	[64]
Nylon 6,6	14 wt%	Formic acid/acetic acid (1:1, v/v)	26kV, 0.4ml/h, 15cm	[62]
Polyindole	1.6 wt%	Acetonitrile	28kV, 0.5ml/h, 20cm	[65]
Polystyrene	15 wt%	DMF	20kV, 0.8ml/h, 20cm	[61]
Polyethylene terephthalate	18 wt%	TFA	15kV, 0.3ml/h, 10cm	[66]

3.4.2. Electrospun adsorbents from polymer composite

When two or more polymers are mixed, the structure and properties of electrospun fibers are different from those of a single polymer. Polymers can interact with each other by forming hydrogen bonds or dipole-dipole interactions [2]. Also, the properties of different polymers can be complementary, conquering the disadvantages of a single polymer during the electrospinning process and in the ultimate nanofibers. Notably, numerous studies are on the combination of natural polymers and synthetic polymers. The majority of natural polymers share a couple of similarities, such as non-toxicity, biodegradability, renewability, high availability, and biocompatibility, which are desirable properties of a promising adsorbent.

Nevertheless, they suffer from several drawbacks, such as weak mechanical properties and wet stability. Lignin, the second abundant natural polymer next to cellulose, possesses alcohol, ether, aromatic, sulfur, or carboxylate groups according to its various extraction processes [67]. However, the electrospinning of pure lignin is limited by its poor chain structure and molecular entanglement [68]. Camire et al. stated that the addition of PVA to the electrospinning solution largely facilitates the formation of lignin-based nanofibers [35]. Keratin, derives from sheep wool, textile industry wastes, and feathers from butchery, was mixed with PA6 for electrospinning [69]. Keratin possessed desirable properties such as amine groups and high molecular weight, while PA6 offset its limitations (weak mechanical property and brittleness).

Similarly, polyvinylidene fluoride (PVDF)/chitin nanocomposites were prepared for indigo carmine dye removal [70]. The composite fibers exhibited improved stability and adsorption capacity compared to the single polymer nanofibers. Poly(acrylic acid) (PAA) fibers are not stable in water, although they can adsorb metal ions via chemical binding affinity [5]. Thus, a binary polymer system of PAA and PVA was developed for the removal of heavy metal ions [5,71]. It was

revealed that both the stability and adsorption capacity of electrospun fibers were improved significantly. Chitosan, possessing numerous promising adsorption characteristics, is also limited by its swelling behavior and poor solubility in organic solvents. It was found that the combination of chitosan and polyisoprene could reduce the swelling ratio of electrospun chitosan nanofibers by 50% [72]. Lou et al. [73] have coated chitosan on the surface of PAN electrospun nanofibers. To do so, chitosan can be dissolved in acidic solvent systems instead of N,N-dimethylformamide which is an organic solvent for PAN electrospun solution. Chitosan attached to the surface of PAN nanofiber tightly by forming hydrogen bonds, which guaranteed high adsorption capacities and solved the problem of insolubility of chitosan in organic solvents in the meanwhile. Chitosan has also been formed composites with PVA and poly(ethylene oxide) (PEO) to ameliorate the mechanical instability of chitosan-based nanofibers [74,75] (Table 3.2).

Table 3.2. Electrospun adsorbents prepared from polymer composites and their optimized electrospinning conditions.

Polymers	**Concentrations**	**Solvents**	**Electrospinning conditions** (voltage, flow rate, tip-to-collector distance)	**Refs**
Cellulose acetate/ beta-cyclodextrin	16%/5%	Acetone: DMF (2:1)	25kV, 1.5ml/h, 15cm	[25]
Chitosan/ poly(acrylamide)	3% (CS:PAA=77:23)	50% acetic acid	24kV, 0.7ml/h, 21cm	[72]
Chitosan/ poly(vinyl alcohol)	3%/7.5%	Acetic acid (90% v/v)	22kV, 1.5ml/h, 15cm	[74]
Chitosan/poly(ethyl ene oxide)	CS:PEO=9:1	Acetic acid	20kV, 0.5ml/h, 13.5cm	[75]
Poly (vinyl alcohol) / Poly(acrylic acid)	7.6% (PVA:PAA=4:1)	Deionized water	13kV, 1ml/h, 10cm	[5]
Poly (vinyl alcohol) / Poly(acrylic acid)	5%/5%	Deionized water	17kV,0.5ml/h, 15cm	[71]
Poly (vinyl alcohol) /Alkali lignin	15% (PVA:AL=7:3)	Distilled water	10kV,0.1ml/h, 10cm	[35]
Poly (vinyl alcohol) /Alkali lignin	10% (PVA:AL=6:4)	Distilled water	20kV,4.8ml/h, 20cm	[68]
PA6/keratin	15% (1:1)	Formic acid	25kV,0.6ml/h, 10cm	[69]
Polyvinylidene difluoride / chitin	15%/1%	Distilled water	18kV,1ml/h, 15cm	[70]
Chitosan/PAN	1:5	Acetic acid	16kV,1ml/h, 15cm	[76]
Chitosan/polymeth ylmethacrylate	0.3:1.25/0.3:1	Acetic acid	18kV, 1ml/h, 15cm	[77]
Polyamidoamine/ PAN	6:9	DMF	16kV,1ml/h, 20cm	[78]

3.4.3. Incorporation of inorganic/organic fillers

Polymers are composed of molecular chains of repeating subunits. Their high molecular weights deliver many physical properties such as viscoelasticity and toughness [2]. Therefore, polymers are widely used as matrix materials in electrospinning, and organic or inorganic fillers are introduced into polymer nanofibers to acquire favorable mechanical, thermal, and chemical

properties. For example, PAN is a well-studied polymer in electrospinning, which is favored by its abundance, easy accessibility, excellent tensile strength, and high thermal and chemical stabilities [79,80]. Nevertheless, the swelling behavior of PAN nanofibers remains a major issue. The addition of ZnO and TiO_2 was able to ameliorate the swelling of PAN-based fibers [79]. Also, the metal nanoparticles (ZnO, TiO_2, Fe_3O_4, and Zr), graphene oxide, magnesium silicate, fumarate ferroxane (Fum-F), and crown ester were successfully incorporated in electrospun PAN fibers to improve the adsorption capacity [48,79-85]. PVA has relatively strong hydrophilicity, so PVA fibers also suffer from swelling in an aqueous solution. With the addition of inorganic nanoparticles, PVA-based nanofibers acquire strengthened physicochemical properties. Water-insoluble PVA nanofibers were prepared with the incorporation of SiO_2, and the effectiveness of adsorption for Mn^{+2} and Ni^{+2} ions was improved by introducing phosphine groups [56]. The hydrogen bonds between water and PVA were replaced by those between silanol groups of TEOS [$Si(OC_2H_5)_4$] and hydroxyl groups of PVA. The average diameter of PVA/SiO_2 nanofibers was smaller than that of pristine PVA nanofibers, implicating the enlarged surface-to-volume ratio. It revealed that nano-porous particles, such as TiO_2 and ZnO, could also be employed to improve the physical and chemical stabilities of PVA fibers [55, 86]. Electrospun PVP fibers could be coated by cerium oxide, magnetic $CuFe_2O_4$, fly ash, TiO_2, and alumina-silica to prepare functional adsorbents [57,87-89].

3.4.3.1. Metal oxide fillers

Overviewing the applications of electrospun adsorbents reported in the last five years, the incorporation of metal oxide nanoparticles into polymeric nanofiber matrices played a vital role in removing heavy metals, toxic dyes, antibiotics, herbicides as well as other wastes and pollutants from aqueous environment. To date, titanium dioxide, ferric oxide, zinc oxide, ceric oxide,

aluminum oxide, and manganese oxide have been used to prepare electrospun adsorbents [34,87,90-92]. These metal oxides have good physical and chemical stability, high surface-to-volume ratio, and non-toxicity [3,53]. Nevertheless, recycling these nano-sized metal oxides is difficult when they are directly used as adsorbents for water treatment. The incorporation in electrospun fiber matrices not only facilitates the recycling of nanoparticles but also maintains their functionalities.

Titanium dioxide has been widely used to remove heavy metal ions and dyes. Saud et al. examined the adsorption capacity of electrospun fly ash/TiO_2/PVP nanofibers for methylene blue [89]. It was worth noting that the addition of fly ash offered extra adsorptive sites for dye molecules. Titanium dioxide has also been entrapped into chitosan nanofibers for the adsorption of Pb (II) and Cu (II) ions [93]. The TiO_2 content of up to 2wt% resulted in the reduced fiber diameters, so the surface area and subsequent adsorption capacity were increased. Cerium oxide modified with mercapto groups was incorporated in PVP fibers and applied for removal of Pb (II) and Cu (II) ions [87]. However, its maximum adsorption capacities for Pb (II) and Cu (II) ions were 90.9 mg/g and 88.3 mg/g, respectively, which were much lower than those of chitosan/TiO_2 nanofibers (710.3 for Cu (II) and 526.5 mg/g for Pb (II)) [87,93]. It was revealed that the combination of chitosan with TiO_2 nanoparticles has a significant impact on adsorption efficiency. TiO_2 not only can ameliorate the swelling of chitosan fibers in aqueous solutions, but also enable chitosan with better uptake of metal ions by electrostatic attraction. ZnO nanoparticles were added in electrospun polymeric adsorbents to remove metal ions and dye molecules. Appiah-Ntiamoah et al. [81] integrated PAN-based polymeric adsorbents with ZnO and $ZnFe_2O_4$ to facilitate the adsorption capacity toward Congo red. The result revealed that the driving adsorption mechanisms shifted from surface charges to chemical bonding after the addition of ZnO, indicating that the concentration of ZnO

had an impact on the strength of the chemical adsorption process; and the heterojunction formed between ZnO and $ZnFe_2O_4$ promote further chemical adsorptions. The adsorption of Congo red was also reported by using zeolitic imidazolate framework (ZIF) incorporated PVA nanofibers. Zeolitic imidazolate framework, featured as high surface area and promising thermal stability, is a novel metal-organic framework material composing of tetrahedral zinc ions [94]. The nanofibers containing ZnO-$ZnFe_2O_4$ and ZIF exhibited the adsorption capacities for Congo red of 263 mg/g and 160 mg/g, respectively [81,94]. The relatively lower adsorption capacity of ZIF/PVA nanofibers might be attributed to the limited adsorptive sites which were mainly on the surface of ZIF/PVA fibers. The pore size on ZIF/PVA fibers was smaller than the size of Congo red molecules, so it impeded them from entering the internal of fibers. Another metal oxide of great interest is the magnetic Fe_3O_4 nanoparticle, which exhibited great potential in the adsorption of heavy metal ions, inorganic pollutants, aqueous contaminants, and so on. Yan et al. reported the electrospun PVA/chitosan nanofibers containing magnetic Fe_3O_4 for Cr (VI) ion removal by oxidation-reduction reaction and electrostatic force [95]. Solid-phase extraction of triazine herbicides has also been reported by Feizbakhsh et al. using the magnetic Fe_3O_4 nanoparticles [96]. Recently, the effects of combining more than one type of metal nanoparticles on adsorption capacity have been investigated. For example, the adsorption capacity of electrospun PVA/TiO_2/ZnO nanofibers for thorium (IV) surpassed that of PVA/TiO_2 fibers [53,55]. Doping both TiO_2 and ZnO nanoparticles was also applied to removing Cr (VI) ions in the electrospun PAN fiber matrix [79]. The addition of metal oxides improved the porous structure of nanofibers and thus delivered a distinguished adsorption capacity. Fe_3O_4 nanoparticles were also actively combined with other metal oxides such as Al_2O_3. Bozorgpour et al. investigated the application of chitosan/Al_2O_3/ Fe_3O_4 composite nanofibers for the adsorption of nitrate and phosphate anions

[97]. Other metal adsorbents with high potential in adsorption are cobalt ferrite, hydrous zirconium oxide, and manganese oxide nanoparticles, which all displayed auspicious performance in the treatment of contaminated aqueous environment [90,98-99].

3.4.3.2. Carbon-based fillers

Recently, incorporating carbon-based materials into the polymeric nanofiber matrices has been recognized as one of the superior methods for adsorbent preparation. Carbon nanotube (CNT) is known for its distinguished mechanical, electrical, thermal, and adsorption properties [100]. Electrospun CNT-impregnated poly(styrene-co-acrylonitrile) nanofibers were developed to remove methylene blue. The driving adsorption mechanism was proved to be a physical process via van der Waals force between MB molecules and CNTs [101]. Nevertheless, the strong van der Waals force between CNTs was likely to induce agglomeration, remaining an obstacle to preparing uniformly distributed solutions [6]. To ameliorate this problem, Bassyouni et al. [6] functionalized CNTs with carboxylic groups via oxidation and mixed them with Fe_3O_4 nanoparticles for Pb (II) removal. To do so, not only the agglomeration of CNTs was reduced, but also the adsorptive sites on the prepared hybrid nanofibrous mats were increased significantly, contributing to a relatively higher adsorption capacity towards Pb (II). A similar study was reported by Beheshti et al. [29] to treat Cr (VI) contamination in an aqueous environment, which combined chitosan, Fe_3O_4, and CNTs. The reduced agglomeration of CNTs is attributed to the incorporation of Fe_3O_4. The maximum adsorptive capacity towards Cr (VI) was 360.1 mg/g, which was higher than that of the aforementioned PVA/chitosan/Fe_3O_4 nanocomposite (213 mg/g) [29,95]. Effectively, the appropriate combination of different adsorbents in polymer matrices offers extraordinary adsorptive effects compared with sole adsorbent systems.

Graphene oxide (GO) was also reported as an effective adsorbent extensively attributed to its auspicious structure and oxygen-containing functionalities, such as epoxide, carbonyl, carboxyl, and hydroxyl groups [102]. Mercante et al. investigated the adsorption performance of electrospun poly(methylmethacrylate) nanofibers coating with reduced GO for removing methylene blue [49]. The reduced GO possessed a stronger π electron structure, and therefore the adsorption efficiency was significantly enhanced. GO is often combined with metal nanoparticles to deliver a chemisorption process to facilitate adsorption efficiency. As an electron acceptor, GO migrates electrons and prevents the charge combination between the metal oxide adsorbents and graphene, offering more adsorptive sites for adsorbates [103,104]. Abdel-Mottaleb et al. [105] reported a ZnO-decorated electrospun PAN/GO fibrous matrix for Cr (VI) removal, which showed a high adsorption capacity of 690 mg/g. GO was also used to combine with electrospun Fe_3O_4/waste PAN nanofibers for Basic Red 46 dye removal by exchanging and sharing electrons with the dye molecules [85].

3.4.3.3. Other fillers

Silica nanoparticles are representative inorganic fillers incorporated in electrospun fabric membranes for the adsorption of pollutants such as heavy metal ions, toxic dye molecules, herbicides, and so on. Like the metal nanoparticles, silica serves as an adsorbent and ameliorates the swelling of electrospun polymeric fibers. Notably, the silica-based materials with mesoporous structures are of great interest, making the adsorptive sites more accessible to the contaminant substances. An electrospun mesoporous polyvinyl alcohol/chitosan/silica nanocomposite adsorbent was synthesized for Red 80 dye removal [106]. The highest adsorption efficiency of PVA/CS/SiO_2 was 322.5 mg/g. A comparison of mesoporous and microporous electrospun PVA/silica nanofibers was presented by Elsherief et al. [107]. The later showed higher adsorptive

efficiency, which might be attributed to the larger surface area-to-volume ratio of microporous structured fibers. Furthermore, a wide range of functional groups has been integrated into the silica-based materials. For example, Kim et al. successfully fabricated the PVA/PAA nanofibers incorporating thiol group-modified silica nanoparticles [108]. The modification of thiol groups induced strong attraction with Cu (II) ions, facilitating the overall adsorptive performance of electrospun nanofibers. Some other researchers have also reported the well-performed metal-silica nanofiber adsorbents, such as magnesium silicate and alumina-silica nanofibers [57,84], where silica reinforced the fiber matrices by conquering the fragile property of inorganic metal oxides.

Cyclodextrins (CDs) are oligosaccharides shaped as a hollow circular cone. Among all types of CDs, beta-cyclodextrins (β-CD), owning seven glucose units, gained much attention as a composite substance in electrospun nanofibers for adsorption. One of its desirable characteristics is that β-CD can form a host-guest complex with the pollutant molecules due to its internal hydrophobicity and external hydrophilicity [25]. It has been widely applied for dye removal from wastewater. Chen et al. have fabricated gelatin/β-CD nanofibers for the adsorption of methylene blue. It was indicated that the maximum adsorption capacity of composite fibers was 47.7 mg/g, and it was better than that of pure gelatin fibers [109]. A similar study was conducted to prepare ε-polycaprolactone (PCL)/β-CD composite fibers for methylene blue removal. The adsorption behavior became better along with the increment of β-CD content, and no doubt that the improvement of dye removal was achieved by the composite fibers comparesd with pure PCL fibers [110]. However, the optimum methylene blue uptake by PCL/β-CD fibers was only 10.52 mg/g, much lower than that of gelatin/β-CD fibers. It might be because of that gelatin also contributed to the adsorptive activity by electrostatic interactions and hydrogen bonding, while PCL acted as the base material has no binding sites for dye molecules.

Applications of natural bio-sorbents for contaminant removal are known to be economical and effective. Not only the biopolymers like chitosan but also the microorganisms and enzymes showed distinguished adsorptive capability. Baker's yeast, a commonly used microorganism in fermentation, has been used to remove uranium (VI) and thorium (IV) ions effectively via electrostatic attraction [111]. A co-polymeric nanofiber matrix immobilizing laccase was also prepared to adsorb phenol and biphenyl A, displaying a better adsorptive effect than that of pure polymeric nanofibers [112].

Molecularly imprinted electrospun nanofibers are featured with specific recognition and high affinity of targeted emerging contaminants, which introduce binding sites with specific sizes using functional monomers or ligands, and exhibits great potential in adsorption applications [113]. Molecular imprinting during the electrospinning process is a relatively straightforward approach to perform, where the templates (targeting contaminant molecules) are dispersed in polymer solutions and removed after electrospinning. Xue et al. [114] have successfully imprinted 2,4-dinitrotoluene (DNT) molecule using PET as the supporting material and polyallylamine (PAM) as the functional macromer. The concentration of 20 wt.% PET and the ratio of 1:1 PAM/DNT gave rise to the optimal adsorption capacity of the prepared imprinted nanofibers [114]. Decoration of the pre-synthesized electrospun matrix with template imprinted polymer layers can also produce electropsun adsorbents. Wu et al. [115] have demonstrated this approach using polyethersulfone as the base material, and the polymerization of dopamine (functional monomer) in the presence of bilirubin (template) was carried out in weakly alkaline solutions. Another alternative approach is to disperse the template-encapsulated nanoparticles in electrospinning solutions. Ardekani et al. [116] prepared bisphenol A (template) imprinted electrospun nylon 6 nanofibers, where 3-aminopropyltriethoxysilane (APTES) was selected as the functional monomer to bind the template.

The molecularly imprinted nanofibers prepared from 12 wt.% of nylon 6 displayed a smooth surface and an average diameter of 145 nm [116].

3.5. Applications of electrospun nanofibers in adsorption of contaminants

The applications of electrospun nanofibers in eradicating impurities have been explored and reported by numerous researchers. Generally, pollutants were discharged either directly from the factories as industrial wastes, such as organic dye solutions, heavy metals, phenolic compounds, etc., or indirectly through soil and groundwater systems as agricultural wastes, such as pesticides, antibiotics, and natural organic matters (NOMs), etc. Especially, heavy metals and organic dye pollutions are of grave concern ascribing to the high toxicity and persistence. The adsorption capacities primarily depend on the interactions between contaminant molecules and the functional sites of adsorbents, which occur in two types of processes: physisorption and chemisorption. Physical adsorption, such as electrostatic attraction and Van der Waals force, forms a multilayer of adsorbate molecules on adsorbent surface, while chemical chelating with the formation of covalent bonds results in a monolayer on the surface. The adsorption of heavy metals, organic dyes, and other contaminants by electrospun adsorbents reported in the last five years has been summarized below.

3.5.1. Adsorption of heavy metals

Heavy metal is recognized as one of the most hazardous contaminants that result in low water quality. Even trace amounts of heavy metals can induce adverse impacts on water quality and threaten human health. Lead (II), copper (II), chromium (VI), uranium (VI), thorium (IV), and cadmium (II) ions are some of the typical contaminants attracting extensive attention from researchers. The most commonly applied polymers (listed in Table 3.3) used to remove heavy

metal ions from the aqueous environment include PVA, PAN, chitosan, polyacrylic acid (PAA), and PA [5,6,29,52,66,79,117]. Some of them, such as PAN, chitosan, PVA, and PAA, are capable of binding metal ions through abundant functional groups without additional fillers [5,51,68,118]. More generally, both organic and inorganic fillers, such as metal nanoparticles, graphene oxide, zeolite etc., are widely used to further improve the adsorption capacity of polymeric fibers.

In particular, metal nanoparticles for the adsorption of heavy metal ions have been explored in numerous studies [87,92,93,98]. The uniqueness of these nanoparticles as adsorbents includes their high surface binding energy, low diffusion resistance inside their structures, and capability of enhancing water permeability of the integrated matrices [92]. These advantages of nanoparticles usually endow the entire matrix with extraordinary adsorptive ability towards heavy metal ions. Moradi et al. [83] used the electrospun Fum-F/PAN nanocomposite for lead removal, which achieved a remarkable adsorption efficiency (97.89%). It was demonstrated that the removal of lead ions was due to the ion exchange and complex formation (Figure 3.4). The carboxyl groups on the Fum-F fiber surface offered binding sites for lead ions. Bassyouni et al. [6] developed the PA6-based electrospun nanofibrous membranes, incorporating multiwall carbon nanotubes (MWCNTs) and Fe_3O_4 nanoparticles. The adsorption mechanism towards Pb (II) ions was mainly attributed to the abundant adsorption sites on the nano-sized fillers. According to the XPS spectra of the prepared adsorbent before and after adsorption, it was confirmed that Pb (II) ions were chemically bonded with carboxyl groups on the surface of the adsorbent [6]. The combination of MWCNTs/Fe_3O_4 as fillers for metal ion removal was also reported to be immobilized onto CS nanofibers, which displayed outstanding adsorption efficiency towards Cr (VI) ions [29]. Razzaz et al. [93] prepared an efficient nanofibrous adsorbent with TiO_2 nanoparticles for the removal of Pb (II) and Cu (II) ions. The addition of TiO_2 not only enhanced the mechanical strength of

chitosan nanofibrous mat but also improved the adsorption efficiency. As a result, the chitosan/TiO_2 nanocomposite adsorbent showed a superior adsorption capacity of 579.10 mg/g for Pb (II) through physisorption.

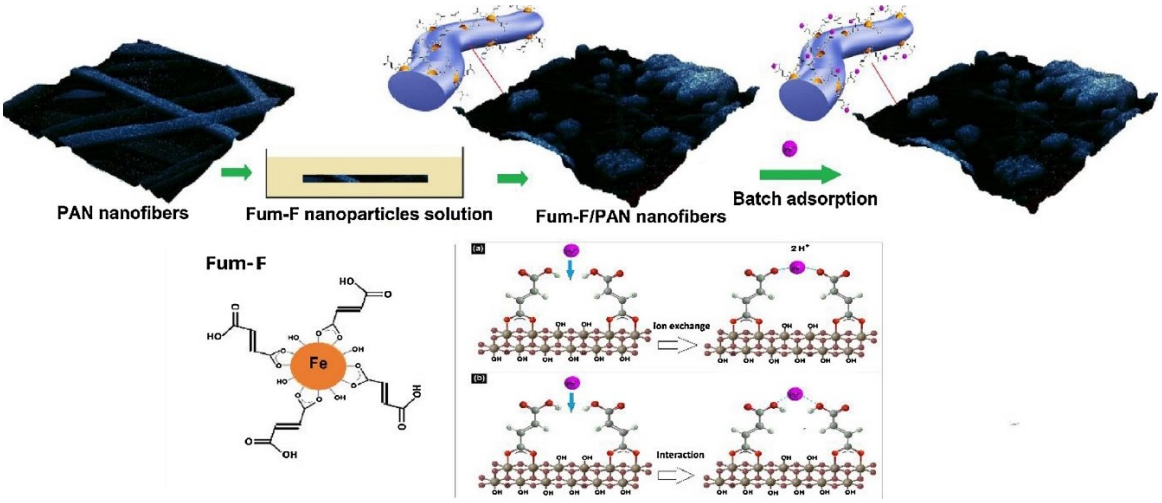

Figure 3.4. Schematic illustration of the lead removal mechanisms using Fum-F/PAN nanocomposite: (a) ion exchange and (b) complex formation (reprinted with permission from Ref [83]).

Nonetheless, the concentration of nanoparticles needs to be optimized to achieve the highest adsorption capacity. An excessive amount of nanoparticles hinders the adsorption capacity instead, owing to the agglomeration and coagulation of nanoparticles. Razzaz et al. [93] demonstrated that up to 2% of TiO_2 could give rise to an increased adsorption capacity towards Pb (II) and Cu (II) ions.

Table 3.3. Recent electrospun nanocomposites for the adsorption of heavy metal ions.

Polymers	Additives	Adsorption capacity (mg/g)
PA6	MWCNTs/Fe_3O_4	Pb (II) 49.3
Ethyl cellulose	γ-Al_2O_3	Pb (II) 134.5
Chitosan		Pb (II) 570
PVA	Sb-TBC, Sr-TBC, La-TBC	Pb (II) 91, 124, 194
Chitosan		Pb (II) 110.2
PAN	Fumarate ferroxane nanoparticles	Pb (II) 357.14
PVA/PAA		Pb (II) 159, Cd (II) 102
PAN		Cu (II) 143.47, Pb (II) 178.57
PEO/chitosan		Cu (II) 310.2, Pb (II) 237.2, Ni (III) 357.1, Cd (II) 248.1
Chitosan	Cobalt ferrite	Pb (II) 283.3, Cr (VI) 179.1
Chitosan	TiO_2	Cu (II) 710.3, Pb (II) 579.1
PVP	Mercapto group modified CeO_2/P123	Cu (II) 263.4, Pb (II) 272.3
Chitosan	Graphene oxide	Cu (II) 423.8, Pb (II) 461.3, Cr (VI) 310.4
PVA		Cu (II) 62.3, Pb (II) 168.2
Chitosan/poly (lactide-co-caprolactone) (P (LLA-CL))	TiO_2	Cu (II) 190.5
PVA/PAA	Thiol-modified silica nanoparticles	Cu (II) 125.47
PAN	EDTA intercalated Mg/Al layered double hydroxides	Cu (II) 120.77
PAN	GO/ZnO	Cr (VI) 690
PAN	TiO_2/ZnO	Cr (VI) 333.43
Chitosan	MWCNTs/Fe_3O_4	Cr (VI) 360.1
PVA/chitosan	Fe_3O_4	Cr (VI) 213
PAN	Branched polyethylenimine	Cr (VI) 637.46
PVA	TiO_2	U(VI) 196.1, Th(IV) 238.1
PAN	Al-O nanoparticles	Th(IV) 472
PVA	Mercapto group modified TiO_2/ZnO	Th(IV) 333.33

It has been proven that the modification of metal nanoparticles with functional groups, such as -SH and -NH_2 groups, contributes to a considerably better adsorption performance [53,55,103,108].

Functional groups can interact with heavy metal ions, offering more binding sites. Abbasizadeh et al. [53] reported the mercapto group functionalized PVA/TiO_2 nanofibrous adsorbent for the adsorption of uranium (VI) and thorium (IV) ions. Physical affinity was the primary adsorption mechanism, and the PVA/TiO_2 nanofibers showed the reduced diameters and narrower distribution of pore size after modification with mercapto groups, leading to the enhanced adsorption capacities. Alipour et al. [55] investigated the effect of mercapto groups on the adsorption capacity of electrospun PVA/TiO_2/ZnO nanofibers towards thorium (IV) ions. The optimized contents of TiO_2 and TMPTMS were 20 wt% and 15 wt%, respectively, which resulted in a smooth surface of nanofibers with no aggregations. The adsorption process was also physisorption, and the maximum adsorption capacities of Th (IV) reported by these two studies were 238.1 and 333.33 mg/g, respectively [53, 55].

Moreover, the integration of surfactants into the structure of nanoparticle/polymer matrix is an effective strategy to improve the adsorption capacity by enabling a significant amount of binding sites on nanofibrous matrix. For example, the maximum adsorption capacities of PVP/CeO_2 incorporating Pluronic P123 as surfactants were 272.3 and 263.4 mg/g for Pb (II) and Cu (II) ions, respectively, which were three times greater than those of PVP/CeO_2 nanofiber adsorbent (90.9 mg/g for Pb (II) ions and 88.3 mg/g for Cu (II) ions) [87]. A similar result was obtained by Vu et al. [22], where the incorporation of surfactant provided doubled adsorption capacity of PVP/TiO_2 for the removal of Cu (II) ions.

Most of current studies on electropsun adsorbents were only conducted and found to be feasible for simulated wastewater samples at laboratory scale. The removal of targeting contaminants from real wastewater is more dynamic and complicated due to variance in the compositions of wastewater, which could impede the overall adsorption capacities. Fan et al. [120] investigated the

performance of β-CD/CS/PVA nanofibers for heavy metal removal in river water. It was found that organic/inorganic substances, such as Ca^{2+}, Mg^{2+} and microorganisms, might interfere the adsorption performance of the adsorbent towards Pb^{2+} and Hg^{2+}. However, it was worth noting that a high removal efficiency (95%) of Cu^{2+} was achieved by applying EDTA intercalated-layered double hydroxides/PAN nanocomposites for the treatment of collected industrial wastewater [121].

3.5.2. Adsorption of organic dyes

Dye molecules in wastewater are of great concern due to their low degradation, toxicity, and stability in water bodies [128]. Considerable research efforts have been devoted to reducing the hazardous effects of synthetic dyes on water and subsequently human health. The most widely applied polymeric matrices for dye removal are PAN, PVP, and PVA [54,57,81]. Other polymers, such as chitosan, cellulose acetate, poly L-lactic acid (PLLA), poly β-cyclodextrin (PCD), polyvinylidene fluoride (PVDF), and poly(methylmethacrylate) (PMMA) have also been reported [4,49,63,64,110,129]. For example, the electrospun PAN/chitosan adsorbents without additional fillers offered substantial adsorption capacity towards acid blue-113, which was mainly driven by chemisorption between the functional groups NH_3^+ (adsorbent) and SO_4^{2-} (dye molecules) [4]. More generally, polymers were modified with functional groups to improve their adsorption efficiency. Olaru et al. [63] reported that the grafting of nicotinoyl groups on cellulose acetate nanofibers boosted the adsorption efficiency for Rhodamine B from 18% to 74%.

Other than functional polymers, additional properties and functions are often delivered by incorporating fillers into the polymeric complex. Additives such as metal oxides, carbon-based materials, zeolites, and silica nanoparticles are attractive and have been employed for the treatment of synthetic dyes in an aqueous system (listed in Table 3.4). Carbonaceous materials displayed

extraordinary performance in eradicating dye molecules due to the large surface area of their nanostructures. Elzain et al. [101] investigated the performance of carbon nanotubes and graphite immobilized on poly (styrene-co-acrylate) to remove methylene blue. It was indicated that the adsorption mainly depended on Van der Waals force. Mercante et al. [49] also developed carbon-based composite adsorbent for methylene blue adsorption through the functionalization of poly(methylmethacrylate) (PMMA) nanofibers with reduced graphene oxide (rGO). The adsorption mechanism depended not only on the physical structure of the nanofiber matrix but also on the strong π–π interactions generated from rGO fillers. Therefore, the adsorption capacity of PMMA/rGO adsorbent for methylene blue (698.51 mg/g) outweighed that of the former study (20.34 mg/g) [49,101]. Silica is another porous material that is of great research interest for adsorption. Mahmoodi et al. [106] demonstrated that silica nanoparticles in PVA/ CS nanofibers led to the higher porosity and smaller pore size. Therefore, the adsorption capacity for Direct red 80 (322 mg/g) was twice that of PVA/CS nanofibers [106].

The adsorption performance of electrospun fibers towards dye molecules can be further improved by combing more than one type of additive. For example, Mukhlish et al. [57] prepared the flexible PVP/Al_2O_3/silica nanofibers with an extraordinary adsorption capacity of 884.95 mg/g towards Reactive red-120. Silica contributed to the suppression of alumina crystallization and subsequent reduction in active surface area, while alumina played a role in enhancing adsorptive performance. Another study demonstrated the synergistic effect of ZnO and $ZnFe_2O_4$ [81]. It was shown that the ZnO-$ZnFe_2O_4$ heterojunction promoted the chemisorption process of Congo red by providing active sites for molecular interactions.

Table 3.4. Recent electrospun nanocomposites for the adsorption of organic dyes.

Polymers	Additives	Organic dyes	Adsorption capacity (mg/g)	Refs
Poly (styrene-co-acrylate)	Carbon nanotube	Methylene blue	24.69	[101]
Poly (styrene-co-acrylate)	Graphite	Methylene blue	20.34	[101]
PAN coated with chitosan		Acid Blue-113	1708	[4]
PAN	$ZnO/ZnFe_2O_4$	Congo red	263	[81]
Nicotinoyl group modified cellulose acetate		Rhodamine B	156.25	[63]
ε-polycaprolactone/ poly β-cyclodextrin		Methylene blue	24.1	[110]
Gelatin/poly β-cyclodextrin		Methylene blue	47.4	[109]
PVA	Zeolitic imidazolate framework	Congo red	160	[54]
PVA/chitosan	silica	Direct red 80	322	[106]
Poly L-lactic acid		Methylene blue	8.7306	[64]
Polyethersufone	Styrene sulfonate/acrylic acid	Methylene blue	478.46	[130]
PAN	Graphite oxide/Fe_3O_4/ carboxylate groups (on the composite)	Basic red 46	19.8	[85]
PVP	Al_2O_3/silica	Reactive red-120	884.95	[57]
Poly(methylmethacrylate)	Graphene oxide	Methylene blue	698.51	[49]
PVA	α-Fe_2O_3/vinyl group (on the nanofiber surface)/polyamido amine	Direct red 80 Acid red 18	703.12 817.81	[91]
Lignin/PVA		Safranine T	140.3	[68]
Polyvinylidene fluoride	Chitin nanowhisker	Indigo carmine	72.6	[70]
Polyethylenimine/ PVDF		Methyl orange	633.3	[129]
PA6 coated with polyaniline		Methyl orange	370	[131]
PAN	Polyamidoamine	Methyl orange	120	[78]
PVP	$CuFe_2O_4$ coated with CeO_2	Methylene orange	100 g/ml (column bed studies)	[88]
PVP	Fly ash/TiO_2	Methylene blue	12.5	[89]

3.5.3. Adsorption of other contaminants

Phenolic compounds have been increasingly detected in waterbody through waste emissions of industries. Because of their detrimental effect on the environment and the human body, they have gained significant attention from researchers. Polymers such as chitosan, PVA, PU, and Nylon 6 have been actively applied to remove phenolic compounds [62,90,126,132]. For example, electrospun PVA/silica nanofibers were proven to be an effective adsorbent for bisphenol A through hydrogen bonding interaction, which reached its maximum adsorption capacity at 2.989 mmol/g [128]. At the same time, the polyurethane (PU)/MnO composite showed promising performance in the removal of nitrophenols through hydrogen bonding and π–π interactions [90]. Molecularly imprinted polymeric nanofibers have also been applied to the removal of bisphenol A from aqueous environment with higher affinity. Ardekani et al. exploited bisphenol A imprinted nylon 6 nanofibers bearing APTES functional monomer [133]. The binding capacity towards bisphenol A was three times higher than the other similar compounds (phenol and naphthol), showing good sensitivity and selectivity. The binding capacity of bisphenol A imprinted nanofibers was also superior (115.1 mg/g) compared to that of non-imprinted nanofibers (46.82 mg/g) [133]. Electrospun nanofibers have also been used for pesticide extraction. Li et al. [84] reported a magnesium silicate/PAN composite adsorbent to remove herbicide for the first time. The free magnesium ions inside the magnesium silicate nanotubes endowed potential for efficient adsorption of cation substances, such as diquat molecules, through strong electrostatic attraction.

Wastewater effluents are also a major source of some emerging environmental contaminants, attributing to their wide use in food products, cosmetic products, and pharmaceuticals [134]. Paraben derivatives are found in many food and cosmetic products as antibacterial preservatives, which show relations with breast cancer and male infertility [135]. Demirkurt et al. [135] applied

imprinted acrylate microsphere incorporating electrospun polystyrene fibers to remove three parabens (benzyl, methyl, and propyl parabens). The adsorption mechanism was based on the specific hydrogen bonding interactions between the carboxylic groups in the microspheres and hydroxyl groups in parabens. Xue et al. [114] have explored the possibility of using imprinted electrospun PET matrix for the adsorption of trace DNT molecules. The binding was caused by the strong dipole-dipole interactions between the benzene rings of DNT and the carbonyl groups of PET, enabling effective and reliable adsorption of DNT molecules.

Table 3.5. Recent electrospun nanocomposites for the adsorption of other contaminants.

Polymers	**Additives**	**Contaminants**	**Adsorption capacity (mg/g)**	**Refs**
Polythiophene/chitosan	Fe_3O_4	Triazine herbicides		[96]
PAN	Fe_3O_4	Tetracycline	315.31	[80]
PAN	Amino-Zr-MOF	Chlorpyrifos		[82]
Chitosan	Fe_3O_4/Al_2O_3	Nitrate and phosphate	160.7 and 135.1	[97]
Polyurethane	MnO nanoparticles	Mono-nitrophenols		[90]
Poly (vinylidene fluoride)	Glycidyl methacrylate) monomer	Boron	18	[136]
Polystyrene	Poly(dibenzo-18-crown-6)	Plasma catecholamines	0.97	[50]
Alginate	Zeolite	Sr (II)	83.31	[60]
Cellulose triacetate	Hydroxyapatite	Bovine serum albumin	176.04	[137]

3.6. Conclusion and Future Prospects

Due to the high surface-to-volume ratio, high porosity, promising compatibility, versatility, and simple operation, numerous studies focused on developing electrospun nanofiber adsorbents and exploring of their potential applications and feasibilities in extensive fields. Various synthetic and natural polymers, such as PVA, PAN, chitosan, PVP, nylon 6, and so on, have been employed to

fabricate fibrous matrices. It allows the construction of polymeric fibers that are suitable in different environmental situations. Regardless of the initial structures and properties of polymers, their adsorption capacities could be improved by either modifying with functional groups (-SH, -NH_2, -S- etc.) or adding functional fillers (metal oxides, carbon-based materials, silica nanoparticles, etc.). On a laboratory scale, heavy metal ions and organic dyes are the most widely used contaminant models, while some other contaminants such as phenolic compounds and pesticides have also been applied to evaluate the adsorption performance of electrospun fibers. Numerous researches have demonstrated that electrospun nanomaterials have great potential to address many existing and emerging environmental issues and safety concerns. Commercial lab-scale and industry-scale electrospinning equipment are available on the market. Compared to industry-scale equipment, the lab-scale apparatuses are usually more advanced, which enable the formation of electrospun fibers with multiple structures. Therefore, an improvement on industry-scale devices can be foreseen in the near future. However, future research in the following areas is required to promote their real applications:

1. Systematical study on the design and optimization of electrospun adsorbents is expected. Till now, many combinations of polymers and fillers have been reported, and most of them were claimed as efficient. However, it is still unclear which combination is the most promising for next stage development and how we can maximize the adsorption capacity while maintaining the adequate mechanical properties of electrospun fibers. The desorption and reuse of adsorbents should also be carefully considered and evaluated.

2. Real environmental samples and conditions need to be applied to study the performance of electrospun adsorbents. Recently, most researches are carried out at a laboratory-scale and based on the standard solutions of heavy metal ions and organic dyes. However, the real conditions are

much more complicated and harsher. It is still necessary to improve the yield and efficiency of the electrospinning technique to realize the mass production of multifunctional fibers at a large scale. Technological advancements in the electrospinning equipment are essential to response to complex spinning process and nanofibrous organizations. More flexible adjustment of the electrospinning process could contribute to the higher efficiency and larger production scale. Also, the actual wastewater contains strong acid, base, and corrosive substances originating from industrial and agricultural wastes. Therefore, the improvement of mechanical properties and stability of electrospun adsorbents is in high demand. We will know better about the performance, stability, and cost of electrospun adsorbents so as to judge their potential in real applications.

3. Safety issues of electrospun adsorbents need to be investigated. The purpose of developing these fibrous adsorption materials is to provide an easily handleable nanomaterial with numerous binding sites by immobilizing the functional groups or fillers on the fiber network. It will be essential to know the electrospun adsorbents won't bring new contaminants to the water system and environment. Therefore, it is necessary to study the stability and degradability of electrospun fibers as well as the migration of nanofillers.

3.7. References

1. Sapountzi, E., Braiek, M., Chateaux, J. F., Jaffrezic-Renault, N., and Lagarde, F. *Recent Advances in Electrospun Nanofiber Interfaces for Biosensing Devices.* Sensors. **17** (2017) p. 29. doi: 10.3390/s17081887.

2. Pereao, O.K., Bode-Aluko, C., Ndayambaje, G., Fatoba, O., and Petrik, L. F. *Electrospinning: Polymer Nanofibre Adsorbent Applications for Metal Ion Removal.* Journal of Polymers and the Environment. **25** (2017): p. 1175-1189. doi: 10.1007/s10924-016-0896-y

3. He, N., Li, L., Wang, P., Zhang, J., Chen, J., and Zhao, J. *Dioxide/Chitosan/poly(lactide-co-caprolactone) composite membrane with efficient Cu(II) adsorption.* Colloids and Surfaces A: Physicochemical and Engineering Aspects. **580 (**2019**)**: p. 123687. doi: 10.1016/j.colsurfa.2019.123687

4. Lou, T., X. Yan, and X.J. Wang. *Chitosan coated polyacrylonitrile nanofibrous mat for dye adsorption.* International Journal of Biological Macromolecules. **135 (**2019**)**: p. 919-925. doi: 10.1016/j.ijbiomac.2019.06.008

5. Zhang, S., Shi, Q., Christodoulatos, C., and Meng, X. *Lead and cadmium adsorption by electrospun PVA/PAA nanofibers: Batch, spectroscopic, and modeling study.* Chemosphere. **233 (**2019**)**: p. 405-413. doi: 10.1016/j.chemosphere.2019.05.190

6. Bassyouni, D., Mohamed, M., El-Ashtoukhy, E., El-Latif, M. A., Zaatout, A., and Hamad, H. *Fabrication and characterization of electrospun Fe3O4/o-MWCNTs/polyamide 6 hybrid nanofibrous membrane composite as an efficient and recoverable adsorbent for removal of Pb (II).* Microchemical Journal. **149 (**2019**)**: p. 103998. doi: 10.1016/j.microc.2019.103998

7. Sekar, A. D., Kumar, V., Muthukumar, H., Gopinath, P., and Matheswaran, M. *Electrospinning of Fe-doped ZnO nanoparticles incorporated polyvinyl alcohol nanofibers for its antibacterial treatment and cytotoxic studies.* European Polymer Journal. **118** (2019): p. 27-35. doi.org/10.1016/j.eurpolymj.2019.05.038

8. Pandey, S., Fosso-Kankeu, E., Spiro, M. J., Waanders, F., Kumar, N., Ray, S. S., Kim, J., Kang, M. *Equilibrium, kinetic, and thermodynamic studies of lead ion adsorption from mine wastewater onto MoS2-clinoptilolite composite*. Mater. Today Chem. **18** (2020): 100376. doi: 10.1016/j.mtchem.2020.100376

9. Pandey, S., Do, J. Y., Kim, J., and Kang, M. *Fast and highly efficient removal of dye from aqueous solution using natural locust bean gum based hydrogels as adsorbent*. Int. J. Biol. Macromol. **143** (2020): p. 60-75. doi:10.1016/j.ijbiomac.2019.12.002

10. Okoro, H. K., Ige, J. O., Iyiola, O. A., Pandey, S., Lawal, I. A., Zvinowanda, C., and Ngila, C.J., *Comprehensive reviews on adverse health effects of human exposure to endocrine - disrupting chemicals*. Fresenius Environ. Bull., **26** (2017): 4623-4636.

11. Pandey, S., and Ramontja, J. *Natural Bentonite Clay and Its Composites for Dye Removal: Current State and Future Potential.* American Journal of Chemistry and Applications, **3** (2016): p. 8-19.

12. Klavarioti, M., Mantzavinos, D., and Kassinos, D. *Removal of residual pharmaceuticals from aqueous systems by advanced oxidation processes.* Environ. Int. **35 (**2019**)**, p. 402-417. doi:10.1016/j.envint.2008.07.009

13. Pal, A., Karina, Y. G., Angela, Y. L., and Reinhard, M. *ReinhardImpacts of emerging organic contaminants on freshwater resources: review of recent occurrences, sources, fate and effects.* Sci. Total Environ. **408 (**2010**)**, p. 6062-6069. doi: 10.1016/j.scitotenv.2010.09.026.

14. Sanches, S., Penetra, A., Rodrigues, A., Ferreira, E., Cardoso, V. V., Benoliel, M. J., Crespo, M. T. B., Pereira, V. J., and Crespo, J. G. *Nanofiltration of hormones and pesticides in different real drinking water sources*. Separ. Purif. Technol. **94 (**2012**)**, p. 44-53. doi:10.1016/j.seppur.2012.04.003

15. Hakizimana, J. N., Gourich, B., Chafi, M., Stiriba, Y., Vial, C., Drogui, P., Naja, J. *Electrocoagulation process in water treatment: A review of electrocoagulation modeling approaches*, Desalination. **404 (**2017**)**, p. 1-21. doi:10.1016/j.desal.2016.10.011

16. Teodosiu,C., Gilca, A., Barjoveanu, G., and Fiore, S. *Emerging pollutants removal through advanced drinking water treatment: A review on processes and environmental performances assessment*. Journal of Cleaner Production. **197** (2018), p. 1210-1221. doi:10.1016/j.jclepro.2018.06.247

17. Pandey, S., Do, J. Y., Kim, J., and Kang, M. *Fast and highly efficient catalytic degradation of dyes using κ-carrageenan stabilized silver nanoparticles nanocatalyst.* Carbohydrate Polymers, **230** (2020): 115597. doi: 10.1016/j.carbpol.2019.115597

18. Fosso-Kankeu, E., Pandey, S., and Ray, S. S. Photocatalysts in advanced oxidation processes for wastewater treatment. Hoboken, NJ, USA: Wiley-Scrivener, 2020, Chapter 6.

19. Wen, M., Li, G., Liu, H., Chen, J., An, T., and Yamashita, H. *Metal-organic framework-based nanomaterials for adsorption and photocatalytic degradation of gaseous pollutants: recent progress and challenges.* Environ.-Sci. Nano. **6 (**2019**)**, p. 1006-1025. doi:10.1039/C8EN01167B

20. Pandey, S., and Tiwari, S. *Facile approach to synthesize chitosan-based composite—Characterization and cadmium (II) ion adsorption studies*. Carbohydrate Polymers, **134** (2015): p. 646-656. doi: 10.1016/j.carbpol.2015.08.027

21. Makhado, E., Pandey, S., and Ramontja, J. *Microwave assisted synthesis of xanthan gum-cl-poly (acrylic acid) based-reduced graphene oxide hydrogel composite for adsorption of*

methylene blue and methyl violet from aqueous solution. International Journal of Biological Macromolecules, 119 (2018): p. 255-269. doi: 10.1016/j.ijbiomac.2018.07.104

22. Vu, D., Li, Z., Zhang, H., Wang, W., Wang, Z., Xu, X., Dong, B., Wang, C. *Adsorption of Cu(II) from aqueous solution by anatase mesoporous TiO2 nanofibers prepared via electrospinning*. Journal of Colloid and Interface Science. **367** (2012), p. 429-435. doi:10.1016/j.jcis.2011.09.088

23. Tucker, N., Stanger, J.J., Staiger, M. P., Razzaq, H., and Hofman, K. *The History of the Science and Technology of Electrospinning from 1600 to 1995.* Journal of Engineered Fibers and Fabrics. **7 (**2012**)**: p. 63-73. doi: 10.1177/155892501200702S10

24. Mirjalili, M. and Zohoori, S. *Review for application of electrospinning and electrospun nanofibers technology in textile industry.* Journal of Nanostructure in Chemistry. **6** (2016): p. 207-213. doi: 10.1007/s40097-016-0189-y

25. Ghorani, B., Kadkhodaee, R., Rajabzadeh, G., and Tucker, N. *Assembly of odour adsorbent nanofilters by incorporating cyclodextrin molecules into electrospun cellulose acetate webs.* Reactive and Functional Polymers. **134 (**2019**)**: p. 121-132. doi: 10.1016/j.reactfunctpolym.2018.11.014

26. Xue, J., Xie, J., Liu, W., and Xia, Y. *Electrospun Nanofibers: New Concepts, Materials, and Applications*. Acc. Chem. Res, **50** (2017): p. 1976−1987. doi: 10.1021/acs.accounts.7b00218

27. Han, T., Yarin, A. L., and Reneker, D. H. *Viscoelastic electrospun jets: Initial stresses and elongational rheometry*. Polymers. **49** (2008): p. 1651-1658. doi:10.1016/j.polymer.2008.01.035

28. Fong, H., Chun, I., and Reneker, D.H. *Beaded nanofibers formed during electrospinning.* Polymer. **40**(1999): p. 4585-4592. doi:10.1016/S0032-3861(99)00068-3

29. Beheshti, H., Irani, M., Hosseini, L., Rahimi, A., and Aliabadi, M. *Removal of Cr (VI) from aqueous solutions using chitosan/MWCNT/Fe3O4 composite nanofibers-batch and column studies.* Chemical Engineering Journal. **284 (**2016**)**: p. 557-564. doi:10.1016/J.CEJ.2015.08.158

30. Haghi, A.K. and Akbari, M. *Trends in electrospinning of natural nanofibers.* Physica Status Solidi a-Applications and Materials Science. **204** (2007): p. 1830-1834. doi:10.1002/pssa.200675301

31. Mokhena, T.C., Jacobs, V., and Luyt, A.S. *A review on electrospun bio-based polymers for water treatment.* Express Polymer Letters. **9** (2015): p. 839-880. doi: 10.3144/expresspolymlett.2015.79

32. Gupta, P., Elkins, C., Long, T. E., Wilkes, G. L. *Electrospinning of linear homopolymers of poly(methyl methacrylate): exploring relationships between fiber formation, viscosity, molecular weight and concentration in a good solvent*.Polymer. **46** (2005): p. 4799-4810. doi.org/10.1016/j.polymer.2005.04.021.

33. Lan, T., Shao, Z., Wang, J., and Gu, M. *Fabrication of hydroxyapatite nanoparticles decorated cellulose triacetate nanofibers for protein adsorption by co-axial electrospinning.* Chemical Engineering Journal. **260 (**2015**)**: p. 818-825. doi:10.1016/j.cej.2014.09.004

34. He, X., Cheng, L., Zhang, X., Xiao, Q., Zhang, W., and Lu, C. *Tissue engineering scaffolds electrospun from cotton cellulose.* Carbohydrate Polymers. **115 (**2015**)**: p. 485-493. doi: 10.1016/j.carbpol.2014.08.114

35. Camire, A., Espinasse, J., Chabot, B., and Lajenunesse, A. *Development of eletropsun lignin nanofibers for the adsorption of pharmaceutical contaminants in wastewater.* Environmental Science and Pollution Research. **27** (2020): p. 3560-3573. doi: 10.1007/s11356-018-3333-z

36. Somsap, J., Kanjanapongkul, K., and Tepsorn, R. *Effect of parameters on the morphology and fibre diameters of edible electrospun chitosan-cellulose acetate-gelatin hybrid nanofibres*. MATEC Web of Conferences. **192 (**2018**)**, p. 03038. doi:10.1051/matecconf/201819203038

37. Li, D., and Xia, Y. *Electrospinning of Nanofibers: Reinventing the Wheel?*. Advanced Materials. **16** (2004), p. 1151-1170. doi:10.1002/adma.200400719

38. Sung, Y. K., Ahn, B. W., and Kang, T. J. *Magnetic nanofibers with core (Fe3O4 nanoparticle suspension)/sheath (poly ethylene terephthalate) structure fabricated by co-axial electrospinning*, Journal of Magnetism and Magnetic Materials. **324** (2012): p. 916-922. doi:10.1016/j.jmmm.2011.03.004

39. Li, D., and Xia, Y. *Direct Fabrication of Composite and Ceramic Hollow Nanofibers by Electrospinning*. Nano Letters. **4** (2004), p. 933-938. doi: 10.1021/nl049590f

40. Wen, H., Yang, C., Yu, D., Li, X., and Zhang, D. *Electrospun zein nanoribbons for treatment of lead-contained wastewater*. Chemical Engineering Journal. **290 (**2016**)**, p. 263-272. doi:10.1016/j.cej.2016.01.055

41. Ma, L., Shi, X., Zhang, X., Dong, S., and Li, L. *Electrospun Cellulose Acetate–Polycaprolactone/Chitosan Core–Shell Nanofibers for the Removal of Cr(VI)*. Phys. Status Solidi A. **216** (2019), p.1900379. doi:10.1002/pssa.201900379

42. Wang, X., Lin, T., and Wang, X. *Scaling up the production rate of nanofibers by needleless electrospinning from multiple ring*. *Fibers and Polymers.* **15** (2014): p. 961-965. doi:10.1007/s12221-014-0961-x

43. Wei, L., Sun, R., Liu, C., Xiong, J., and Qin, X. *Mass production of nanofibers from needleless electrospinning by a novel annular spinneret*. Materials & Design. **179** (2019): p. 107885. doi:10.1016/j.matdes.2019.107885

44. Niu, H., Lin, T., & Wang, X. *Needleless electrospinning. i. a comparison of cylinder and disk nozzles.* Journal of Applied Polymer Science. **114** (2009): p. 3524-3530. doi:10.1002/app.30891

45. Varesano, A., Carletto, R. A., and Mazzuchetti, G. *Experimental investigations on the multi-jet electrospinning process.* Journal of Materials Processing Technology. **209** (2009): p.5178-5185. doi: 10.1016/j.jmatprotec.2009.03.003

46. Moon, S., Gil, M., and Lee, K. J. *Syringeless electrospinning toward versatile fabrication of nanofiber web.* Scientific Reports. **7**(2017): p. 41424. doi:10.1038/srep41424wec

47. Bhardwaj, N. and Kundu, S.C. *Electrospinning: A fascinating fiber fabrication technique.* Biotechnology Advances. **28** (2010): p. 325-347. doi:10.1016/j.biotechadv.2010.01.004

48. Tas, S., Kaynan, O., Ozden-Yenigun, E., and Nijmeijer, K. *Polyacrylonitrile (PAN)/crown ether composite nanofibers for the selective adsorption of cations.* Rsc Advances. **6** (2016): p. 3608-3616. doi:10.1039/C5RA23214G

49. Mercante, L.A., Facure, M. H. M., Locilento, D. A., Sanfelice, R. C., Migliorini, F. L., Mattoso, H, C., and Correa, D. S. *Solution blow spun PMMA nanofibers wrapped with reduced graphene oxide as an efficient dye adsorbent.* New Journal of Chemistry. **41** (2017): p. 9087-9094. doi:10.1039/C7NJ01703K

50. Chen, L., Zhu, X., Huang, D., Xu, Z., Shen, J., and Zhang, W. *Polystyrene/poly(dibenzo-18-crown-6) composite nanofibers for the selective adsorption of plasma catecholamines.* Rsc Advances. **7** (2017): p. 13263-13271. doi: 10.1039/C7RA00430C

51. Dai, Z., Ren, P., Cao, Q., Gao, X., He, W., Xiao, Y., Jin, Y., and Ren, F. *Synthesis of TiO2@lignin- based carbon nanofibers composite materials with highly efficient photocatalytic to methylene blue dye*. J Polym Res. **27(**2020**)**: p. 108. doi: 10.1007/s10965-020-02068-7

52. Tian, H., Yuan, L., Wang, J, Wu, H., Wang, H., Xiang, A., Ashok, B., and Rajulu, A. J. *Electrospinning of polyvinyl alcohol into crosslinked nanofibers: An approach to fabricate functional adsorbent for heavy metals.* Journal of Hazardous Materials. **378 (**2019**)**: p. 120751. doi: 10.1016/j.jhazmat.2019.120751

53. Abbasizadeh, S., Keshtkar, A.R., and Mousavian, M.A. *Preparation of a novel electrospun polyvinyl alcohol/titanium oxide nanofiber adsorbent modified with mercapto groups for uranium(VI) and thorium(IV) removal from aqueous solution.* Chemical Engineering Journal. **220** (2013): p. 161-171. doi:10.1016/j.cej.2013.01.029

54. Fan, X., Yu, L., Li, L., Yang, C., Wen, J., Ye, X., Cheng, J., and Hu, Y. *Characterization and application of zeolitic imidazolate framework-8@polyvinyl alcohol nanofibers mats prepared by electrospinning.* Materials Research Express. **4** (2017): p. 026404. doi: 10.1088/2053-1591/aa5a84

55. Alipour, D., Keshtkar, A.R., and Moosavian, M.A. *Adsorption of thorium(IV) from simulated radioactive solutions using a novel electrospun PVA/TiO2/ZnO nanofiber adsorbent functionalized with mercapto groups: Study in single and multi-component systems.* Applied Surface Science. **366** (2016): p. 19-29. doi:10.1016/j.apsusc.2016.01.049

56. Islam, M.S., Rahaman, M.S., and Yeum, J.H. *Phosphine-functionalized electrospun poly(vinyl alcohol)/silica nanofibers as highly effective adsorbent for removal of aqueous manganese and nickel ions.* Colloids and Surfaces a-Physicochemical and Engineering Aspects. **484** (2015): p. 9-18. doi:10.1016/j.colsurfa.2015.07.023

57. Mukhlish, M.Z. B., Horie, Y., and Nomiyama, T. *Flexible Alumina-Silica Nanofibrous Membrane and Its High Adaptability in Reactive Red-120 Dye Removal from Water.* Water Air and Soil Pollution. **228** (2017): p. 16. doi:10.1007/s11270-017-3546-7

58. Li, Y., Zhang, J., Xu, C., and Zhou, Y. *Crosslinked chitosan nanofiber mats fabricated by one-step electrospinning and ion-imprinting methods for metal ions adsorption.* Science China-Chemistry. **59** (2016): p. 95-105. doi:10.1007/s11426-015-5526-3

59. Haider, S. and Park, S. Y. *Preparation of the electrospun chitosan nanofibers and their applications to the adsorption of Cu(II) and Pb(II) ions from an aqueous solution.* Journal of Membrane Science. **328** (2009): p. 90-96. doi:10.1016/j.memsci.2008.11.046

60. Zhang, Y., Lin, X., Hu, S., Zhang, X., and Luo, X. *Core-shell zeolite@Alg-Ca particles for removal of strontium from aqueous solutions.* Rsc Advances. **6** (2016): p. 73959-73973. doi:10.1039/C6RA11112B

61. Liu, F., Song, D., Huang, X., and Xu, H. *Electrospun polystyrene nanofibers as a novel adsorbent to transfer an organic phase from an aqueous phase.* Journal of Separation Science. **39** (2016), p. 1326–1330. doi:10.1002/jssc.201501182

62. Jasni, M.J.F., Arulkumar, M., Sarhishkumar, P., Rahim, A., Yusoff, M., Buang, N. A., and Gu, F. L. *Electrospun nylon 6,6 membrane as a reusable nano-adsorbent for bisphenol A*

removal: Adsorption performance and mechanism. Journal of Colloid and Interface Science. **508 (**2017**)**: p. 591-602. doi:10.1016/j.jcis.2017.08.075

63. Olaru, N., Anghel, N., Pascariu, P., and Ailiesei, G. *Synthesis and testing of cellulose acetate nicotinate as adsorbent for rhodamine B dye.* Journal of Applied Polymer Science. **136** (2019): p. 9. doi:10.1002/app.47772

64. Bai, L., Jia, L., Yan, Z., Liu, Z., and Liu, Y. *Plasma-etched electrospun nanofiber membrane as adsorbent for dye removal.* Chemical Engineering Research and Design. **132 (**2018**)**: p. 445-451. doi: 10.1016/j.cherd.2018.01.046

65. Cai, Z., Song, X., and Zhai, T. *Electrospun Polyindole Nanofibers as a Nano-adsorbent for Heavy Metal Ions Adsorption for Wastewater Treatment.* Fibers and Polymers. **18** (2017): p. 502-513. doi 10.1007/s12221-017-6988-z

66. Sereshti, H., Amini, F., and Najarzadekan, H. *Electrospun polyethylene terephthalate (PET) nanofibers as a new adsorbent for micro-solid phase extraction of chromium(VI) in environmental water samples.* Rsc Advances. **5** (2015): p. 89195-89203. doi: 10.1039/C5RA14788C

67. Naseem, A., Tabasum, S., Zia, K. M., Zuber, M., Ali, M., and Noreen, A. *Lignin-derivatives based polymers, blends and composites: A review.* International Journal of Biological Macromolecules. **93 (**2016**)**: p. 296-313. doi:10.1016/j.ijbiomac.2016.08.030

68. Zhang, W., Yang, P., Li, X., Zhu, Z., Chen, M., Zhou, X. *Electrospun lignin-based composite nanofiber membrane as high-performance absorbent for water purification.* International Journal of Biological Macromolecules. **141 (**2019**)**: p. 747-755. doi:10.1016/j.ijbiomac.2019.08.221

69. Aluigi, A., Varesano, A., Claudia, V., and Rio, A. D. *Adsorption of copper(II) ions by keratin/PA6 blend nanofibres.* European Polymer Journal. **47 (**2011**)**: p. 1756-1764. doi.org/10.1016/j.eurpolymj.2011.06.009.

70. Gopi, S., Balakrishnan, P., Pius, A., and Thomas, S. *Chitin nanowhisker (ChNW)-functionalized electrospun PVDF membrane for enhanced removal of Indigo carmine.* Carbohydrate Polymers. **165 (**2017**)**: p. 115-122. doi:10.1016/j.carbpol.2017.02.046

71. Park, J., Kang, J., Lee, S., and Kim, S. *Electrospun poly(acrylic acid)/poly(vinyl alcohol) nanofibrous adsorbents for Cu(II) removal from industrial plating wastewater.* Rsc Advances. **7** (2017): p. 18075-18084. doi: 10.1039/C7RA01362K

72. Nthunya, L., Masheane, M. L., Malinga, S. P., Nxumalo, E. N., and Mhlanga, S. D. *Electrospun chitosan-based nanofibres for removal of phenols from drinking water*. WATER SA. **44** (2018), p. 377–386. doi:10.4314/wsa.v44i3.05

73. Lou, T., Yan, X., and Wang, X. *Chitosan coated polyacrylonitrile nanofibrous mat for dye adsorption.* International Journal of Biological Macromolecules. **135 (**2019**)**: p. 919-925. doi:10.1016/j.ijbiomac.2019.06.008

74. Abdolmaleki, A.Y., Zilouei, H., and Khorasani, S. N. *Optimization and characterization of electrospun chitosan/poly(vinyl alcohol) nanofibers as a phenol adsorbent via response surface methodology.* Polymers for Advanced Technologies. **28** (2017): p. 1872-1878. doi:10.1002/pat.4075

75. Aliabadi, M., Irani, M., Ismaeili, J., Piri, H., and Parnian, M. J. *Electrospun nanofiber membrane of PEO/Chitosan for the adsorption of nickel, cadmium, lead and copper ions from aqueous solution.* Chemical Engineering Journal. **220 (**2013**)**: p. 237-243. doi:10.1016/j.cej.2013.01.021

76. Huang, M., Tu, H., Chen, J., Liu, R., Liang, Z., Jiang, L., Shi, X., Du, Y., and Deng, H. *Chitosan-rectorite nanospheres embedded aminated polyacrylonitrile nanofibers via shoulder-to-shoulder electrospinning and electrospraying for enhanced heavy metal removal.* Applied Surface Science. **437 (**2018**)**: p. 294-303. doi:10.1016/j.apsusc.2017.12.150

77. Li, Z., Li, T., An, L., Fu, P., Gao, C., Zhang, Z. *Highly efficient chromium(VI) adsorption with nanofibrous filter paper prepared through electrospinning chitosan/polymethylmethacrylate composite.* Carbohydrate Polymers. **137 (**2016**)**: p. 119-126. doi:10.1016/j.carbpol.2015.10.059

78. Hou, C., Yang, H., Xu, Z., and Wei, Y. *Preparation of PAN/PAMAM Blend Nanofiber Mats as Efficient Adsorbent for Dye Removal.* Fibers and Polymers. **16** (2015): p. 1917-1924. doi: 10.1007/s12221-015-5335-5

79. Parlayici, S., Yar, A., Pehlivan, E., and Avci, A. *ZnO-TiO2 doped polyacrylonitrile nano fiber-Mat for elimination of Cr (VI) from polluted water.* Journal of Analytical Science and Technology. **10 (**2019**)**: p. 12. doi:10.1186/s40543-019-0183-3

80. Liu, Q., Zhang, Y., ZHonf, L., Cheng, X. *Removal of tetracycline from aqueous solution by a Fe3O4 incorporated PAN electrospun nanofiber mat.* Journal of Environmental Sciences. **28 (**2015**)**: p. 29-36. doi:10.1016/j.jes.2014.04.016

81. Appiah-Ntiamoah, R., Baye, A. F., Gadisa, B. T., Abebe, M. W., and Kim, H. *In-situ prepared ZnO-ZnFe2O4 with 1-D nanofiber network structure: An effective adsorbent for toxic dye effluent treatment.* Journal of Hazardous Materials. **373 (**2019**)**: p. 459-467. doi:10.1016/j.jhazmat.2019.03.108

82. Bahrami, H., Rezaei, B., and Jafari, M.T. *Coupling of a novel electrospun polyacrylonitrile/amino-Zr-MOF nanofiber as a thin film for microextraction-corona discharge-ion mobility spectrometry for the analysis of chlorpyrifos in water samples.* Analytical Methods. **11** (2019): p. 1073-1079. doi: 10.1039/C8AY02518E

83. Moradi, G., Dabirian, F., Mohammadi, P., Rajabim L., Babaei, M., and Shiri, N. *Electrospun fumarate ferroxane/polyacrylonitrile nanocomposite nanofibers adsorbent for lead removal from aqueous solution: Characterization and process optimization by response surface methodology.* Chemical Engineering Research and Design. **129 (**2018**)**: p. 182-196. doi:10.1016/j.cherd.2017.09.022

84. Li, Y., Zhao, R., Chao, S., Sun, B., Zhang, N., Qiu, J., Wang, C., and Li, X. *A flexible magnesium silicate coated electrospun fiber adsorbent for high-efficiency removal of a toxic cationic herbicide.* New Journal of Chemistry. **41** (2017): p. 15601-15611. doi:.1039/C7NJ03168H

85. Rahimi, K., Mirzaei, R., Akbari, A., and Mirghaffari, N. *Preparation of nanoparticle-modified polymeric adsorbent using wastage fuzzes of mechanized carpet and its application in dye removal from aqueous solution.* Journal of Cleaner Production. **178 (**2018**)**: p. 373-383. doi:10.1016/j.jclepro.2017.12.213

86. Hallaji, H., Keshtkar, A. R., and Moosavian, M. A. *A novel electrospun PVA/ZnO nanofiber adsorbent for U(VI), Cu(II) and Ni(II) removal from aqueous solution.* Journal of the Taiwan Institute of Chemical Engineers. **46** (2015): p. 109-118. doi.org/10.1016/j.jtice.2014.09.007

87. Yari, S., Abbassizadeh, S., Mousavi, S. E., Moghaddam, M. S., and Moghaddam, A. Z. *Adsorption of Pb(II) and Cu(II) ions from aqueous solution by an electrospun CeO2 nanofiber adsorbent functionalized with mercapto groups.* Process Safety and Environmental Protection. **94 (**2015**)**: p. 159-171. doi: 10.1016/j.psep.2015.01.011

88. Zou, L., Wang, Q., Shen, X., Wang, Z., Jing, M., and LuO, Z. *Fabrication and dye removal performance of magnetic CuFe2O4@CeO2 nanofibers.* Applied Surface Science. **332 (**2015**)**: p. 674-681. doi:10.1016/j.apsusc.2015.01.176

89. Saud, P.S., Pant, B., Park, M., Chae, S., Park, S., El-Newehy, M., Al-Deyab, S. S., and Kim, H. *Preparation and photocatalytic activity of fly ash incorporated TiO2 nanofibers for effective removal of organic pollutants.* Ceramics International. **41** (2015): p. 1771-1777. doi:10.1016/j.ceramint.2014.09.123

90. Eskandarpour, N. and Sereshti, H. *Electrospun polyurethane fibers doped with manganese oxide nanoparticles as an effective adsorbent for determination of priority pollutant mono-*

nitrophenols in water samples. Journal of Environmental Chemical Engineering. **7** (2019): p. 102926. doi:10.1016/j.jece.2019.102926

91. Fard, G. C., Mirjalili, M., Almasian, A., and Najafi, F. *PAMAM grafted α-Fe2O3 nanofiber: Preparation and dye removal ability from binary system.* Journal of the Taiwan Institute of Chemical Engineers. **80 (**2017**)**: p. 156-167. doi:10.1016/j.jtice.2017.04.018

92. Pouya, E. S., Fatoorehchi, H., and Foroughi-Dahr, M. *Batch removal of Pb (II) ions from aqueous medium using gamma-Al2O3 nanoparticles/ethyl cellulose adsorbent fabricated via electrospinning method: An equilibrium isotherm and characterization study.* Polish Journal of Chemical Technology. **20** (2018): p. 32-39. doi: 10.2478/pjct-2018-0020

93. Razzaz, A., Ghorban, S., Hosayni, L., Irani, M., and Aliabadi, M. *Chitosan nanofibers functionalized by TiO2 nanoparticles for the removal of heavy metal ions.* Journal of the Taiwan Institute of Chemical Engineers. **58 (**2016**)**: p. 333-343. doi:10.1016/j.jtice.2015.06.003

94. Hu, Y., Liu, Z., Xu, J., Huang, Y., and Song, Y. *Evidence of Pressure Enhanced CO2 Storage in ZIF-8 Probed by FTIR Spectroscopy.* Journal of the American Chemical Society. **135** (2013): p. 9287-9290. doi: 10.1021/ja403635b

95. Yan, E., Cao, M., Jiang, J., Gao, J., Jiang, C., Ba, X., Yang, X., and Zhang, D. *A novel adsorbent based on magnetic Fe3O4 contained polyvinyl alcohol/chitosan composite nanofibers for chromium (VI) removal.* Solid State Sciences. **72 (**2017**)**: p. 94-102. doi:10.1016/j.solidstatesciences.2017.08.014

96. Feizbakhsh, A., and Ehteshami, S. *Modified Magnetic Nanoparticles as a Novel Sorbent for Dispersive Magnetic Solid-Phase Extraction of Triazine Herbicides in Aqueous Media.* Journal of Aoac International. **100** (2017): p. 198-205. doi: 10.5740/jaoacint.16-0054.

97. Bozorgpour, F., Ramandi, H. F., Jafari, P., Samadi, S., Yazd, S.S., and Aliabadi, M. *Removal of nitrate and phosphate using chitosan/Al2O3/Fe3O4 composite nanofibrous adsorbent: Comparison with chitosan/Al2O3/Fe3O4 beads.* International Journal of Biological Macromolecules. **93 (**2016**)**: p. 557-565. doi:10.1016/j.ijbiomac.2016.09.015

98. Aliabadi, M. *Removal of Pb(II) and Cr(VI) Ions from Aqueous Solutions Using Chitosan/Cobalt Ferrite Nanofibrous Adsorbent.* Fibers and Polymers. **17** (2016): p. 1162-1170. doi: 10.1007/s12221-016-6555-z

99. Wang, X., Pan, S., Zhang, M., Qi, J., Sun, X., Gu, C., Wang, L., and Li, J. *Modified hydrous zirconium oxide/PAN nanofibers for efficient defluoridation from groundwater.* Science of The Total Environment. **685 (**2019**)**: p. 401-409. doi:10.1016/j.scitotenv.2019.05.380

100. Choi, E.Y., Choi, L.W. and Kim, C.K. *Noncovalent functionalization of multi-walled carbon nanotubes with hydroxyl group-containing pyrene derivatives for their composites with polycarbonate.* Carbon. **95 (**2015**)**: p. 91-99. doi:10.1016/j.carbon.2015.08.038

101. Elzain, A.A., El-Aassar, M. R., Hashem, F. S., Mohamed, F. M., and Ali, A. S. M. *Removal of methylene dye using composites of poly (styrene-co-acrylonitrile) nanofibers impregnated with adsorbent materials.* Journal of Molecular Liquids. **291 (**2019**)**: p. 111335. doi:10.1016/j.molliq.2019.111335

102. Ray, S. C., in: Ray, S. C. (Eds.), In Micro and Nano Technologies, Applications of Graphene and Graphene-Oxide Based Nanomaterials, William Andrew Publishing, Inc. Elsevier, 2015, p. 39-55.

103. Ghaedi, M., Hajjatti, S., Mahmudi, Z., Tyahi, I., Agarwal, S., Maity, A., and Gupta, V. K. *Modeling of competitive ultrasonic assisted removal of the dyes – Methylene blue and Safranin-O using Fe3O4 nanoparticles.* Chemical Engineering Journal. **268 (**2015**)**: p. 28-37. doi:10.1016/j.cej.2014.12.090

104. Yousef, S., A. Mohamed, and M. Tatariants, *Mass production of graphene nanosheets by multi-roll milling technique.* Tribology International. **121 (**2018**)**: p. 54-63. doi:10.1016/j.triboint.2018.01.040

105. Abdel-Mottaleb, M.M., Khalil, A., Osman, T. A., and Khattab, A. *Removal of hexavalent chromium by electrospun PAN/GO decorated ZnO.* Journal of the Mechanical Behavior of Biomedical Materials. **98 (**2019**)**: p. 205-212. doi:10.1016/j.jmbbm.2019.06.025

106. Mahmoodi, N.M., Mokhtari-Shourijeh, Z., and Abdi, J. *Preparation of mesoporous polyvinyl alcohol/chitosan/silica composite nanofiber and dye removal from wastewater.* Environmental Progress & Sustainable Energy. **38 (**2019**)**: p. S100-S109. doi: 10.1002/ep.12933

107. Elsherief, M.A., Morsi, R. E., Shabaan, M., Salem, H., Dayeem, S. A., and Elsabee, M. Z. *Tuning of nanoporous silica by electrospinning and sol-gel methods for efficient beryllium uptake.* Separation Science and Technology. **55** (2020): p. 35-46. doi:10.1080/01496395.2018.1563159

108. Kim, J., Kang, T., Kim, H., Shin, H. J., and Oh, S. *Preparation of PVA/PAA nanofibers containing thiol-modified silica particles by electrospinning as an eco-friendly Cu (II) adsorbent.* Journal of Industrial and Engineering Chemistry. **77 (**2019**)**: p. 273-279. doi:10.1016/j.jiec.2019.04.048

109. Chen, Y., Ma, Y., Lu, W., Guo, Y., Zhu, Y., Lu, H., and Song, Y. *Environmentally Friendly Gelatin/β-Cyclodextrin Composite Fiber Adsorbents for the Efficient Removal of Dyes from Wastewater.* Molecules. **23** (2018): p. 2473. doi: 10.3390/molecules23102473

110. Guo, R., Wang, R., Yin, J., Jiao, T., Huang, H., Zhao, X., Zhang, L., Li, Q., Zhou, J., and Peng, Q. *Fabrication and Highly Efficient Dye Removal Characterization of Beta-Cyclodextrin-Based Composite Polymer Fibers by Electrospinning.* Nanomaterials. **9** (2019): p. 17. doi: 10.3390/nano9010127

111. Hosseini, M., Keshtkar, A.R., and Moosavian, M.A. *Electrospun chitosan/baker's yeast nanofibre adsorbent: preparation, characterization and application in heavy metal adsorption.* Bulletin of Materials Science. **39** (2016): p. 1091-1100. doi: 10.1007/s12034-016-1260-5

112. El-Aassar, M.R., Alsohaimi, I. H., Ali, A. S. M., and Elzain, A. A. *Removal of phenol and Bisphenol A by immobilized Laccase on poly (Acrylonitrile-co-Styrene/Pyrrole) nanofibers.* Separation Science and Technology. **55** (2020): p. 2670-2678. doi:10.1080/01496395.2019.1648511

113. Patel, K. D., Kim, H., Knowles, J. C., and Poma, A. *Molecularly imprinted polymers and Electrospinning: manufacturing convergence for next-level applications.* Advanced Functional Materials. **30**(2020): p. 2001955. doi:10.1002/adfm.202001955

114. Xue, X., Lu, R., Li, Y., Wang, Q., Li, J., and Wang, L. *Molecularly imprinted electrospun nanofibers for adsorption of 2,4-DINITROTOLUENE in water*. The Analyst. **143**(2018): p. 3465-3471. doi:10.1039/c8an00734a

115. Wu, K., Yang, W., Jiao, Y., and Zhou, C. *A surface molecularly imprinted electrospun polyethersulfone (pes) fiber mat for selective removal of bilirubin.* Journal of Materials Chemistry B. **5**(2017): p. 5763-5773. doi:10.1039/c7tb00643h

116. Zhu, T., Xu, D., Wu, Y., Li, J., Zhou, M., Tian, T., . . . Li, G. *Surface molecularly imprinted electrospun affinity membranes with multimodal pore structures for efficient separation of proteins*. Journal of Materials Chemistry B. **1**(2013), p. 6449. doi:10.1039/c3tb20973c

117. Ardekani, R., Borhani, S., and Rezaei, B. *Simple preparation and characterization OF molecularly imprinted Nylon 6 nanofibers for the extraction of bisphenol A from wastewater*. Journal of Applied Polymer Science. **136**(2018): p. 47112. doi:10.1002/app.47112

118. Umma Habiba, Amalina M. Afifi, Areisman Salleh, Bee Chin Ang., *Chitosan/(polyvinyl alcohol)/zeolite electrospun composite nanofibrous membrane for adsorption of Cr6+, Fe3+ and Ni2+*. Journal of Hazardous Materials. **322** (2017), p. 182-194. doi:10.1016/j.jhazmat.2016.06.028

119. Jing, R., Yan, C., Liu, Q., Yang, Q., Lu, G., Song, Y., and Li, Y. *Preparation of amidoxime-modified polyacrylonitrile nanofibrous adsorbents for the extraction of copper(II) and lead(II) ions and dye from aqueous media*. Journal of Applied Polymer Science. **135** (2018): p. 45697. doi:10.1002/app.45697

120. Fan, J., Luo, J., Zhang, X., Zhen, B., Dong, C., Li, Y., . . . Chen, H. *A novel ELECTROSPUN β-CD/CS/PVA nanofiber membrane for simultaneous and rapid removal of Organic micropollutants and heavy metal ions from water*. Chemical Engineering Journal. **378** (2019): p. 122232. doi: 10.1016/j.cej.2019.122232

121. Chen, H., Lin, J., Zhang, N., Chen, L., Zhong, S., Wang, Y., . . . Ling, Q. *Preparation of MGAL-EDTA-LDH Based ELECTROSPUN nanofiber membrane and its adsorption properties of copper (II) from wastewater*. Journal of Hazardous Materials. **345** (2018): p. 1-9. doi: 10.1016/j.jhazmat.2017.11.002

122. Li, Y., Qiu, T., and Xu, X. *Preparation of lead-ion imprinted crosslinked electro-spun chitosan nanofiber mats and application in lead ions removal from aqueous solutions*. European Polymer Journal. 49 (2013): p. 1487-1494

123. Shooto, N.D., Dikio, C.W., Wankasi, D., Sikhwivhilu, L. M., Mtunzi, F. M., and Dikio, E. D. *Novel PVA/MOF Nanofibres: Fabrication, Evaluation and Adsorption of Lead Ions from Aqueous Solution*. Nanoscale Res Lett. **11 (**2016**)**, p. 414. doi: 10.1186/s11671-016-1631-2

124. Najafabadi, H. H., Irani, M., Rad, L.R., Haratameh, A.H., Haririan, I. *Removal of Cu^{2+}, Pb^{2+} and Cr^{6+} from aqueous solutions using a chitosan/graphene oxide composite nanofibrous adsorbent*. RSC Advances. **5 (**2015**)**, p. 16532-16539. doi: 10.1039/C5RA01500F

125. Chen H., Lin J., Zhang N., Chen, L., Zhong, S., Wang, Y., Zhang, W., and Ling, Q. *Preparation of MgAl-EDTA-LDH based electrospun nanofiber membrane and its adsorption properties of copper(II) from wastewater*. J Hazard Mater. **345 (**2018**)**: p. 1-9. doi: 10.1016/j.jhazmat.2017.11.002

126. Zhao, R., Li, X., Sun, B., Li, Y., Li, Y., Yang, R., and Wang, C. *Branched polyethylenimine grafted1 electrospun polyacrylonitrile fiber membrane: A novel and effective adsorbent for Cr(VI) remediation in wastewater*. J. Mater. Chem. A. 5 (2017), p. 1133-1144. doi: 10.1039/C6TA09784G

127. Broujeni, B. R., and Nilchi, A. *Preparation and characterization of polyacrylonitrile nanofiber adsorbent modified with 6-amino-1-hexanethiol hydrochloride for the adsorption of thorium (IV) ion from aqueous solution.* Desalination and water treatment. 133 (2018), p. 122-133. doi: 10.5004/dwt.2018.23001

128. Wang, D., and Wang, J. *Electrospinning Polyvinyl alcohol/silica-based nanofiber as highly efficient adsorbent for simultaneous and sequential removal of Bisphenol A and Cu(II) from water*, Chemical Engineering Journal. **314 (**2017**)**: p. 714-726. doi:10.1016/j.cej.2016.12.037

129. Ma, Y., Zhang, B., Ma, H., Yu, M., Li, L., and Li, J. *Polyethylenimine nanofibrous adsorbent for highly effective removal of anionic dyes from aqueous solution*. Sci. China Mater. **59 (**2016**)**, p. 38-50. doi:10.1007/s40843-016-0117-y

130. Chen, S., Du, Y., Zhang, X., Xie, Y., Shi, Z., Ji, H., Zhao, W., Zhao, C. *One-step electrospinning of negatively-charged polyethersulfone nanofibrous membranes for selective removal of cationic dyes*, Journal of the Taiwan Institute of Chemical Engineers. **82 (**2018**)**, p. 179-188. doi:10.1016/j.jtice.2017.11.018

131. Zarrini, K., Rahimi, A. A., Alihosseini, F., and Fashandi, H. *Highly efficient dye adsorbent based on polyaniline-coated nylon-6 nanofibers*. Journal of Cleaner Production. **142 (**2017**)**, p. 3645-3654. doi: 10.1016/j.jclepro.2016.10.103

132. Nthunya, L., Masheane, M. L., Malinga, S. P., Nxumalo, E. N., and Mhlanga, S. D. *Electrospun chitosan-based nanofibres for removal of phenols from drinking water*. WATER SA. **44** (2018), p. 377–386. doi:10.4314/wsa.v44i3.05

133. Ardekani, R., Borhani, S., and Rezaei, B. *Selective molecularly imprinted polymer nanofiber sorbent for the extraction of bisphenol a in a water sample*. Polymer International. **69** (2020): p. 780-793. doi:10.1002/pi.6013

134. Richardson, S. D., and Kimura, S. Y. *Emerging environmental contaminants: Challenges facing our next generation and potential engineering solutions*. Environmental Technology & Innovation. **8** (2017): p. 40-56. doi:10.1016/j.eti.2017.04.002

135. Demirkurt, M., Olcer, Y., Demir, M., and Eroglu, A. *Electrospun polystyrene fibers knitted around imprinted acrylate microspheres as sorbent for paraben derivatives*. Analytica Chimica Acta. **1014** (2018): p. 1-9. doi:10.1016/j.aca.2018.02.016

136. Nallappan, M.L., Nasef, M. M., Ting, T. M., and Arshad, A. *An Optimized Covalent Immobilization of Glucamine on Electrospun Nanofibrous Poly(vinylidene fluoride) Sheets Grafted with Oxirane Groups for Higher Boron Adsorption.* Fibers and Polymers. **19** (2018): p. 1694-1705. doi: 10.1007/s12221-018-8110-6

137. Lan, T., Shao, Z., Wang, J., and Gu, M. *Fabrication of hydroxyapatite nanoparticles decorated cellulose triacetate nanofibers for protein adsorption by co-axial electrospinning.* Chemical Engineering Journal. **260 (**2015**)**: p. 818-825. doi:10.1016/j.cej.2014.09.004

Connecting Statement to Chapter 4

In Chapter 3, a comprehensive summary and thorough review of electrospun nanomaterials and their roles in water treatment were provided, demonstrating their great potential to address many existing and emerging environmental issues. Additionally, the feasibility of employing CA to obtain electrospun fibers has been proved, while the drawback of CA was revealed that its adsorption capacity was limited. Chitosan (CS), an amino polysaccharide derived by the acetylation of chitin, is one of the promising electrospun polymers possessing desirable characteristics, such as non-toxicity, biocompatibility, biodegradability, eco-friendly, and bioactivity (Haider & Park, 2009). CS-based nanofibers for heavy metal and dye adsorption have been extensively investigated. Nevertheless, CS tends to be swollen in aqueous media (Phan et al., 2019). Therefore, CA and CS compensate each other, performing better adsorption processes. Furthermore, according to our previous intermolecular interaction study, we expected that CA with abundant methyl groups and CS featured with amino groups could exhibit superior adhesion energy toward humic acid (HA). Herein, CA and CS derived from wastes and residues were recycled into value-added adsorbent materials in Chapter 4, followed by the investigation of the properties of CA/CS electropsun fibers, as well as the interactions between the CA/CS fibrous adsorbents and HA.

Chapter 4. Electrospun cellulose acetate/chitosan fibers for humic acid removal: construction guided by intermolecular interaction study

4.1. Abstract

Humic substance is a ubiquitous class of natural organic matter (NOM) in soil and aquatic ecosystems, which severely affects the terrestrial and aquatic environments as well as water-based engineering systems. In our previous work, the adsorption of humic acid (HA) on self-assembled monolayers with different functional groups (OH-SAMs, CH_3-SAMs, NH_2-SAMs, and COOH-SAM) has been reported, where amino groups exhibited superior adhesion energy towards HA, followed by methyl groups and hydroxyl groups. Therefore, guided by the intermolecular interaction study, chitosan (CS) and cellulose acetate (CA) containing -NH_2 and -CH_3 groups derived from waste materials were selected to fabricate electrospun fibrous adsorbents for the removal of HA from aqueous solutions in this work. The effect of CA/CS ratios on the structure and adsorption performance of electrospun fibers was investigated in detail. The results revealed that all the samples (CA/CS=3:1, 1:1, 1:3) showed the high adsorption capacities (> 152 mg/g) towards HA at pH 4. It was because of the abundant functional groups on the surface of fibers. Especially, the CA/CS 1:1 sample had a uniform fibrous morphology with the average diameter of 335±242 nm, which led to the highest tensile strength of 2.97±0.59 MPa and adsorption capacity of 184.72 mg/g. The adsorption of HA onto CA/CS fibers was non-spontaneous and exothermic in nature. It followed the pseudo-first-order kinetic model and was primarily driven by electrostatic interaction. The adsorption isotherm was better fitted by Langmuir model. Therefore, this work demonstrates the feasibility to use intermolecular interaction mechanisms to guide the design of functional materials. Moreover, it provides a biodegradable efficient adsorbent that is promising for the applications in water treatment.

Keywords: electrospinning, adsorption, cellulose acetate, chitosan, humic acid, intermolecular interactions

4.2. Introduction

Humic acid (HA) is a natural organic compound that is originated from the decompositions of dead animal and plant substances. As a prominent source of organic matter, ubiquitous amounts of HA present in surface water, ocean water, upload streams and so on. Nevertheless, the presence of HA in the water system, especially in portable water, remains as a critical concern associated with organoleptic issues, environmental problems, and even health risks. Accumulation of HA in the water body not only gives rise to unfavorable taste, color, and odor, but also induces complexation effects with heavy metal ions and other chemical substances such as biocides [1]. Schmitt et al. [2] demonstrated that HA, as a natural organic matter (NOM), facilitated the movement of metal ions in aqua systems. Similarly, an adverse effect of HA on the removal of organohalides and nitroaromatic contaminants was concluded by Klausen et al. [3]. Additionally, Cl_2 used in the water treatment process reacts actively with the functional groups (hydroxyl groups, carbonyl groups, carboxyl groups etc.) of HA, giving rise to carcinogenic and reproductive issue-related organochlorines as a disinfection by-product [4-5]. Considering the above potential adverse effects, an effective strategy for HA eradication is of great importance and necessity.

Up to date, enormous efforts have been devoted in the removal of HA from aqueous environment, including electrocoagulation, advanced oxidation process (photocatalysis), ultrafiltration, fenton oxidation treatment, and biological treatments [6-11]. Besides them, adsorption is also considered as a promising method for HA removal attributing to its simple operation, low initial cost, and the sustainability of adsorbents. Numerous adsorptive materials have been studied on the eradication of HA, comprising of magnetic nanocomposite, activated carbon, graphene oxide, clays, nano-silica, and so on [12-16]. However, the powdered-form sorbents have several drawbacks, such as low bulk density, affinity to water vapor, and dustiness [17]. Electrospinning is a cost-effective and relatively simple technique in terms of the setup and the operation [18]. It is capable of

generating long and uniform fibers, which have unique properties, such as porous structure, large specific surface area, good interconnectivity, and structural stability, and thus are novel adsorbents for water treatment [19-20].

Regardless of the diversified adsorptive materials involved, understanding the interaction mechanisms and the attractive forces between the contaminants and adsorbents is fundamental to develop an auspicious removal strategy. In our previous work [21], the intermolecular forces between HA and multiple self-assembled monolayers with different functional groups (OH-SAMs, CH_3-SAMs, NH_2-SAMs, and COOH-SAM) were revealed. Remarkably, amino groups exhibited superior adhesion energy towards HA molecules over other functional groups, followed by methyl groups and hydroxyl groups. Therefore, inspired by the intermolecular interaction study, chitosan (CS) and cellulose acetate (CA), featured with abundant amino and methyl groups respectively, were employed to fabricate highly efficient electrospun adsorbents for HA removal from aqueous solutions in this work. Both CS and CA can be obtained from waste materials (e.g., crab shell and cigarette filters), and are biodegradable, relatively cost effective, and non-toxic [22-23]. The morphology and structure of electrospun CA/CS fibers were characterized by scanning electron microscopy (SEM) and Fourier-transform infrared (FT-IR) spectroscopy. Additionally, the effects of CA/CS ratio, pH value, adsorbent dosage, contact time, initial concentration, and temperatures on the adsorption capacity towards HA were studied in detail.

4.3. Experimental methods

4.3.1. Materials

Cellulose acetate (CA, M_w = 75-95 kDa, acetyl content 39.95 wt.%, degree of substitution ~ 2.47, characterized by Celanese) from cigarette filters was kindly provided by Celanese Corporation

(Irving, US). Chitosan (CS, M_w = 190-310 kDa, degree of deacetylation 75-85%, characterized by Dr. Simpson) derived from crab shells was kindly provided by Dr. Benjamin Simpson, Department of Food Science and Agricultural Chemistry, McGill University (Quebec, Canada). Acetic acid (CH_3COOH, 100%) and humic acid (sodium salt, $C_9H_8Na_2O_4$ 45-70%) were purchased from Fisher Scientific (Mississauga, Canada). Deionized water was used to prepare the electrospinning solutions and HA solutions. Sulfuric acid (H_2SO_4, ACS reagent grade) and sodium hydroxide (NaOH, ACS reagent grade) were used to adjust the pH values of HA solutions.

4.3.2. Fabrication of electrospun CA/CS adsorbents

Three CA/CS ratios (3:1, 1:1, and 1:3, w/w) were applied to fabricate electrospun adsorbents. For 3:1 and 1:1 mixture, desired amounts of polymers (total solid concentration of 7 wt.%) were dissolved in 85 wt.% acetic acid solution [24] and stirred for 48 h at room temperature, while the 1:3 sample (5 wt.% solid content) was added into 85 wt.% acetic acid solution and stirred for 48 h at 40 °C. Electrospinning conditions were optimized in our preliminary experiment to allow the steady generation of fibers. Specifically, homogeneous CA/CS mixture solutions were forced through a stainless-steel needle with a diameter of 0.6 mm at the rate of 0.8 mL h^{-1}, and the applied voltage was fixed at 25-30 kV. A stainless-steel drum rotating at 10 rpm was chosen as the collector, and the nozzle-to-collector distance was set at 10 cm. The obtained electrospun fibrous films were vacuum dried at room temperature for 24 h to remove the residual trace solvent.

4.3.3. Characterization of electrospun CA/CS adsorbents

Fourier-transform infrared spectroscopy (FT-IR) spectra of electrospun CA/CS adsorbents were obtained by Varian Excalibur 3100 FT-IR spectrometer (Varian, Melbourne, Australia) equipped with an attenuated total reflectance (ATR) accessory (Specac, Orpington, UK). The FT-IR spectra

were recorded as the average of 64 scans with a resolution of 4 cm^{-1}. To observe the morphologies of CA/CS fibers, they were first coated with platinum/gold (thickness: 4 nm) by the Leica EM ACE200 coater (Leica, Wetzlar, Germany). The scanning electron microscopy (SEM) images were then obtained by Hitachi SU-3500 (Hitachi, Tokyo, Japan) operating at 30 kV. In SEM images, fiber diameters were determined with the ImageJ image-visualization software developed by the National Institute of Health. Six hundred random positions were selected and measured for each sample [18]. Uniaxial tensile tests were performed to study the mechanical properties of electrospun CA/CS fibers. Three specimens with dimensions of 30 mm × 10 mm × 14.5 μm (length × width × thickness) were tested for each type of films using an Instron 5965 tester (Instron, Massachusetts, USA) at a fixed velocity of 1 mm min^{-1}. The tensile strength (σ) of CA/CS fibrous films was calculated using the following equation:

$$\sigma = \frac{F}{A} \qquad (4-1)$$

where F (N) is the maximum load at break, and A (mm^2) is the cross-sectional area.

4.3.4. Adsorption of humic acid

Adsorption experiments of HA molecules were carried out as functions of CA/CS ratios (1:3, 1:1, 3:1), pH levels (4, 6, 8, 10), adsorbent dosages (0.4, 0.8, 1.2, 1.6, 2 mg), contact times (5, 10, 15, 30, 45, 60, 90, 120 min), initial concentrations (10, 20, 30, 40 ppm), and temperatures (25 ℃, 45 ℃, 55℃) under batch conditions. The stock solution with a concentration of 100 ppm HA was prepared. Adsorption experiments were conducted in 25 ml glass bottles with white polypropylene caps which contained 20 ml of HA solutions with required concentrations. Specific dosages of adsorbents were then added to the solutions, which were shaken for required time intervals at 155 rpm. The concentrations of HA before and after adsorption were determined using a Hitachi UV-

2000 UV-vis spectroscopy (Hitachi, Tokyo, Japan) at a wavelength of 278 nm. The adsorption capacity and efficiency were calculated using the following equations:

$$q_e(mg\ g^{-1}) = \frac{(C_0 - Ce) \times V}{m} \qquad (4-2)$$

$$adsotpion\ efficiency\ (\%) = \frac{(C_0 - Ce)}{C_0} \times 100 \qquad (4-3)$$

where C_0 (mg/L) is the initial HA concentration in the solution; Ce (mg/L) is the equilibrium HA concentration; V (L) is the volume of HA solution; and m (g) is the mass of electrospun CA/CS adsorbent.

4.3.4.1 Adsorption kinetics

The experimental data was fitted into two kinetic models to investigate the adsorption kinetics: pseudo-first-order kinetic model and pseudo-second-order model, which are shown in the following equations:

$$\ln(q_e - q_t) = \ln q_e - k_1 t \qquad (4-4)$$

$$\frac{t}{q_t} = \frac{1}{k_2 {q_e}^2} + \frac{t}{q_e} \qquad (4-5)$$

where q_e (mg/g) and q_t (mg/g) are the adsorption capacities of the adsorbent at equilibrium and at time t (min), respectively; and k_1 (min^{-1}) and k_2 (g mg^{-1} min^{-1}) are the rate constants of pseudo-first-order adsorption and pseudo-second-order adsorption, respectively.

4.3.4.2 Adsorption isotherm

The Langmuir and Freundlich isotherm equations were applied to interpret the experimental results. The linear form of Langmuir isotherm equation and Freundlich isotherm equation can be written as follows [25]:

$$\frac{C_e}{q_e} = \frac{C_e}{q_{max}} + \frac{1}{q_{max}K_L} \qquad (4-6)$$

$$\ln(q_e) = \ln(K_F) + \frac{1}{n}\ln(C_e) \qquad (4-7)$$

where C_e (mg/L) is the concentration of HA in the solution at equilibrium; q_e (mg/g) is the adsorption capacity of the adsorbent at equilibrium; q_{max} (mg/g) is the maximum adsorption capacity of the adsorbent; K_L (L/mg) and K_F (L/mg) are the Langmuir constant and Freundlich constant, respectively; and 1/n is the adsorption intensity, which gives an indication of the favourability of adsorption.

4.3.4.3 Adsorption thermodynamics

Adsorptive performance of electrospun CA/CS adsorbents was examined at various temperatures. The experimental data was used to calculate thermodynamic parameters including Gibbs free energy change (ΔG^0), enthalpy change (ΔH^0), and entropy change (ΔS^0), which can be calculated by the equations as follows:

$$\Delta G^0 = -RTlnK_c \qquad (4-8)$$

$$lnK_c = \frac{\Delta S^0}{R} - \frac{\Delta H^0}{RT} \qquad (4-9)$$

where K_c is the equilibrium constant; R is the gas constant (8.314 J/(K mol)), and T (K) is the temperature. The values of ΔH^0 and ΔS^0 were obtained from the slope and intercept of the Van't Hoff plot of ln Kc versus 1/T [26].

4.3.5. Statistical analysis

Experimental results were represented as the mean of three batches ± SD. Statistical evaluation was carried out by analysis of variance (ANOVA) followed by multiple-comparison tests using Duncan's multiple-range test at the 95% confidence level. All of the analyses were conducted using SAS statistical software (SAS Institute, Inc., Cary, NC) with a probability of $p < 0.05$ considered to be significant.

4.4. Results and discussion

4.4.1. Structure and morphology of electrospun CA/CS adsorbents

Electrospun fibrous adsorbents with three CA/CS ratios (3:1, 1:1, and 1:3, w/w) were fabricated, and the interactions between CS and CA were investigated by FT-IR. As shown in Fig. 4.1, pure CS exhibited the adsorption peaks at 3290 cm^{-1} (N-H and O-H stretching), 2875 cm^{-1} (C-H stretching), 1667 cm^{-1} (C=O stretching of amide I), and 1583 cm^{-1} (N-H bending of amide II), and the bands at 983 cm^{-1} and 1017 cm^{-1} could be assigned to typical saccharide structures [24]. For pure CA sample, its carbonyl and hydroxyl groups had the peaks at 1750 cm^{-1} (C=O vibration) and 3450 cm^{-1} (O-H stretching), and the adsorption bands at 1372, 1224, and 1030 cm^{-1} were corresponding to methyl groups and C-O and ether C-O-C of pyranose rings, respectively [27]. The electrospun films with three different CA/CS ratios showed similar characteristic adsorption patterns except the broad peak of O-H and N-H groups at 3450 cm^{-1} shifted to lower wavenumbers

with the increase of CS contents, which revealed the hydrogen bonding interactions between the amine groups of CS and acetyl/hydroxyl groups of CA [24].

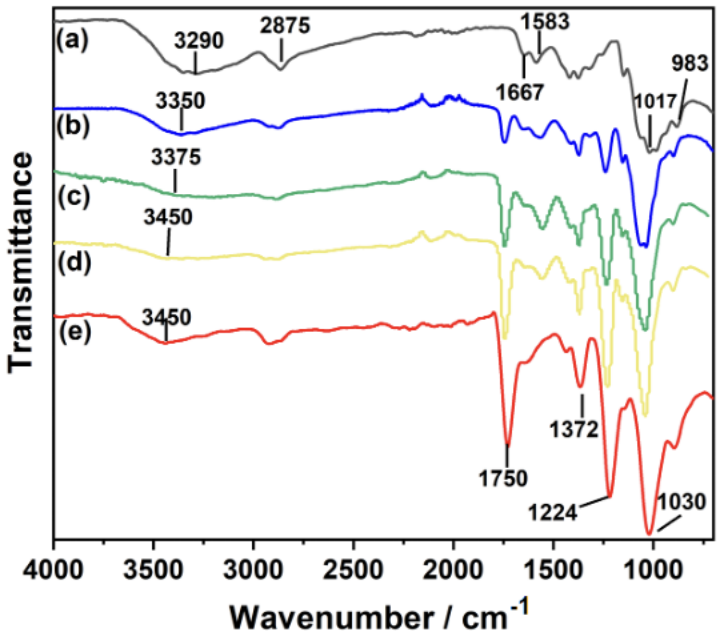

Figure 4.1. Fourier-transform infrared spectroscopy spectra of (a) CS powder; (b) CA/CS=1:3; (c) CA/CS=1:1; (d) CA/CS=3:1; and (e) CA powder.

The morphologies of electrospun CA/CS adsorbents with different polymer ratios were studied by SEM as shown in Fig 4.2. All the samples were composed of tiny fibers with semi-micron scaled diameters, which enabled the large surface area and interconnected porous structure and were desirable for adsorbents [28,29]. The average fiber diameters of CA/CS 3:1, 1:1, and 1:3 films were 277±319 nm, 335±242 nm, and 405±306 nm, respectively. Although there was no significant difference in diameters, the CA/CS 1:1 fibers were more uniform and less beady compared to the other two samples. The relatively thick and nonuniform fibers in CA/CS 1:3 films might be attributed to the poor electrospinnability of CS [30], and the presence of micron-sized beads in CA/CS 3:1 films might be due to the addition of 15 wt.% water in the electrospinning solution

which resulted in a less desirable solvent of CA and affected the dissolution of CA at a high concentration [31]. Similar beady structure has been reported by Du and Hsieh when CA was dissolved in and electrospun from 85 wt.% acetic acid solution [32].

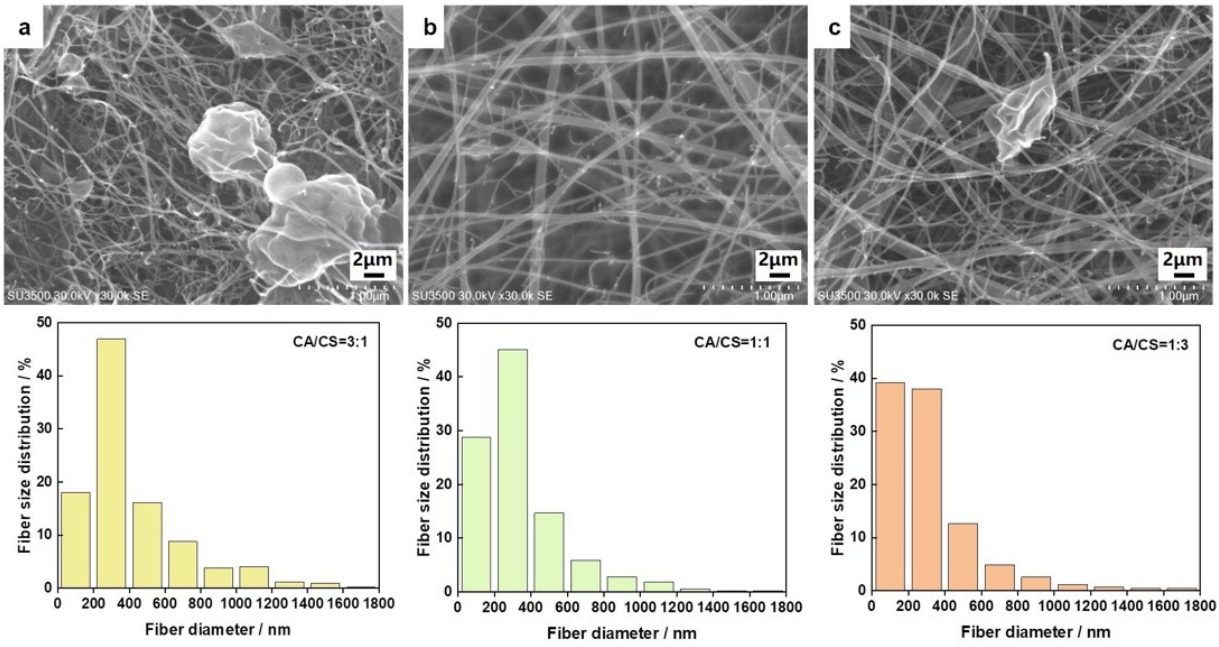

Figure 4.2. SEM images and fiber diameter distributions of electrospun adsorbents with CA/CS ratios of (a) 3:1, (b) 1:1, and (c) 1:3.

4.4.2. Mechanical properties of electrospun CA/CS adsorbents

Good mechanical properties and structural integrity of adsorbents are the prominent requirements for the removal of contaminants, which enable the adsorbents to conquer the water flow and become more stable during adsorption [33]. Mechanical properties of electropsun CA/CS films with different compositions were investigated by tensile tests. As shown in Fig. 4.3, the tensile strength of CA/CS 3:1, 1:1, and 1:3 films were 0.44±0.01 MPa, 2.97±0.59 MPa, and 0.22±0.04 MPa, respectively. The significantly higher tensile strength of CA/CS 1:1 films was attributed to their homogeneous fibrous structure, which could lead to more uniform stress distribution, and

subsequently increased amount of energy could be absorbed by the film [34]. It was worth noting that the elongation at break of CA/CS 1:1 films was also obviously higher than the other two samples. Similar phenomenon was observed in the electrospun assembled prolamin proteinnanofabrics, where the optimized fibers exhibited the highest tensile strength and elongation at break because of their uniform structure and hydrogen bonding interactions between the amine groups of CS and acetyl/hydroxyl groups of CA [24,35].

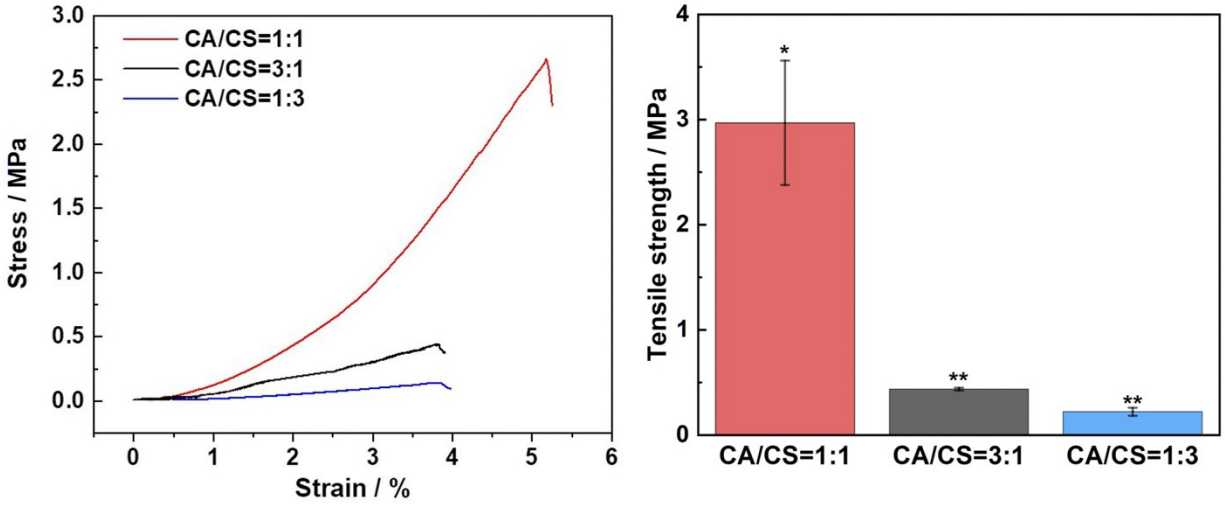

Figure 4.3. Mechanical properties of electrospun CA/CS adsorbents with different compositions. Different symbols on the top of columns indicate the significant difference ($p < 0.05$).

4.4.3. Adsorption of HA

4.4.3.1. Effect of pH on HA adsorption

The effect of the initial pH on HA removal by electrospun CA/CS adsorbents was investigated at the pH levels ranging from 3 to 10. As shown in Fig. 4.4, with increasing pH levels, the adsorption capacities of all the samples decreased. It was in accordance with our previous results that the adhesion energy of HA interacting with the charged NH_2-SAMs and non-polar CH_3-SAMs

decreased with increasing the pH from 4 to 8 [21]. The maximum adsorption capacity reached up to 422.75 mg/g at pH 3. However, it was a consequence of coagulation and further precipitation of HA. The sedimentation of HA at low pH level could be explained by the loss of colloidal stability [36]. This phenomenon has also been reported by Abate and Masini [36] and Brigante et al. [37]. Humic acid typically has pKa values of 3.39, 4.78 and 6.06 [38], and the pKa of the primary amine of chitosan is ~6.5 [39]. Therefore, the electrostatic attraction existed at pH 4 between the deprotonated carboxylic groups of HA and protonated amino groups of CS in the adsorbents, and the hydrophobic moieties of HA could interact with CH_3^- groups of CA via the hydrophobic attraction, leading to the adsorption of HA on electrospun CA/CS fibers. When the pH values further increased, the attractive force was weakened, and even repulsive interaction was generated between the adsorbents and HA. At the same time, the spherical-shaped HA molecules with small sizes at low pH could be stretched into linear shapes at high pH due to the increasing electrostatic repulsion between adjacent negatively charged groups, so the adsorption capacities decreased at high pH values [40]. It was worth noting that CA/CS 1:1 fibers showed superior adsorptive performance over the CA/CS 3:1 and 1:3 adsorbents at all pH levels. Bead-free and homogeneous fibers can result in a large surface area and subsequent high adsorption capacity [41]. This result demonstrated that both functional groups and homogeneous fibrous structure contributed to the adsorption capacity of electrospun CA/CS fibers. Therefore, the CA/CS 1:1 film and pH 4 were selected for the following studies.

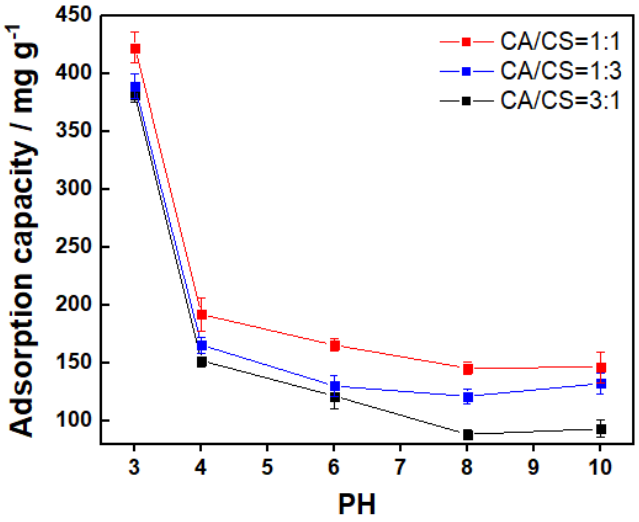

Figure 4.4. Effect of pH on the adsorption capacities of CA/CS 3:1, 1:1, and 1:3 adsorbents for HA removal (adsorbent dosage: 0.0011g; initial concentration of HA solution: 30 ppm; volume: 20 mL; contact time: 90 min; shaking speed: 155 rpm; temperature: 25 ºC).

4.4.3.2. Effect of adsorbent dosage on HA adsorption

The adsorption capacity of CA/CS 1:1 films toward HA is shown in Fig 4.5. The dosages of CA/CS films were adjusted from 0.0004 to 0.002 g while the other factors remained constant. It was obvious that the adsorption capacity of electrospun films remained steady when the adsorbent dosage was changed from 0.0004 to 0.0012 g. Further addition of the adsorbent (from 0.0012 to 0.002 g) led to the decrease of adsorption capacity for HA molecules. This phenomenon was attributed to the obvious decrease in HA concentration [42]. Thus, 0.0012 g of electrospun CA/CS adsorbents in 20 ml 30 ppm HA solution were chosen to conduct the following adsorption tests.

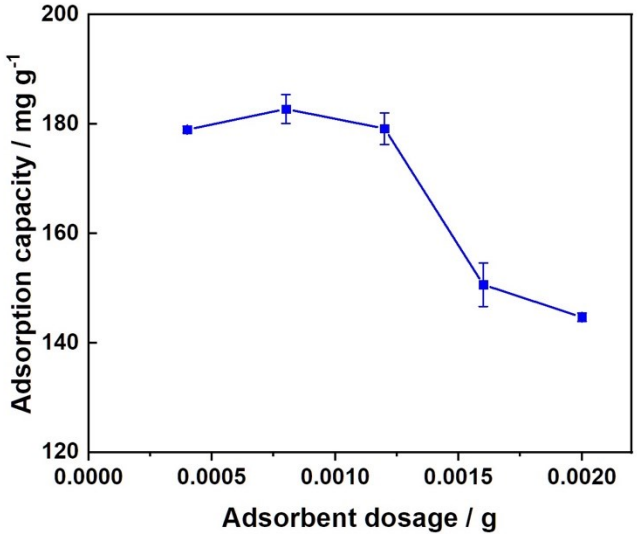

Figure 4.5. Effect of adsorbent dosage on HA removal using CA/CS 1:1 adsorbent (pH: 4.0; initial concentration of HA solution: 30 ppm; volume: 20 mL; contact time: 90 min; shaking speed: 155 rpm; temperature: 25 °C).

4.4.3.3. Effects of contact time and initial HA concentration

According to the result of adsorbent dosage study, the effects of initial HA concentration (ranging from 10 to 40 ppm) and contact time were investigated. As shown in Fig 4.6, rapid adsorptions of HA were observed in the first 45 min, and then the curves tended to be flat during 60 min to 120 min. It could be explained by the availability of relatively abundant adsorption sites for HA molecules at the beginning. As the adsorption process proceeded, the active sites were occupied gradually until the equilibrium adsorption capacity reached at 60 minutes. The electrospun CA/CS adsorbents showed a relatively higher adsorption rate for HA removal compared to many previously reported adsorbents; for example, the adsorption of HA on Fe_3O_4-$Mg(OH)_2 \cdot Al(OH)_3$ nanoparticles was 81.23 mg/g within 120 min at an initial concentration of 40 ppm and pH=5 [43], and hexadecyltrimethylammonium bromide modified-bentonites showed a capacity of 47.85 mg/g within 210 min at an initial concentration of 20 ppm and pH=3.2 [44]. The higher initial concentration of HA led to the increased adsorption capacity. It was because of that, in one aspect,

more HA molecules in solution could better conquer the resistance between the mass transfer of HA from aqueous environment to the solid adsorbents [42]; and in another, strong repulsive forces among neighboring HA molecules attached on the adsorbent surface prevented the further adsorption [45]. Notably, the performance of CA/CS adsorbents was also satisfactory at low concentration of HA molecules (the adsorption capacity reached up to 90.25 mg/g with 10 ppm initial HA concentration) [46-47].

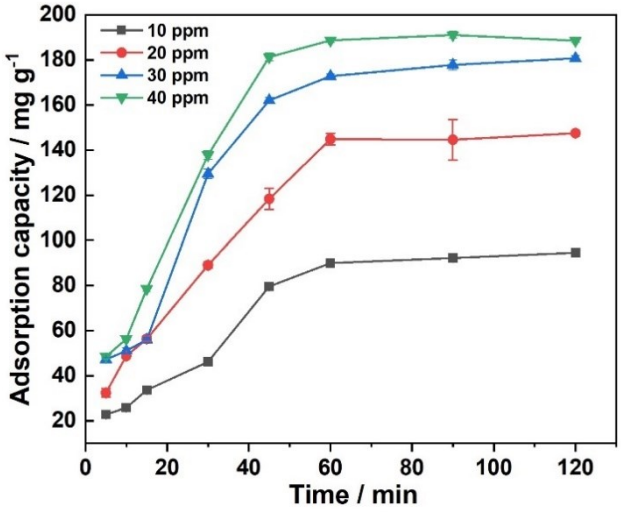

Figure 4.6. Effects of contact time and HA concentration on the adsorption capacities (pH: 4.0; adsorbent dosage: 0.0012 g; volume: 20 mL; shaking speed: 155 rpm; temperature: 25 ºC).

4.4.3.4. Adsorption isotherm

To analyze the process of adsorbing HA onto electrospun CA/CS fibers and predict the maximum adsorption capacity, adsorption isotherm was simulated by employing Langmuir and Freundlich isotherm models. The characterization of Langmuir model is to assume that monolayer adsorption occurs at homogeneous adsorption sites on the surface of adsorbents and the interactions among all the adsorbed molecules are negligible [48], while the Freundlich isotherm model describes multilayer adsorptions with interactions of adsorbates at heterogeneous sites [48]. The result of adsorption isotherm analysis is presented in Table 4.1. It was evident that the adsorption of HA

onto electrospun CA/CS fibers was better fitted by Langmuir model with a correlation coefficient of 0.992, so the removal of HA in this study was a homogeneous monolayer adsorption process. The predicted maximum adsorption capacity of CA/CS 1:1 film obtained from fitting by Langmuir model was 238.10 mg/g, which was higher than those of many adsorbents reported in previous literatures (listed in Table 4.2). It indicated that it is feasible to use intermolecular interaction mechanisms to guide the design of highly efficient adsorbents. The adsorbents derived from metal oxide nanoparticles [42,49] had the better capacities due to their large surface-to-volume ratios, but it is much easier to handle electrospun films compared to powdered form adsorbents [17].

Table 4.1. Summary of Langmuir and Freundlich constants for HA adsorption using electrospun CA/CS 1:1 adsorbents.

Langmuir Model			**Freundlich Model**		
K_L (L/mg)	q_{max} (mg/g)	R^2	n	K_f ((mg/g) $(L/mg)^{1/n}$)	R^2
0.15	238.10	0.99	2.58	9.00	0.94

Table 4.2. List of previously reported maximum adsorption capacities towards HA.

Adsorbent	**q_m (mg/g)**	**Reference**
Algerian bentonite	54.8	[50]
Fe_3O_4-SiO_2 microsphere	128.64	[51]
TiO_2-coated zeolite	5.94	[52]
Polyacrylamide/chitosan semi-IPN hydrogel	160	[53]
Crosslinked chitosan-epichlorohydrin beads	44.84	[54]
Fly ash	36	[55]
ZrO_2-poly(ether sulfone)	50.5	[56]
Fe_3O_4-$Mg(OH)_2 \cdot Al(OH)_3$	353.82	[42]
Fe_3O_4-hexadecyl trimethylammonium bromide	350	[49]
Cellulose acetate/Chitosan nanofiber	238.10	This study

4.4.3.5. Adsorption kinetics

Kinetic study reveals information on adsorption rate and mechanisms by fitting the experimental data into kinetic models. In this study, pseudo-first-order and pseudo-second-order kinetic models were examined to investigate the adsorption kinetics of HA on electrospun CA/CS 1:1 fibers, and

the results are presented in Table 4.3. The values of q_{e1} and k_1 were obtained from the intercept and slope of $\ln(q_e-q_t)$ versus t plots according to Equation (4-3), while q_{e2} and k_2 were calculated from the (t/q_t) versus t plots according to Equation (4-4). It was revealed that the adsorption of HA on electrospun CA/CS 1:1 fibers was better fitted by pseudo-first-order kinetic model. Therefore, the adsorption was primarily driven by electrostatic interactions [53].

Table 4.3. Summary of pseudo-first-order and pseudo-second-order kinetic model parameters for HA adsorption on electrospun CA/CS 1:1 fibrous films.

	Pseudo-first-order			**Pseudo-second-order**		
q_e, experimental (mg/g)	q_{e1}, calculated (mg/g)	k_1 (min^{-1})	R^2	q_{e2}, calculated (mg/g)	k_2 ($g(mg\ min^{-1})^{-1}$)	R^2
180.73	181.22	0.05	0.98	236.41	0.12	0.95

4.4.3.6. Adsorption thermodynamics

Thermodynamic study gives a hint on the interactions between HA and electrospun CA/CS 1:1 fibers with respect to the temperature. When the temperature increased from 25 ℃ to 55 ℃, the adsorption capacities of CA/CS films were reduced. As listed in Table 4.4, the positive values of ΔG° indicated the non-spontaneous process of HA adsorption at the range of temperature studied, which is also reported by Zulfikar et al. [44]. The values of ΔG° became more positive with the increase of temperature, which represented a higher energy barrier and confirmed the favourability of adsorption at lower temperature [44]. The negative ΔH° value revealed the exothermic process of HA adsorption, which is supported by the lower adsorption capacity of CA/CS films at higher temperatures. The negative ΔS° value indicated the decreasing degree of freedom of the HA molecules and consequently decreasing randomness at the solid-liquid interface. The results is similar to the thermodynamic studies reported by Derakhshani and Naghizadeh [57].

Table 4.4. Summary of thermodynamic parameters for HA adsorption on electrospun CA/CS 1:1 fibrous films

Temperature (°C)	ΔG° (kJ/mol)	ΔH° (kJ/mol)	ΔS° (kJ/mol)	R^2
25	3.52	-25.40	-0.097	0.96
45	5.46			
55	6.43			

4.5. Conclusion

Guided by probing the intermolecular interaction mechanisms between HA and different substrates, in this work, highly efficient adsorbents were successfully fabricated by electrospinning CA/CS acetic acid solutions for HA removal from aqueous solutions. The adsorption was mainly driven by the electrostatic attraction between the deprotonated carboxylic groups of HA and protonated amino groups of CS in the adsorbents, as well as the hydrophobic attraction between the hydrophobic moieties of HA and -CH_3 groups of CA. These interactions varied at different pH values, initial HA concentrations, and temperatures. Besides the roles of functional groups of CS and CA, the fiber morphologies could also significantly affect the adsorption capacities. The CA/CS 1:1 adsorbent exhibited the uniform fibrous structure and highest tensile strength among all the samples. Its predicted maximum adsorption capacity towards HA reached 238.10 mg/g, which was higher than those of many adsorbents reported in previous literatures. The adsorption process was fast (within 45 min) and effective even at a low initial HA concentration. Therefore, the obtained adsorbents are promising for the application in wastewater treatment.

4.6. References

1. Liu, S., Lim, M., and Amal, R. TiO_2-coated Natural Zeolite: Rapid Humic Acid Adsorption and Effective Photocatalytic Regeneration. *Chem. Eng. Sci.* 2014; 105: 46-52. doi: 10.1016/j.ces.2013.10.041
2. Schmitt, D., Saravia, F., Frimmel, F. H., and Schuessler, W. NOM-facilitated Transport of Metal Ions in Aquifers: Importance of Complex-dissociation Kinetics and Colloid Formation. *Water Res.* 2001; 37: 3541-3550. doi: 10.1016/S0043-1354(01)00525-5
3. Klausen, J., Vikesland, P. J., Kohn, T., Burris, D. R., Ball, W. P., and Roberts, A. L. Longevity of Granular Iron in Groundwater Treatment Processes: Solution Composition Effects on Reduction of Organohalides and Nitroaromatic Compounds. *Enviro. Sci. Technol.* 2003; 37: 1208-1218. doi: 10.1021/es025965s
4. Khodadadi, M., Al-Musawi, T.J., Kamranifar, M., Saghi, M. H., and Panahi, A. H. A Comprehensive Study of Using Barberry Stem Powder and Ash as Adsorbents for Adsorption of Humic Acid. *Environ. Sci. Pollut. Res.* 2019; 26: 26159-26169. doi: 10.1007/s11356-019-05879-4
5. Richardson, S. D., and Meyers, R. A. (Ed.). Encyclopedia of Environmental Analysis and Remediation. Berlin: Wiley; 1998.
6. Abdellatif, E. G., Mohammad, A., Ahmed, K., Ignasi, S., and Ahmed, A. W. Corrosion Behavior of Pure Titanium Anodes in Saline Medium and Their Performance for Humic Acid Removal by Electrocoagulation. *Chemosphere.* 2020; 246: 125674. doi: 10.1016/j.chemosphere.2019.125674
7. Algamdi, M. S., Alsohaimi, I. H., Lawler, J., Ali, H. M., Aldawsari, A.M., and Hassan, H. M. A. Fabrication of Graphene Oxide Incorporated Polyethersulfone Hybrid Ultrafiltration

Membranes for Humic Acid Removal. *Sep. Purif. Technol*. 2019; 223: 17-23. doi: 10.1016/j.seppur.2019.04.057

8. Geng, N., Chen, W., Xu, H., Ding, M., Liu, Z., and Shen, Z. A Sono-photocatalyst for Humic Acid Removal from Water: Operational Parameters, Kinetics and Mechanism. *Ultrason. Sonochem*. 2019; 57: 242-252. doi: 10.1016/j.ultsonch.2019.03.022
9. Hasani, G., Maleki, A., Daraei, H., Ghanbari, R., Safari, M., Mckay, G., Yetilmezsoy, K., Ilhan, F., and Marzban, N. A Comparative Optimization and Performance Analysis of Four Different Electrocoagulation-flotation Processes for Humic Acid Removal from Aqueous Solutions. *Process Saf. Environ. Prot*. 2019; 121: 103-117. doi: 10.1016/j.psep.2018.10.025
10. Moura, M.N., Martín, M.J., and Burguillo, F.J. A Comparative Study of the Adsorption of Humic Acid, Fulvic Acid and Phenol onto Bacillus Subtilis and Activated Sludge. *J. Hazard. Mater.* 2007; 149: 42–48. doi: 10.1016/j.jhazmat.2007.02.074
11. Wei, M., Wang, K., Hsiao, T., Lin, I., Wu, H., Wu, Y., Liu, P., and Chang, S. Effects of UV Irradiation on Humic Acid Removal by Ozonation, Fenton and Fe◦/Air Treatment: THMFP and Biotoxicity Evaluation. *J. Hazard. Mater*. 2011; 195: 324-331. doi:10.1016/j.jhazmat.2011.08.044
12. Akbari, F., Khodadadi, M., Panahi, A. H., and Naghizadeh, A. Synthesis and Characteristics of a Novel $FeNi_3$ /SiO_2 /TiO_2 Magnetic Nanocomposites and its Application in Adsorption of Humic Acid from Simulated Wastewater: Study of Isotherms and Kinetics. *Environ. Sci. Pollut. Res.* 2019; 26: 32385-32396. doi: 10.1007/s11356-019-06371-9
13. Barhoumi, A., Ncib, S., Chibani, A., Brahmi, K., Bouguerra, W., and Elaloui, E. High Rate Humic Acid Removal from Cellulose and Paper Industry Wastewater by Combining

Electrocoagulation Process with Adsorption onto Granular Activated Carbon. *Ind. Crops Prod.* 2019; 140: 111715. doi: 10.1016/j.indcrop.2019.111715

14. Gueu, S., Finqueneisel, G., Zimmy, T., Bartier, D., and Yao, B. Physicochemical Characterization of Three Natural Clays Used as Adsorbent for the Humic Acid Removal from Aqueous Solution. *Adsorpt. Sci. Technol*. 2018; 37: 77-94. doi: 10.1177/0263617418811469
15. Mulyati, S., Armando, M. A., Mawardi, H., Azmi, F. A., Pratiwi, W. P., Fadzlina, A., Akbar, R., and Syawaliah. Enhancement of Polyethersulfone (PES) Membrane Performance by Modification with Rice Husk Nanosilica for Removal of Organic Matter in Water. *IOP Conf. Ser.: Mater. Sci. Eng.* 2018; 334: 012040. doi: 10.1088/1757-899X/334/1/012040
16. Tahmasebi, F., Alimohammadi, M., Nabizadeh, R., Khoobi, M., Karimian, K., and Zarei, A. Performance Evaluation of Graphene Oxide Coated on Cotton Fibers in Removal of Humic Acid from Aquatic Solutions. *Environ. Eng*. 2019; 36: 894-902. doi:10.1007/s11814-019-0277-z
17. Kutorglo, E. M., Kovačovič, J., Trunov, D., Hassouna, F., Fučíková, A., Kopecký, D., Sedlářová, I., and Šoóš, M. Preparation of Carbon-based Monolithic CO2 Adsorbents with Hierarchical Pore Structure. *Chem. Eng. J.* 2020; 388: 124308. doi: 10.1016/j.cej.2020.124308
18. Wang, Y., Yang, J., Du, R., and Chen, L. Transition Metal Ions Enable the Transition from Electrospun Prolamin Protein Fibers to Nitrogen-Doped Freestanding Carbon Films for Flexible Supercapacitors. *ACS Appl. Mater. Interfaces*. 2017; 9: 23731-23740. doi: 10.1021/acsami.7b05159

19. Aliabadi, M., Irani, M., Ismaeili, J., Piri, H., and Parnian, M. J. Electrospun Nanofiber Membrane of PEO/Chitosan for the Adsorption of Nickel, Cadmium, Lead and Copper Ions from Aqueous Solution. *Chem. Eng. J.* 2013; 220: 237-243. doi: 10.1016/j.cej.2013.01.021
20. Zhang, Y., Wang, F., and Wang, Y. Recent Developments of Electrospun Nanofibrous Materials as Novel Adsorbents for Water Treatment. *Mater. Today Commun*. 2021; 27: 102272. doi: 10.1016/j.mtcomm.2021.102272
21. Xie, L., Lu, Q., Mao, X., Wang, J., Han, L., Hu, J., Lu, Q., Wang, Y., and Zeng, H. Probing the Intermolecular Interaction Mechanisms Between Humic Acid and Different Substrates with Implications for its Adsorption and Removal in Water Treatment. *Water Res*. 2020; 176: 115766. doi:10.1016/j.watres.2020.115766
22. Ghorani, B., Kadkhodaee, R., Rajabzadeh, G., and Tucker, N. Assembly of Odour Adsorbent Nanofilters by Incorporating Cyclodextrin Molecules into Electrospun Cellulose Acetate Webs. *React. Funct. Polym*. 2019; 134: 121-132. doi:10.1016/j.reactfunctpolym.2018.11.014
23. Lakhdhar, I., Belosinschi, D., Mangin, P., and Chabotet, B. Development of a Bio-based Sorbent Media for the Removal of Nickel Ions from Aqueous Solutions. *J. Environ. Chem. Eng.* 2016; 4: 3159-3169. doi: 10.1016/j.jece.2016.06.026
24. Gopi, S., Pius, A., Kargl, R., Kleinschek, K. S., and Thomas, S. Fabrication of Cellulose Acetate/Chitosan Blend Films as Efficient Adsorbent for Anionic Water Pollutants. *Polym. Bull.* 2019; 76: 1557–1571. doi:10.1007/s00289-018-2467-y
25. Wen, Y., Tang, Z., Chen, Y., and Gu, Y. Adsorption of Cr(VI) from Aqueous Solutions Using Chitosan-coated Fly Ash Composite as Biosorbent. *Chem. Eng. J*. 2011; 175: 110-116. doi: 10.1016/j.cej.2011.09.066

26. Naghizadeh, A., Ghasemi, F., Derakhshani, E., and Shahabi, H. Thermodynamic, Kinetic and Isotherm Studies of Sulfate Removal from Aqueous Solutions by Graphene and Graphite Nanoparticles. *Desalin. Water Treat*. 2017; 80: 247-254. doi: 10.5004/dwt.2017.20891

27. Monisha, S., Selvasekarapandian, S., Mathavan, T., Benial, A. M. F., Manohran, S., and Karthikeyan, S. Preparation and Characterization of Biopolymer Electrolyte Based on Cellulose Acetate for Potential Applications in Energy Storage Devices. *J. Mater. Sci.: Mater. Electron*. 2016; 27: 9314–9324. doi:10.1007/s10854-016-4971-x

28. Wu, J., Wang, N., Wang, L., Dong, H., Zhao, Y., and Jiang, L. Electrospun Porous Structure Fibrous Film with High Oil Adsorption Capacity. *ACS Appl. Mater. Interfaces*. 2012; 4: 3207-3212. doi:10.1021/am300544d

29. Guo, Z., Huang, J., Xue, Z., and Wang, X. Electrospun Graphene Oxide/Carbon Composite Nanofibers with Well-developed Mesoporous Structure and Their Adsorption Performance for Benzene and Butanone. *Chem. Eng. J*. 2016; 306: 99-106. doi:https://doi.org/10.1016/j.cej.2016.07.048.

30. He, N., Li, L., Wang, P., Zhang, J., Chen, J., and Zhao, J. Dioxide/Chitosan/Poly(lactide-co-caprolactone) Composite Membrane with Efficient Cu(II) Adsorption. *Colloids Surf., A.* 2019; 580: 123687. doi: 10.1016/j.colsurfa.2019.123687

31. Pereira, A. G. B., Fajardo, A. R., Gerola, A. P., Rodrigues, J. H., Nakamura, C. V., Muniz, E. C., and Hsieh, Y. L. First Report of Electrospun Cellulose Acetate Nanofibers Mats with Chitin and Chitosan Nanowhiskers: Fabrication, Characterization, and Antibacterial Activity. *Carbohydr. Polym*. 2020; 250: 116954. doi: 10.1016/j.carbpol.2020.116954

32. Du, J., and Hsieh, Y. Cellulose/Chitosan Hybrid Nanofibers from Electrospinning of Their Ester Derivatives. *Cellulose*, 16 (2009), pp. 247-260. doi: 10.1007/s10570-008-9266-9

33. Mahfoudhi, N., and Boufi, S. Nanocellulose as a Novel Nanostructured Adsorbent for Environmental Remediation: A Review. *Cellulose*. 2017; 24: 1171-1197. doi: 10.1007/s10570-017-1194-0

34. Alaskar, A., Albidah, A., Alqarni, A. S., Alyousef, R., and Mohammadhosseini, H. Performance Evaluation of High-strength Concrete Reinforced with Basalt Fibers Exposed to Elevated Temperatures. *J. Build. Eng*. 2021; 35: 102108. doi:10.1016/j.jobe.2020.102108

35. Wang, Y., and Chen, L. Fabrication and Characterization of Novel Assembled Prolamin Protein Nanofabrics with Improved Stability, Mechanical Property and Release Profiles. J. *Mater. Chem*. 2012; 22: 21592-21601. doi: 10.1039/C2JM34611G

36. Abate, G., and Masini, J. C. Influencce of pH and Ionic Strength on Removal Processes of a Sedimentary Humic Acid in a Suspension of Vermiculite. *Colloids Surf., A.* 2003; 226: 25-34. doi: 10.1016/S0927-7757(03)00418-7

37. Brigante, M., Zanini, G., and Avena, M. On the Dissolution Kinetics of Humic Acid Particles: Effects of pH, Temperature and Ca^{2+} Concentration. *Colloids Surf., A.* 2007; 294: 64-70. doi: 10.1016/j.colsurfa.2006.07.045

38. Lu, Q., Huang, J., Maan, O., Liu, Y., and Zeng, H. Probing Molecular Interaction Mechanisms of Organic Fouling on Polyamide Membrane Using a Surface Forces Apparatus: Implication for Wastewater Treatment. *Sci. Total Environ*. 2018; 622-623: 644-654. doi: 10.1016/j.scitotenv.2017.12.022

39. Wang, Q., Chen, X., Liu, N., Wang, S., Liu, C., Meng, X., and Liu, C. Protonation Constants of Chitosan with Different Molecular Weight and Degree of Deacetylation. *Carbohydr. Polym*. 2006; 65: 194-201. doi: 10.1016/j.carbpol.2006.01.001

40. Ngah, W. S. W., Hanafiah, M. A. K. M., and Yong, S. S. Adsorption of Humic Acid from Aqueous Solutions on Crosslinked Chitosan-epichlorohydrn Beads: Kinetics and Isotherm Studies. *Colloids Surf., B.* 2008; 65: 18-24. doi: 10.1016/j.colsurfb.2008.02.007

41. Krasian, T., Punyodom, W., and Worajittiphon, P. A Hybrid of 2D Materials (MoS_2 and WS_2) as an Effective Performance Enhancer for Poly(lactic acid) Fibrous Mats in Oil Adsorption and Oil/Water Separation. *Chem. Eng. J.* 2019; 369: 563-575. doi: 10.1016/j.cej.2019.03.092

42. Zulfikar, M. A., Afrita, S., Wahyuningrum, D., and Ledyastuti, M. Preparation of Fe_3O_4-Chitosan Hybrid Nano-particles Used for Humic Acid Adsorption. *Enviro. Nanotechnol. Monit. Manag*. 2016; 6: 64-75. doi: 10.1016/j.enmm.2016.06.001

43. Wang, R., Wen, T., Wu, X., and Xu, A. Highly Efficient Removal of Humic Acid from Aqueous Solutions by Mg/Al Layered Double Hydroxides–Fe_3O_4 Nanocomposites. *RSC Adv*. 2014; 4: 21802-21809. doi: 10.1039/C4RA02212B

44. Bousba, S., Bougdah, N., Messikh, N., and Magri, P. Adsorption Removal of Humic Acid from Water Using a Modified Algerian Bentonite. *Phys. Chem. Res*. 2018; 6: 613-625. doi: 10.22036/pcr.2018.129154.1482

45. Rao, M. M., Ramesh, A., Rao, G. P. C., and Seshaiah, K. Removal of Copper and Cadmium from the Aqueous Solutions by Activated Carbon Derived from Ceiba Pentandra Hulls. *J. Hazard. Mater*. 2006; 129: 123-129. doi: 10.1016/j.jhazmat.2005.08.018

46. Lin, J., and Zhan, Y. Adsorption of Humic Acid from Aqueous Solution onto Unmodified and Surfactant-modified Chitosan/Zeolite Composites. *Chem. Eng. J*. 2012; 200: 202-213. doi: 10.1016/j.cej.2012.06.039

47. Liu, J., Cao, J., Chen, H., and Zhou, D. Adsorptive Removal of Humic Acid from Aqueous Solution by Micro-and Mesoporous Covalent Triazine-based Framework. *Colloids Surf., A*. 2015; 481: 276-282. doi:10.1016/j.colsurfa.2015.05.021

48. Ngah, W. S. W., Fatinathan, S., and Yosop, N. A. Isotherm and Kinetic Studies on the Adsorption of Humic Acid onto Chitosan-H_2SO_4 Beads. *Desalination*. 2011; 272: 293-300. doi: 10.1016/j.desal.2011.01.024

49. Tang, Z., Zhao, X., Zhao, T., Wang, H., Wang, P., Wu, F., and Giesy, J. P. Magnetic Nanoparticles Interaction with Humic Acid: In the Presence of Surfactants. *Environ. Sci. Technol.* 2016; 50: 8640-8648. doi: 10.1021/acs.est.6b01749

50. Wang, Q., Chen, X., Liu, N., Wang, S., Liu, C., Meng, X., and Liu, C. Protonation Constants of Chitosan with Different Molecular Weight and Degree of Deacetylation. *Carbohydr. Polym*. 2006; 65: 194-201. doi: 10.1016/j.carbpol.2006.01.001

51. Tang, Y., Liang, S., Yu, S., Gao, N., Zhang, J., Guo, H., and Wang, Y. Enhanced Adsorption of Humic Acid on Amine Functionalized Magnetic Mesoporous Composite Microspheres. Colloids Surf., A. 2012; 406: 61-67. doi: 10.1016/j.colsurfa.2012.04.050

52. Liu, S., Lim, M., and Amal, R. TiO_2-coated Natural Zeolite: Rapid Humic Acid Adsorption and Effective Photocatalytic Regeneration. *Chem. Eng. Sci*. 2014; 105: 46-52. doi: 10.1016/j.ces.2013.10.041

53. Liu, Z., and Zhou, S. Removal of Humic Acid from Aqueous Solution Using Polyacrylamide/Chitosan Semi-IPN Hydrogel. *Water Sci. Technol*. 2018; 2017: 16-26. doi: 10.2166/wst.2018.064

54. Tahmasebi, F., Alimohammadi, M., Nabizadeh, R., Khoobi, M., Karimian, K., and Zarei, A. Performance Evaluation of Graphene Oxide Coated on Cotton Fibers in Removal of Humic Acid from Aquatic Solutions. *Environ. Eng*. 2019; 36: 894-902. doi: doi.org/10.1007/s11814-019-0277-z

55. Wang, S., Terdkiatburana, T., and Tade, M. O. Single and Co-adsorption of Heavy Metals and Humic Acid on Fly Ash. *Sep. Purif. Technol*. 2008; 58: 353-358. doi: 10.1016/j.seppur.2007.05.009

56. Thuyavan, Y. L., Anantharaman, N., Arthanareeswaran, G., and Ismail, A. F. Adsorptive Removal of Humic Acid by Zirconia Embedded in a Poly(ether sulfone) Membrane. *Ind. Eng. Chem. Res*. 2014; 53: 11355-11364. doi: 10.1021/ie5015712

57. Derakhshani, E., and Naghizadeh, A. Optimization of Humic Acid Removal by Adsorption onto Bentonite and Montmorillonite Nanoparticles. *J. Mol. Liq*. 2018; 259: 76-81. doi: 10.1016/j.molliq.2018.03.014

Connecting Statement to Chapter 5

In Chapter 4, we demonstrated the feasibility of recycling CA and CS into high-performance adsorbents for HA removal. To further improve the mechanical properties and removal efficiency of the electrospun fibers, we hypothesized a core-sheath structured fiber. Specifically, with the incorporation of CNCs as a load-bearing component in the core of the fibers, and the concentration of CS (with abundant amino groups for binding HA) at the outer layer of the fibers, we expected the fibrous adsorbents to exhibit improved mechanical properties and removal efficiency. The properties of these core-sheath fibers were systematically investigated in comparison with the uniaxial fibers. Additionally, their performance in removing HA was evaluated.

Chapter 5. Electrospun cellulose acetate/chitosan fibers for humic acid removal: improved efficiency and robustness with a core-sheath design

5.1. Abstract

Recycling biomass wastes into functional materials has attracted much attention, and a rational structural design can make more effective use of each component. In our previous work, the feasibility of using intermolecular interaction mechanisms to guide the fabrication of electrospun cellulose acetate (CA)/chitosan (CS) adsorbents for humic acid (HA) removal has been demonstrated. Herein, a core-sheath structure was designed via one-step co-axial electrospinning, where a mixture of CS and CA was employed as the sheath layer to efficiently adsorb HA, and cellulose nanocrystals (CNCs) derived from waste cotton fabrics were incorporated in the CA core as load-bearing components. Compared to the non-layered electrospun CS/CA fibers, all the CS/CA/CNCs fibers with core-sheath structures exhibited smaller diameters, greater homogeneity, and significantly improved mechanical strength. Especially, the tensile strength of electrospun 3:1CS/CA-5%CNC fibers reached 5.08±0.61 MPa, which was 23 times higher than that of the non-layered 3:1 CS/CA fibers. Meanwhile, their maximum adsorption capacities towards HA had no significant difference. Even after the complete hydrolysis of CA into cellulose, the electrospun fibers maintained the fibrous structure and showed a higher tensile strength (6.87±0.25 MPa), while exhibiting an acceptable adsorption capacity towards HA (82.69±5.90 mg/g). Therefore, this work demonstrates the importance of rational design in the efficient preparation of functional materials and the feasibility of using electrospun core-sheath fibers derived from biomass wastes for the removal of water contaminants.

Keywords: co-axial electrospinning, cellulose nanocrystals, cellulose acetate, chitosan, adsorbents

5.2. Introduction

Fair utilization and recycling of biomass wastes is an important consideration of the circular economy where as much value as possible is retained towards zero waste [1]. Nevertheless, a great amount of biomass wastes from agriculture, forestry, and fisheries were instead processed annually by combustion and landfilling, leading to a series of environmental problems [2-4]. Forestry biomass was reported to be the largest source of biomass input in Canada that reached 12.3 million metric tonnes in 2015 [5]. Among the wood-derived compounds, cellulose acetate (CA) is recognized as one of the most important derivatives in terms of its considerable commercial contribution [6]. CA has been extensively used to produce consumer products comprising cigarette filter, textile fibers, films, plastics, and others [7], where the majority of them have no sustainable disposal methods. Also, industrial applications of chitosan (CS) and cellulose in agriculture, pharmaceutical, and textile sectors are expanding exponentially to meet the market demand, which will generate wastes continuously in the foreseeable future [8]. Recycling and converting these biomass wastes and residues into value-added products is a wise strategy to relieve pressure on the environment.

Recently, electrospun fibrous membranes have drawn extensive attention from a broad range of fields owing to their high porosity, large specific area, simple operation, and good interconnectivity [9-11]. Among them, electrospun CA materials have specifically shown great potential in water treatment [10, 12]. In our previous work, the feasibility of using intermolecular interaction study to guide the fabrication of electrospun CA/CS adsorbents for efficient humic acid (HA) removal has been demonstrated, and the superior adsorption performance towards HA was due to the electrostatic and hydrophobic interactions [13]. It is worth noting that adsorption mainly relies on the active sites on the outer surface of adsorbents for the uptake of contaminants [14], and the mechanical strength of the adsorbent plays a vital role in commercial applications because it

guarantees the integrity of electrospun fibrous membranes during water treatment [9]. Therefore, to further improve the performance and mechanical properties of the adsorbents, rationally-designed structures of the fibrous composites are extremely important, which can also contribute to the cost saving in water treatment by using a minimum amount of functional components [15]. Co-axial electrospinning is a double-fluid process where two individual solutions are spun simultaneously through the coaxial capillaries to obtain nanofibers with core-sheath structures [16, 17]. The unique features endow co-axial electrospinning with several advantages over the conventional configuration in terms of flexibility and selection of polymers/solvents when designing and constructing functional materials [18-20]. Given these advantages, co-axial electrospinning has been used to prepare adsorbents with excellent removal effects. For example, core-sheath structure of cellulose triacetate (core)- hydroxyapatite (sheath) fibers were developed for adsorbing bovine serum albumin, which reached a maximum adsorption capacity of 176.04 mg/g [16].

In this study, CA from cigarette filter, CS from crab shells, and cellulose nanocrystals (CNCs) from waste cotton textile were selected to fabricate the core-sheath structured adsorbents via one-step co-axial electrospinning. Specifically, a mixture of CS and CA was employed as the sheath layer to efficiently adsorb HA, and CNCs were incorporated in the CA core as load-bearing components. The effect of CNC contents on the structure and mechanical properties of the core-sheath CS/CA-CNCs fibers was studied via scanning electron microscopy (SEM), Fourier-transform infrared (FTIR) spectroscopy, and uniaxial tensile test. Additionally, the adsorption performance of the core-sheath CS/CA-CNCs fibers and the hydrolyzed fibers was investigated and compared.

5.3. Materials and Methods

5.3.1. Materials

CA tow from cigarette filters was kindly provided by Celanese Corporation (Irving, USA. M_w = 75–95 kDa, acetyl content of 39.95 wt %, degree of substitution of ~2.47). CS derived from crab shells was kindly provided by Dr. Benjamin K. Simpson (Department of Food Science and Agricultural Chemistry, McGill University, Quebec, Canada. Molecular weight 190–310 kDa, degree of deacetylation 75–85%). CNCs with lengths and diameters of 111.76 ± 38.73 nm and 11.18 ± 2.33 nm were extracted from waste cotton fabrics via sulfuric acid hydrolysis [21]. Acetic acid (CH_3COOH, 100%), HA (sodium salt, $C_9H_8Na_2O_4$ 45–70%), sodium hydroxide (NaOH, ACS reagent grade), and sulfuric acid (H_2SO_4, ACS reagent grade) were purchased from Fisher Scientific (Mississauga, Canada). All the reagents were used as received without further purification. Deionized water was used to prepare the electrospinning solutions and HA solutions.

5.3.2. Core-sheath CS/CA-CNCs fibers fabrication

For the co-axial electrospinning configuration, the CS/CA ratios of 1:1 w/w and 3:1 w/w optimized in our previous work were chosen to make the sheath layer [13], and the core layer was prepared by adding CNCs (3 wt % and 5 wt % of CA dry weight) in 12 wt % CA solution. A summary of sample compositions and electrospinning conditions is listed in Table 5.1. The core and sheath fluids were loaded into two syringes and forced through stainless-steel needles with concentric structures. The inner and outer diameters of the needle were 0.66 mm and 1.57 mm, respectively. A stainless-steel drum rotating at 10 rpm was used to collect the fibers, and the obtained fibrous membranes were vacuum dried in a desiccator at room temperature for 24 h to remove the solvent residue. In order to investigate the effect of deacetylation, 1:1CS/CA-5%CNCs and 3:1CS/CA-

5%CNCs were immersed in 20 mL of 0.5 M NaOH/ EtOH solution and stirred for 1 h at room temperature. The membranes were then washed with distilled water several times until the pH level of the wastewater was neutral, and vacuum dried in a desiccator at room temperature for 24 h. The deacetylated fibers were coded as 1:1CS/CL-5%CNCs and 3:1CS/CL-5%CNCs.

Table 5.1. Various compositions and optimized electrospinning conditions of the core-sheath CS/CA-CNCs fibers.

Samples	Core		Sheath		Electrospinning conditions applied voltage (kV), tip-to-collector distance (cm), flow rate (mL/h)
	CA content (wt %)	CNCs content (wt %)	Total solid content (wt %)	CA/CS ratio	
1:1CS/CA-5%CNCs	12	5	7	1:1	22, 11.5, 0.8 (sheath)-0.4 (core)
1:1CS/CA-3%CNCs	12	3	7	1:1	22, 11.5, 0.8 (sheath)-0.4 (core)
3:1CS/CA-5%CNCs	12	5	5	3:1	30, 9.5, 0.8 (sheath)-0.4 (core)
3:1CS/CA-3%CNCs	12	3	5	3:1	30, 9.5, 0.8 (sheath)-0.4 (core)

5.3.3. Core-sheath CS/CA-CNCs fibers characterization

Morphological characterization of the core-sheath CS/CA-CNCs fibers was carried out with a Hitachi SU-3500 scanning electron microscope (SEM, Hitachi, Tokyo, Japan) operating at 30 kV. Prior to the SEM observation, the samples were coated with 4 nm of gold/platinum coating using a Leica EM ACE200 coater (Leica, Wetzlar, Germany). Fiber diameters were measured with the ImageJ image-visualization software developed by the National Institute of Health. Specifically, SEM images under a magnification of ×10k were selected, and for each sample, six hundred random positions were selected and measured from the image [22]. FTIR spectra of the core-sheath CS/CA-CNCs fibers were recorded on a Varian Excalibur 3100 FTIR spectrometer (Varian,

Melbourne, Australia) equipped with an attenuated total reflectance accessory (Specac, Orpington, UK) as the average of 64 scans with a resolution of 4 cm^{-1}. Uniaxial tensile test of the CS/CA-CNCs fibers was carried out to evaluate their tensile strength and elongation at break. Seven specimens with dimensions of 30 mm × 10 mm (length × width) were tested for each sample using an ADMET eXpert 7601 Test System (ADMET, Massachusetts, USA) at a fixed crosshead velocity of 1 mm min^{-1}. The initial grip separation distance was fixed at 10 mm. The thickness of each specimen was measured using the ImageJ image-visualization software. The tensile strength (σ) of CA/CS fibrous films was calculated using the following equation:

$$\sigma = \frac{F}{A} \qquad (5-1)$$

where F (N) is the maximum load at break, and A (mm^2) is the cross-sectional area.

5.3.4. Adsorption experiment

Adsorption of HA were determined as functions of CS/CA ratios in the sheath, CNC contents in the core, and adsorption time under the following optimized conditions (pH=4.0, adsorbent dosage: 1.2 mg, volume of HA solution: 20 mL, initial concentration of HA solution: 30 ppm, shaking speed: 155 rpm, and temperature: 25 °C) [13]. Stock solution with a concentration of 100 ppm HA was prepared and then diluted to obtain 30 ppm HA solution. Sulfuric acid was used to adjust the pH value of HA solution to pH 4.0. Batch experiment was carried out in 25 mL glass bottles with white polypropylene caps, and 1.2 mg of adsorbents was added and shaken for desirable time intervals at 155 rpm. The concentrations of HA in the solutions before and after the adsorption process were determined using a Hitachi UV-2000 UV–vis spectrophotometer (Hitachi, Tokyo, Japan) at a wavelength of 278 nm. The adsorption capacity was calculated using the following equation:

$$q_e(mg\ g^{-1}) = \frac{(C_0 - Ce) \times V}{m} \qquad (5-2)$$

where C_0 (mg/L) is the initial HA concentration in the solution; *Ce* (mg/L) is the equilibrium HA concentration; V (L) is the volume of HA solution; and m (g) is the mass of electrospun adsorbent.

5.3.5. Statistical Analysis

All experimental results were expressed as the mean of at least three replicas ± SD. Statistical interpretations of the experimental result were carried out by analysis of variance (ANOVA) followed by multiple comparison tests using Duncan's multiple-range test at the 95% confidence level. All of the analyses were conducted using SPSS statistical software (version 27, IBM, NY, USA) with a probability of $p < 0.05$ considered to be significant.

5.4. Results and Discussion

5.4.1. Core-sheath CS/CA-CNCs fiber structure

Figure 5.1 shows the morphology and corresponding diameter distribution of the core-sheath-structured fibers with various CNC contents. The average fiber diameters of 1:1CS/CA-5%CNCs, 1:1CS/CA-3%CNCs, 3:1CS/CA-5%CNCs, and 3:1CS/CA-3%CNCs samples were 174.7±89.6, 158.8±66.0, 172.4±84.3, and 168.1±63.2 nm, respectively. All the CS/CA-CNCs adsorbents exhibited fine fibrous structures, which facilitated the adsorption of water contaminants [23, 24]. The average fiber diameters of both 1:1CS/CA-CNCs and 3:1CS/CA-CNCs samples increased when the loading amount of CNCs was adjusted from 3 wt % to 5 wt %. It was because the viscosity of electrospun solutions increased perceptibly as the CNCs content rose [25, 26], and the higher viscosity induced stronger resistance to the stretching force generated axially by the electric field [9, 27]. The high viscosity also caused the formation and deposition of a few convex- and

concave-shaped fibers as shown in Figures 5.1b and 5.1e. In addition, the variance in fiber diameters became greater as the loading level of CNCs increased, which was indicated by the large standard deviation and more spread-out distribution of the fiber diameters (Figure 5.1). In another word, the homogeneity of the 1:1CS/CA-3%CNCs and 3:1CS/CA-3%CNCs fibers were greater than that of the samples with 5 wt % of CNCs. Different amounts of CNCs could have an impact on the dispersible degree of CNCs in the core layer solution. Hence, the wider distribution of fiber diameters could be explained by the unstable formation and status of the Taylor cone in the presence of high amount of CNCs. Similar phenomena were also observed and reported by Ni et al. [28] and Patiño Vidal et al. [29].

Compared to the non-layered CS/CA fibers reported in our previous work [13], all the fiber diameters of the core-sheath CS/CA-CNCs fibers were smaller with greater uniformity in terms of diameter distributions. This observation could be associated with the poor electrospinnability of CS and a lower mass proportion of CS in the core-sheath fibers. After alkali hydrolysis, both 1:1CS/CA-5%CNCs and 3:1CS/CA-5%CNCs maintained their fiber integrity and porous structure. Nevertheless, the CS/CL-CNCs fibers swelled in water due to the improved hydrophilicity.

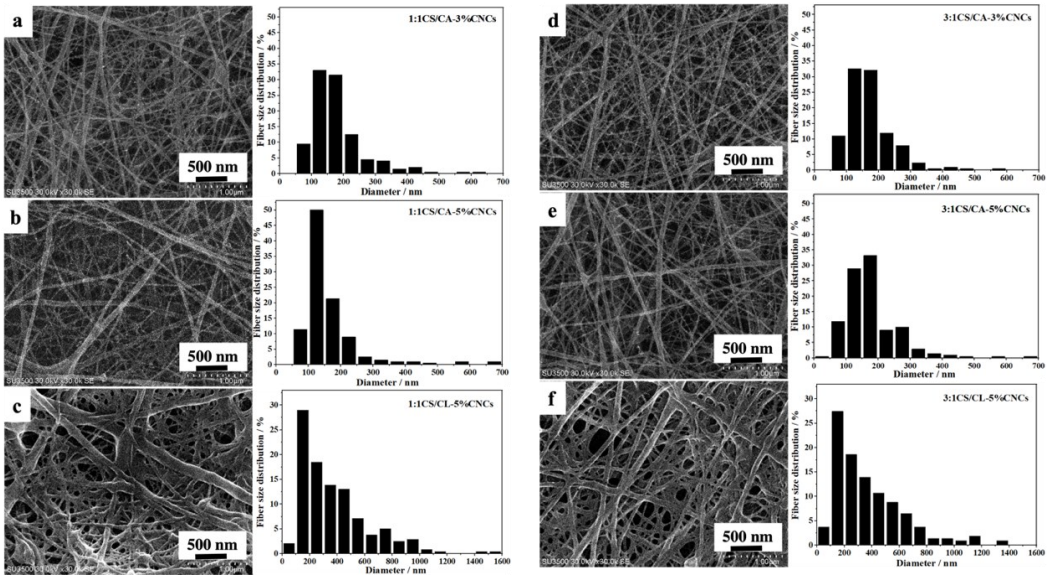

Figure 5.1. SEM images and fiber diameter distributions of (a) 1:1CS/CA-3%CNCs, (b) 1:1CS/CA-5%CNCs, (c) 1:1CS/CL-5%CNCs, (d) 3:1CS/CA-3%CNCs, (e) 3:1CS/CA-5%CNCs, and (f) 3:1CS/CL-5%CNCs fibers.

The interactions among various components of the core-sheath fibers were investigated by FTIR analysis. As shown in Figures 5.2a-5.2d, the core-sheath CS/CA-CNCs fibers with various CS/CA ratios and CNCs loading levels displayed analogous absorbance patterns, except the peaks corresponding to O-H stretching and N-H stretching vibrations [10, 30]. Particularly, the broad peak at 3450 cm^{-1} shifted slightly to a lower wavenumber (3420 cm^{-1}) as the mass proportion of CS rose, which disclosed the formation of intermolecular hydrogen bonds between hydroxyl groups of CA and amine groups of CS. In addition, the absorption bands at 1735 cm^{-1} and 1644 cm^{-1} were attributed to the carbonyl groups of CA and C=O stretching of the acetyl groups in CS, respectively [31, 32], but the absorption bands introduced by the addition of CNCs were implicit. It was due to the low contents of CNCs (up to 5 wt %) embedded in the core. The characteristic peaks of CA appeared in all the core-sheath CS/CA-CNCs fibers (Figures 5.2a-5.2d) at 1735 cm^{-1}, 1370 cm^{-1}, 1225 cm^{-1}, and 1040 cm^{-1}, corresponding to the stretching of carbonyl groups, methyl groups, C-O, and ether C-O-C of pyranose rings, respectively [33, 34]. After the alkali hydrolysis, these four characteristic peaks were absent, but a strong absorption at 3330 cm^{-1} was observed (Figures 5.2e and 5.2f) [35]. Furthermore, the spectra of both CS/CL-CNCs fibers were similar to that of cellulose (waste cotton fabrics). These results revealed the successful deacetylation of CA. It was worth noting that the absorption peak corresponding to C=O stretching of the acetyl groups of CS (1644 cm^{-1}) could still be observed in the spectra of CS/CL-CNCs samples, which proved the retention of CS in the deacetylated fibers.

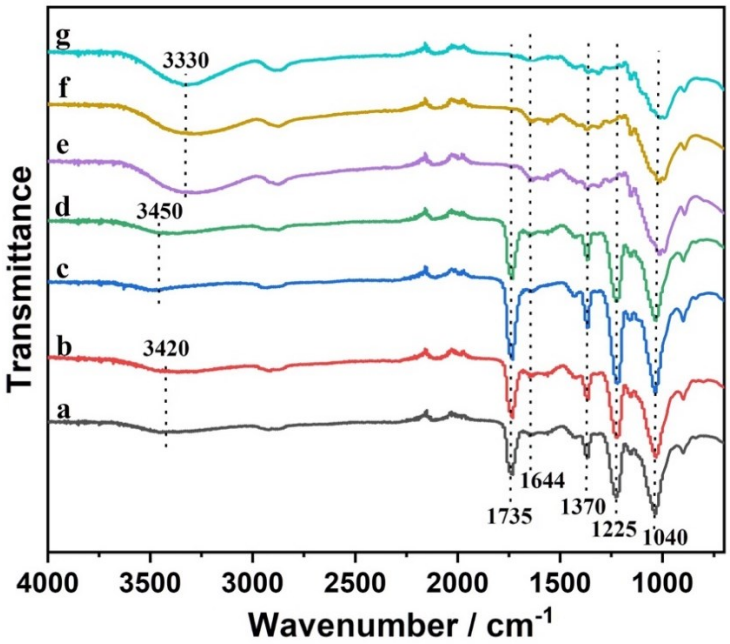

Figure 5.2. FTIR spectra of electrospun fibers: (a) 3:1CS/CA-3%CNCs, (b) 3:1CS/CA-5%CNCs, (c) 1:1CS/CA-3%CNCs, (d) 1:1CS/CA-5%CNCs, (e) 1:1CS/CL-5%CNCs, and (f) 3:1CS/CL-5%CNCs, and (g) cellulose (waste cotton fabrics).

5.4.2. Core-sheath CS/CA-CNCs fiber mechanical properties

The effects of CNCs and alkali hydrolysis on the mechanical properties of electrospun fibers were investigated. As shown in Figure 5.3, the content of CNCs in the core of CS/CA fibers had remarkable effects on their tensile strengths. Our former non-layered 1:1 and 3:1 CS/CA fibers had a tensile strength of 2.97±0.59 and 0.22±0.04 MPa [13], which were much lower than those of the core-sheath fibers containing CNCs. With further increase of CNCs loading levels from 3 wt % to 5 wt %, both 1:1CS/CA-CNCs and 3:1CS/CA-CNCs core-sheath fibers showed considerable improvements in the tensile strength, specifically from 4.50±0.35 to 10.91±0.89 MPa and 3.45±0.55 to 5.08±0.61 MPa, respectively. The distinguishable enhancement of the strength, on one hand, was because the stress could be transferred and diverted from CS/CA fabrics to the rigid

CNCs [25]; on the other hand, the interaction between CNCs and fiber matrix also contributed to the resistance of loading forces [36]. Additionally, the dissimilarity of fibers in elongation at break was less noticeable, and the incorporation of CNCs immobilized the CS/CA fibers to a certain extent, leading to an overall decreased elongation at break [21]. It was worth noting that the deacetylation of 1:1CS/CL-5%CNCs and 3:1CS/CL-5%CNCs fibers induced a further reinforcement of tensile strength to 11.87±1.2 and 6.87±0.25 MPa, respectively. It might be due to the conversion of CA into cellulose that facilitated the formation of hydrogen bonds within electrospun fibers [31].

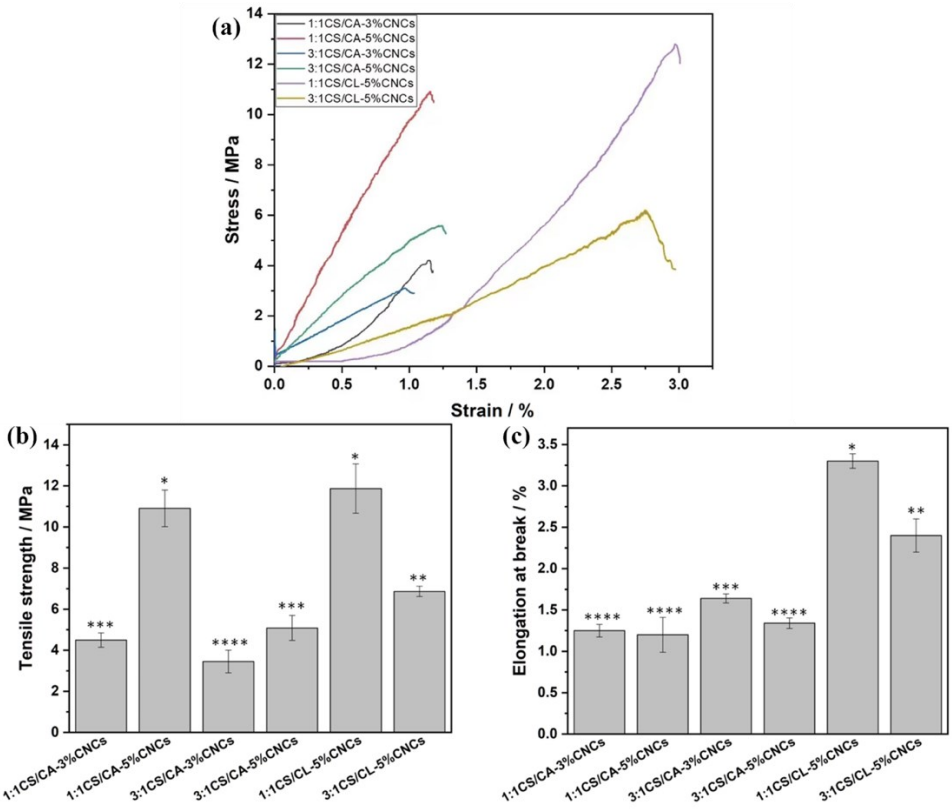

Figure 5.3. Typical stress-strain curves (a), tensile strength (b), and elongation at break (c) of various CS/CA-CNCs fibers before and after deacetylation (different asterisks on the top of columns represent significant difference ($p < 0.05$)).

5.4.3. Core-sheath CS/CA-CNCs fiber adsorption capacity

Figure 5.4a shows the experimental adsorption capacity of core-sheath CS/CA-CNCs fibers under the optimal conditions (pH= 4.0, adsorbent dosage: 1.2 mg, volume of HA solution: 20 mL, initial concentration of HA solution: 30 ppm, shaking speed: 155 rpm, and temperature: 25 °C) [13]. The core-sheath 3:1CS/CA-CNCs fibers exhibited obviously higher adsorption capacities towards HA than the 1:1CS/CA-CNCs fibers. It was because the adsorption predominantly relied on the electrostatic attraction between the deprotonated carboxylic groups of HA and the protonated amino groups of CS [37], and more CS existed in the sheath layer of 3:1CS/CA-CNCs fibers. The adsorption capacity of 3:1CS/CA-5%CNCs fibers was 151.41±1.76 mg/g, which had no significant difference compared to that of our former non-layered 3:1CS/CA fibers, and was achieved by using less amount of CS in the electrospun fibers. This result demonstrated the importance of rationale design in the fabrication of electrospun adsorbents. It was noted that the content of CNCs didn't show any significant impact on the adsorption capacity. Therefore, the core-sheath 1:1CS/CA-5%CNCs and 3:1CS/CA-5%CNCs fibers that exhibited better mechanical properties were selected for the following study. As shown in Figure 5.4b, the adsorption of HA on both samples increased sharply and then gradually plateaued after 10 h. The initial fast increases in adsorption capacity implied the great availability of active sites, high specific surface area, and porous structure of electrospun fibers [14]. The alkali hydrolysis reduced the adsorption capacities to 84.8 and 102.69 mg/g for 1:1CS/CL-5%CNCs and 3:1CS/CL-5%CNCs, respectively. This result was attributed to the following two reasons: on one hand, the interaction between hydrophobic moieties of HA and methyl groups of CA in the adsorbent also contributed to the adsorption of HA, but these methyl groups were removed during the deacetylation of CA; on the other hand, the hydroxyl groups of cellulose in the deacetylated fibers negatively affected the

electrostatic interaction between the amine groups of CS and HA molecules [38]. However, these adsorption capacities towards HA were still acceptable compared to some adsorbents reported in previous studies [39-43]. For example, Wan Ngah et al. reported an adsorption capacity of 44.84 mg/g of HA (10 mg/L, 100mL) using 0.05 g of chitosan- epichlorohydrin beads [42]. Similar to the current study, Thuyavan et al. also demonstrated a membrane type of adsorbent based on zirconia-embedded poly (ether sulfone), which exhibited an adsorption capacity of 50.5 mg/g towards HA and a tensile stress of up to 4.73 MPa [40].

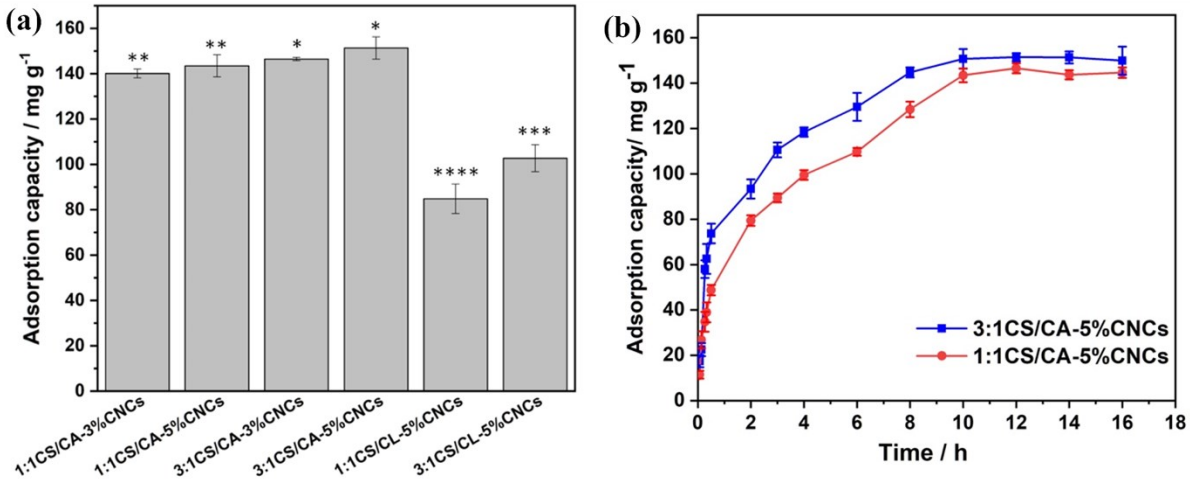

Figure 5.4. Maximum adsorption capacity of various core-sheath fibers (a), and effect of contact time on the adsorption capacity (b) (different asterisks on the top of columns represent significant difference ($p < 0.05$)).

5.5. Conclusion

This work demonstrated the importance of rational design in the fabrication of electrospun adsorbents, and provided an effective method to recycle the waste materials through one-step co-axial electrospinning. All the coaxial CS/CA-CNCs fibers exhibited smaller diameters and greater homogeneity compared to the non-layered ones. The presence of CNCs in the core of fibers significantly improved the tensile strength, and a comparable maximum adsorption capacity to that

of the non-layered ones was achieved by the core-sheath design with lower total CS content. Additionally, the deacetylated CS/CL-CNCs samples maintained the fibrous structure and showed an even higher tensile strength of 6.87±0.25 MPa as well as an acceptable adsorption capacity of 82.69±5.90 mg/g towards HA.

5.6. References

1. Osman, A.I., et al., *Reusing, recycling and up-cycling of biomass: A review of practical and kinetic modelling approaches.* Fuel Processing Technology, 2019. **192**: p. 179-202.

2. Zhou, C. and Y. Wang, *Recent progress in the conversion of biomass wastes into functional materials for value-added applications.* Science and technology of advanced materials, 2020. **21**(1): p. 787-804.

3. Deshmukh, A.R., et al., *Biodegradable films based on chitosan and defatted Chlorella biomass: Functional and physical characterization.* Food Chemistry, 2021. **337**: p. 127777.

4. Zhang, Y., et al., *Biomass chitosan derived cobalt/nitrogen doped carbon nanotubes for the electrocatalytic oxygen reduction reaction.* Journal of Materials Chemistry A, 2018. **6**(14): p. 5740-5745.

5. Canada, S., *Results of the Bioproducts Production and Development Survey 2015 (Catalogue no. 18-001-X).* 2017.

6. Hamed, O.A., et al., *Cellulose acetate from biomass waste of olive industry.* Journal of Wood Science, 2015. **61**(1): p. 45-52.

7. Cao, L., et al., *A novel process for obtaining high quality cellulose acetate from green landscaping waste.* Journal of Cleaner Production, 2018. **176**: p. 338-347.

8. Namboodiri, M.M.T. and K. Pakshirajan, *Chapter 10 - Valorization of waste biomass for chitin and chitosan production*, in *Waste Biorefinery*, T. Bhaskar, et al., Editors. 2020, Elsevier. p. 241-266.

9. Zhang, Y., F. Wang, and Y. Wang, *Recent developments of electrospun nanofibrous materials as novel adsorbents for water treatment.* Materials Today Communications, 2021. **27**: p. 102272.

10. Hamad, A.A., et al., *Electrospun cellulose acetate nanofiber incorporated with hydroxyapatite for removal of heavy metals.* International Journal of Biological Macromolecules, 2020. **151**: p. 1299-1313.

11. Su, H., et al., *Highly sensitive formaldehyde sensors based on CuO/ZnO composite nanofibrous mats using porous cellulose acetate fibers as templates.* International Journal of Biological Macromolecules, 2022. **206**: p. 653-660.

12. Goetz, L.A., et al., *Superhydrophilic anti-fouling electrospun cellulose acetate membranes coated with chitin nanocrystals for water filtration.* Journal of Membrane Science, 2016. **510**: p. 238-248.

13. Zhang, Y., F. Wang, and Y. Wang, *Electrospun Cellulose Acetate/Chitosan Fibers for Humic Acid Removal: Construction Guided by Intermolecular Interaction Study.* ACS Applied Polymer Materials, 2021. **3**(10): p. 5022-5029.

14. Pavithra, S., et al., *Batch adsorption studies on surface tailored chitosan/orange peel hydrogel composite for the removal of Cr(VI) and Cu(II) ions from synthetic wastewater.* Chemosphere, 2021. **271**: p. 129415.

15. Lu, F., et al., *3D hierarchical carbon nanofibers/TiO2@MoS2 core-shell heterostructures by electrospinning, hydrothermal and in-situ growth for flexible electrode materials.* Materials & Design, 2020. **189**: p. 108503.

16. Lan, T., et al., *Fabrication of hydroxyapatite nanoparticles decorated cellulose triacetate nanofibers for protein adsorption by coaxial electrospinning.* Chemical Engineering Journal, 2015. **260**: p. 818-825.

17. Wen, H.-F., et al., *Electrospun zein nanoribbons for treatment of lead-contained wastewater.* Chemical Engineering Journal, 2016. **290**: p. 263-272.

18. Anka, F.H. and K.J. Balkus, *Novel Nanofiltration Hollow Fiber Membrane Produced via Electrospinning.* Industrial & Engineering Chemistry Research, 2013. **52**(9): p. 3473-3480.

19. Merkle, V., et al., *Gelatin shells strengthen polyvinyl alcohol core–shell nanofibers.* Polymer, 2013. **54**(21): p. 6003-6007.

20. Tu, H., et al., *Incorporation of Layered Rectorite into Biocompatible Core–Sheath Nanofibrous Mats for Sustained Drug Delivery.* ACS Biomaterials Science & Engineering, 2021. **7**(9): p. 4509-4520.

21. Huang, S., et al., *Cellulose Nanocrystals Derived from Textile Waste through Acid Hydrolysis and Oxidation as Reinforcing Agent of Soy Protein Film.* Polymers, 2020. **12**(4).

22. Wang, Y., et al., *Transition Metal Ions Enable the Transition from Electrospun Prolamin Protein Fibers to Nitrogen-Doped Freestanding Carbon Films for Flexible Supercapacitors.* ACS Applied Materials & Interfaces, 2017. **9**(28): p. 23731-23740.

23. Hong, H.-J., et al., *Carboxymethlyated cellulose nanofibrils(CMCNFs) embedded in polyurethane foam as a modular adsorbent of heavy metal ions.* Carbohydrate Polymers, 2018. **195**: p. 136-142.

24. Guo, Z., et al., *Electrospun graphene oxide/carbon composite nanofibers with well-developed mesoporous structure and their adsorption performance for benzene and butanone.* Chemical Engineering Journal, 2016. **306**: p. 99-106.

25. Wang, X., et al., *Electrospun polyvinylidene fluoride-based fibrous nanocomposite membranes reinforced by cellulose nanocrystals for efficient separation of water-in-oil emulsions.* Journal of Membrane Science, 2019. **575**: p. 71-79.

26. Jiang, L., et al., *Improving mechanical properties of electrospun cellulose acetate nanofiber membranes by cellulose nanocrystals with and without polyvinylpyrrolidone.* Cellulose, 2020. **27**(2): p. 955-967.

27. Dodero, A., et al., *Chitosan-based electrospun membranes: Effects of solution viscosity, coagulant and crosslinker.* Carbohydrate Polymers, 2020. **235**: p. 115976.

28. Ni, X., et al., *Electrospun cellulose nanocrystals/poly(methyl methacrylate) composite nanofibers: Morphology, thermal and mechanical properties.* Carbohydrate Polymers, 2019. **206**: p. 29-37.

29. Patiño Vidal, C., et al., *Development of an antibacterial coaxial bionanocomposite based on electrospun core/shell fibers loaded with ethyl lauroyl arginate and cellulose nanocrystals for active food packaging.* Food Packaging and Shelf Life, 2022. **31**: p. 100802.

30. Drabczyk, A., et al., *Physicochemical Investigations of Chitosan-Based Hydrogels Containing Aloe Vera Designed for Biomedical Use.* Materials, 2020. **13**(14).

31. Phan, D.-N., et al., *Fabrication of electrospun chitosan/cellulose nanofibers having adsorption property with enhanced mechanical property.* Cellulose, 2019. **26**(3): p. 1781-1793.

32. Monisha, S., et al., *Preparation and characterization of biopolymer electrolyte based on cellulose acetate for potential applications in energy storage devices.* Journal of Materials Science: Materials in Electronics, 2016. **27**(9): p. 9314-9324.

33. Khatri, Z., et al., *Effect of deacetylation on wicking behavior of co-electrospun cellulose acetate/polyvinyl alcohol nanofibers blend.* Carbohydrate Polymers, 2012. **87**(3): p. 2183-2188.

34. Song, J., N.L. Birbach, and J.P. Hinestroza, *Deposition of silver nanoparticles on cellulosic fibers via stabilization of carboxymethyl groups.* Cellulose, 2012. **19**(2): p. 411-424.

35. Liu, C. and R. Bai, *Preparation of chitosan/cellulose acetate blend hollow fibers for adsorptive performance.* Journal of Membrane Science, 2005. **267**(1): p. 68-77.

36. Zhou, C., et al., *Construction of chevaux-de-frise from cellulose nanocrystals to enable mechano-bactericidal activity on recycled waste cotton films.* Green Chemistry, 2022.

37. Xie, L., et al., *Probing the intermolecular interaction mechanisms between humic acid and different substrates with implications for its adsorption and removal in water treatment.* Water Research, 2020. **176**: p. 115766.

38. de Mesquita, J.P., C.L. Donnici, and F.V. Pereira, *Biobased Nanocomposites from Layer-by-Layer Assembly of Cellulose Nanowhiskers with Chitosan.* Biomacromolecules, 2010. **11**(2): p. 473-480.

39. Tahmasebi, F., et al., *Performance evaluation of graphene oxide coated on cotton fibers in removal of humic acid from aquatic solutions.* Korean Journal of Chemical Engineering, 2019. **36**(6): p. 894-902.

40. Thuyavan, Y.L., et al., *Adsorptive Removal of Humic Acid by Zirconia Embedded in a Poly(ether sulfone) Membrane.* Industrial & Engineering Chemistry Research, 2014. **53**(28): p. 11355-11364.

41. Zulfikar, M.A., et al., *Preparation of Fe3O4-chitosan hybrid nano-particles used for humic acid adsorption.* Environmental Nanotechnology, Monitoring & Management, 2016. **6**: p. 64-75.

42. Wan Ngah, W.S., M.A.K.M. Hanafiah, and S.S. Yong, *Adsorption of humic acid from aqueous solutions on crosslinked chitosan–epichlorohydrin beads: Kinetics and isotherm studies.* Colloids and Surfaces B: Biointerfaces, 2008. **65**(1): p. 18-24.

43. Lin, J. and Y. Zhan, *Adsorption of humic acid from aqueous solution onto unmodified and surfactant-modified chitosan/zeolite composites.* Chemical Engineering Journal, 2012. **200-202**: p. 202-213.

Connecting Statement to Chapter 6

In Chapter 5, we successfully constructed core-shell structured fibers through one-step co-axial electrospinning. The overall mechanical properties of the CA/CS electrospun fibers were improved significantly by incorporating CNCs in the core of the fibers as a load-bearing component. Additionally, the removal efficiency of the fibers was improved, as evidenced by the comparable adsorption capacity obtained using core-sheath fibers with less mass proportion of CS. However, the adsorption process ceased upon reaching the maximum adsorption capacity, limiting the performance of the fibrous fibers. In Chapter 6, we aimed to extend the saturation point by incorporating TiO_2 nanoparticles in the CA/CS fibers, followed by the study on the synergistic effects of adsorption and photodegradation.

Chapter 6. One-step electrospinning of cellulose acetate/chitosan/TiO_2 fibrous membranes: efficient humic acid removal by synergistic adsorption and photocatalysis

6.1. Abstract

The removal of contaminants in water purification is limited by the adsorption equilibrium, while the efficiency of photocatalytic oxidation is highly dependent on the adsorption process at the surface of photocatalysts. What would happen if photocatalytic oxidation were combined with biopolymer-based adsorbents? In this work, nano-sized TiO_2 was employed as a model photocatalyst and incorporated in our previously developed highly efficient adsorbents - cellulose acetate (CA)/chitosan (CS) fibrous membranes by one-step electrospinning to continuously and synergistically remove humic acid (HA) from aqueous solutions. The effect of TiO_2 contents on the structure and properties of TiO_2-CA/CS composites was studied by scanning electron microscopy (SEM), Fourier transform infrared spectroscopy (FTIR), and tensile test, and the adsorption-photocatalysis experiment was carried out as a function of TiO_2 content, pH level, fiber composition, and irradiation time. The results indicated that TiO_2 was uniformly fixed in the electrospun CA/CS fibers. When the content of TiO_2 was 2 wt %, the composite fabric exhibited the highest tensile strength (21.84±0.85 MPa) and could continuously remove HA (87.79% in 3h without obvious saturation or fiber damage) at a low adsorbent dosage of 0.3 g/L. The HA removal efficiency of the TiO_2-CA/CS fibers under UV irradiation was higher than those of TiO_2-CA and CA/CS fibers, which also indicated a successful synergistic strategy.

Keywords: electrospinning, adsorption, photodegradation, synergistic effect, humic acid removal

6.2. Introduction

The demand for clean and readily available water is increasing, especially in the face of rapid industrialization and population growth. However, challenges for water supply systems, such as climate change, water scarcity, and urbanization, are still evolving. The World Health Organization (WHO) has emphasized that water reuse is becoming an important strategy to address the water

crisis (WHO, 2022). Water purification is an essential step in effectively implementing this measure into practice. Efforts have been made to develop various water treatment processes, including biological treatment, chemical coagulation, precipitation, membrane separation, oxidation, and adsorption (Marinho et al., 2019; Nidheesh and Singh, 2017; Roy and Saha, 2021; Yadav et al., 2019; Zhang et al., 2008a; Zhang et al., 2021b). Among them, adsorption is often considered superior to many other water treatment processes because the design of adsorbents is facile and it is easy to operate the adsorption equipment (Qiu et al., 2020). Our previous work demonstrated an efficient biodegradable electrospun cellulose acetate (CA)/chitosan (CS) fibrous adsorbent for humic acid (HA) removal; however, it reached the maximum adsorption capacity after 1 hour (Zhang et al., 2021a). Replacing or regenerating adsorbents can be a time-consuming and costly process. Numerous other approaches have been proposed to address the accumulation of HA in aqueous environments. These include aluminum salt coagulation of HA (Liu et al., 2009; Sudoh et al., 2015), electrochemical combustion of HA (Liao et al., 2008), ultrafiltration membrane separation (Szymański et al., 2016), and gamma radiation treatment (Sasaki et al., 2018). The treatment processes were often limited in terms of removal efficiency, material and energy consumption, and management of residuals and by-products (Tung et al., 2019).

Heterogenous photocatalysis employing semiconductor titanium dioxide (TiO_2) exhibited high efficacy for in-suit HA degradation (Birben et al., 2017; Liu et al., 2014; Tung et al., 2019). The remarkable photoactivity, chemical stability, non-toxicity, and abundance of TiO_2 have brought it tremendous attention for environmental remediation (Khorsandi et al., 2015). However, the use of powdery TiO_2 in water treatment can be challenging due to its tendency of agglomeration and subsequent reduced photocatalytic activities (Gebru and Das, 2017; Wang et al., 2013). It was also observed that the solution opacity increased at a higher catalyst concentration, leading to a

reduction of light penetration (Tung et al., 2019). Additional steps such as coagulation and sedimentation are required for recovery and reuse, which increase the risk of secondary contamination in the water system (Xu et al., 2013). Electrospinning is a facile and flexible technology to generate ultrafine fibrous membranes with large surface-to-volume ratios, which are desirable and reliable substrates for TiO_2 immobilization (Marinho et al., 2021). Enclosing the photocatalysts within such a membrane can overcome the aforementioned limitations and facilitate the reuse of photocatalysts in subsequent cycles. Moreover, the nature of the photocatalytic process is surface-oriented, and the efficiency of photo-oxidation is inseparable from the initial adsorption of the targeted contaminants onto the surface of photocatalysts (Rahman et al., 2021; Rao et al., 2016). Previous studies primarily focused on either adsorptive or photocatalytic properties of TiO_2 (Bi et al., 2021; Joung et al., 2006; Liao et al., 2012; Zhang et al., 2008b). It is hypothesized that by incorporating TiO_2 into CA/CS membranes via one-step electrospinning, the CA/CS matrix can provide the large active surface area and high affinity for the adsorption of HA and facilitate the subsequent surface-oriented photodegradation of HA, while TiO_2 nanoparticles fixed in the fibers can oxidize the adsorbed HA by creating reactive oxygen species (ROS) to enable the postponed saturation point of the membrane and higher removal capacity. Therefore, this study intends to explore the synergistic effects of adsorption and photooxidation processes facilitated by TiO_2 within the electrospun CA/CS matrix, which have been seldom reported in the context of HA removal and biopolymer-based fibers. In this work, the morphological and structural properties of electrospun TiO_2-CA/CS fibers were studied and characterized by scanning electron microscopy (SEM) and Fourier transform infrared (FT-IR) spectroscopy. The impacts of TiO_2 content, pH level, fiber composition, and reaction conditions on the removal of HA were examined, and the synergistic effect of surface adsorption and photocatalytic oxidation was confirmed by comparing

the removal efficiencies of TiO_2-CA, TiO_2-CA/CS, and CA/CS fibers. By combining traditional membrane adsorption with nanomaterial catalysis, this work is expected to inspire new ideas for the rational design of efficient adsorbents for water treatment.

6.3. Experimental methods

6.3.1. Materials

Cellulose acetate (CA) tow that is used to produce cigarette filters was kindly provided by Celanese Corporation (Irving, US) with a molecular weight of 75-95 kDa, acetyl content of 39.95 wt %, and degree of substitution of ~2.47. Chitosan (CS) synthesized from crab shell with a molecular weight of 190-310 kDa and degree of deacetylation of 75-85%, was provided by Dr. Benjamin Simpson (Department of Food Science and Agricultural Chemistry, McGill University, Quebec, Canada). Acetic acid (CH_3COOH, glacial), humic acid (sodium salt, $C_9H_8Na_2O_4$ 45–70%), titanium dioxide (TiO_2, particle size of ~ 20 nm), sodium hydroxide (NaOH, ACS reagent grade), and sulfuric acid (H_2SO_4, ACS reagent grade) were all purchased from Fisher Scientific (Mississauga, ON, Canada) and used as received without further purification. Deionized water was used throughout all experiments.

6.3.2. One-step electrospinning of TiO_2-CA/CS fibrous membranes

Desired amounts of CA and CS were dissolved in 85 wt % acetic acid solution and stirred for 48 h. Different amounts of TiO_2 nanoparticles were also dispersed in 85 wt % acetic acid solution by using Vortex at 3000 rpm, and the suspensions were subsequently sonicated for 90 min and added into the CA/CS solutions, which were placed in the sonication bath for another 90 min. The prepared TiO_2-CA/CS composite solutions were forced through a stainless-steel needle with a

diameter of 0.66 mm, and the fibers were collected on a stainless-steel drum rotating at 10 rpm. Electrospinning conditions were optimized in our preliminary experiment to allow the steady generation of fibers. The summary of sample compositions and the optimized electrospinning conditions is listed in Table 6.1. The electrospun fabrics were vacuum-dried in a desiccator at room temperature overnight to expel possible solvent residues. In order to confirm the synergistic effect of photocatalysis and adsorption, electrospun TiO_2-CA fibrous membranes were prepared by the same method as abovementioned.

Table 6.1. Solution compositions and optimized electrospinning conditions of various fibrous membranes.

Samples	CA content (wt %)	CS content (wt %)	TiO_2 content (wt %)	Electrospinning conditions		
				Applied voltage (kV)	Tip-to-collector distance (cm)	Flow rate (mL h^{-1})
›TiO_2-CA/CS	3	3	1	23.5	11.5	1
›TiO_2-CA/CS	3	3	2	26	11.5	1.2
›TiO_2-CA/CS	3	3	3	30	10	1.6
TiO_2-CA	11	0	2	20	12	0.8

6.3.3. Characterization of TiO_2-CA/CS fibrous membranes

Morphological observation of TiO_2-CA/CS fibrous membranes was done using a Hitachi SU-3500 SEM (Hitachi, Tokyo, Japan) operating at 30 kV. All samples were coated with 4 nm of platinum/gold layers using a Leica EM ACE200 coater (Leica, Wetzlar, Germany) prior to the observation. To measure the fiber diameters, SEM images of various samples under a magnification of ×10 k were selected from which four hundred random positions were measured for each sample using the ImageJ image-visualization software (developed by the National Institute of Health) (Wang et al., 2017). The chemical structure of the electrospun fibers was

analysed with a Varian Excalibur 3100 FT-IR spectrometer (Varian, Melbourne, Australia) equipped with an attenuated total reflectance accessory (Specac, Orpington, UK). Each FT-IR spectrum was recorded in transmittance mode as the average of 64 scans with a resolution of 4 cm^{-1}. Uniaxial tensile testing of the fibrous membranes was carried out on an ADMET eXpert 7601 testing machine (ADMET, Norwood, MA, USA) at the fixed initial grip-separation distance of 10 mm and crosshead velocity of 1 mm min^{-1}. Five specimens with dimensions of 30 mm × 10 mm (length × width) from each sample were measured according to the ASTM D-638-V standard (Selling et al., 2011). The thickness of each sample was measured from SEM images using the ImageJ image-visualization software. The tensile strength (σ) of the electrospun membranes was determined and calculated from the following equation:

$$\sigma = \frac{F}{A} \qquad (6-1)$$

6.3.4. Synergistic removal of HA

The performance of TiO_2-CA/CS fibrous membranes towards HA removal was investigated by batch experiments. The removal rate of HA was determined as the functions of TiO_2 content, treatment time, and pH level of the solution under the optimized conditions as follows: membrane dosage of 0.3 g L^{-1} (approximately 20mm × 10mm, length × width), HA solution volume of 20 mL, HA initial concentration of 30 ppm, and stirring speed of 150 rpm (Zhang et al., 2021a). Stock solution with a concentration of 100 ppm HA was prepared and further diluted to obtain HA solutions with lower concentrations. Sulfuric acid and sodium hydroxide were used to adjust the pH levels of HA solutions. Batch experiments were carried out in 25 mL glass vials, and a 20 W UV lamp with a standard wavelength of 365 nm was used as the light source. The distance between the lamp and the water surface was 10 cm. The performance of the TiO_2-CA/CS membranes

towards HA removal in dark conditions was also evaluated. To calculate the HA concentration before and after the treatment, a calibration curve was prepared with a series of standard solutions with known HA concentrations. The UV-vis absorbance of the solutions at 271 nm was measured using a Hitachi UV-2000 UV-vis spectrophotometer (Hitachi, Tokyo, Japan). The removal efficiency was calculated as follows:

$$\text{removal efficiency } (\%) = \frac{(C_0 - C_i)}{C_0} \times 100\% \qquad (6-2)$$

where C_0 (mg/L) is the initial HA concentration in the solution and C_i (mg/L) is the equilibrium HA concentration.

The kinetics of photocatalyzed oxidation were studied by applying and modeling the experimental data into the Langmuir-Hinshelwood kinetic model:

$$\mathrm{r} = -\frac{dC}{dt} = \frac{k_r K C}{1 + KC} \qquad (6-3)$$

where r (mg/ (L min)) represents the rate of reaction that changes with time; C (mg/L) is the concentration of HA solution at time t (min); k_r (mg/(L min)) is the rate constant of the reaction; and K (L/mg) is the equilibrium constant for adsorption of the substrate onto the catalyst. Equation (6-3) can be integrated between the limits: $C=C_0$ at $t=0$ and $C=C$ at $t=t$, which is expressed as:

$$\ln\left(\frac{C_0}{C}\right) + K(C_0 - C) = k_r K t \qquad (6-4)$$

where C_0 (mg/L) is the initial HA concentration in the solution (Kumar et al., 2008).

6.3.5. Statistical analysis

Statistical interpretations of the results were evaluated by analysis of variance (ANOVA) followed by multiple comparison tests of the means using Duncan's multiple-range test at a 95% confidence level. All statistical analyses were done using SPSS statistical software (version 27, IBM, Armonk, NY, USA) with a $p < 0.05$ considered to be significant. The results were expressed as the mean of at least three replicates ± standard deviation.

6.4. Results and Discussion

6.4.1. Structure of TiO_2-CA/CS fibrous membranes

FT-IR was employed to understand the component interactions and characteristic chemical information of TiO_2-CA/CS fibrous membranes. As shown in Figure 6.1, all the samples had the characteristic peaks of CA at 3500 cm^{-1}, 1750 cm^{-1}, and 1372 cm^{-1} (representing O-H stretching, C=O vibration, and CH_3 groups of the acetyl moiety) (Monisha et al., 2016; Zhang et al., 2021a), and the typical infrared diffraction peaks of CS at 3350 cm^{-1} (-OH and -NH groups) and 1600 cm^{-1}, 1100 cm^{-1}, and 885 cm^{-1} (amine groups) (Sharaf et al., 2021). Compared to the spectrum of TiO_2-CA, all the other samples showed downfield shifts from the peak at 3500 cm^{-1} to the broad peak at 3350 cm^{-1}, which revealed the hydrogen bonding interactions between the amine groups of CS and acetyl groups of CA (Gopi et al., 2019). After introducing TiO_2 nanoparticles, TiO_2-CA and TiO_2-CA/CS fibers exhibited new and similar adsorption patterns in the wavenumber range of 350 cm^{-1} to 750 cm^{-1}, which was assigned to the vibration of Ti-O-Ti network and confirmed the successful incorporation of TiO_2 into the CA/CS fibrous matrix (Tsiourvas et al., 2011). However, the change in TiO_2 contents didn't affect the intensities of the characteristic peaks, suggesting that the incorporation of TiO_2 nanoparticles did not significantly impact the structure of CA/CS fibers.

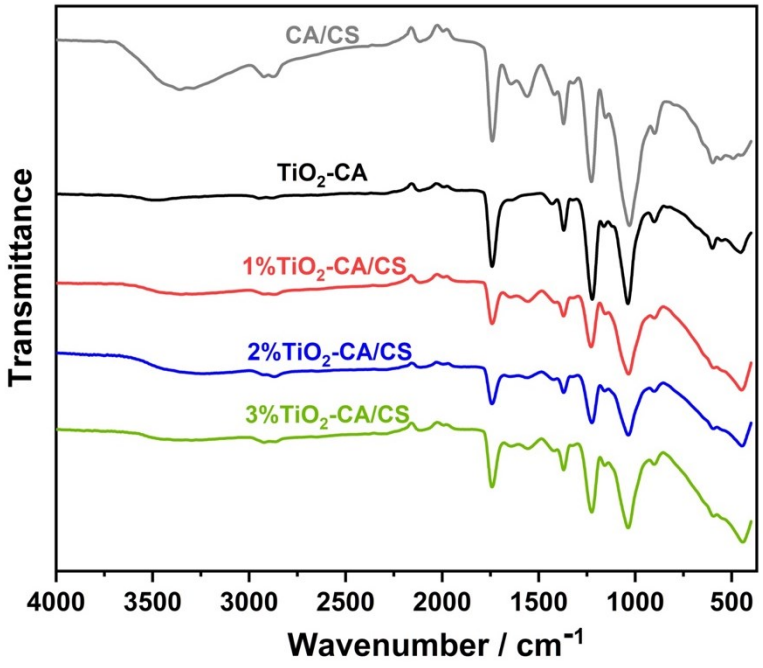

Figure 6.1. FTIR spectra of CA/CS, TiO_2-CA, 1%TiO_2-CA/CS, 2%TiO_2-CA/CS, and 3%TiO_2-CA/CS electrospun fibers.

To investigate the effect of TiO_2 on the electrospun fibers, the morphologies of the fabrics with various compositions were observed by SEM and the images are shown in Figure 6.2. All the samples exhibited ultrafine and continuous fibrous structures with nano-scaled diameters, which are highly desirable for the adsorption and photocatalysis processes (Erhayem and Sohn, 2014; Liu et al., 2014; Lv et al., 2011). The average fiber diameters of 1%TiO_2-CA/CS, 2%TiO_2-CA/CS, and 3%TiO_2-CA/CS were 16.0±7.7, 12.6±4.2, and 15.08±8.2 nm, respectively, and were much smaller than those of TiO_2-CA (149.9±39.2 nm) and the electrospun CA/CS fibers reported in our previous study (Zhang et al., 2021a). It might be due to the higher voltage applied, the shorter tip-to-collector distances, and consequently the enhanced electrical field during electrospinning, resulting in a better stretch of the fibers (He et al., 2015; Kiennork et al., 2015). It was observed that more concave/convex fibers and beads were presented in the 3% TiO_2-CA/CS sample. These

were caused by the formation of an unstable Taylor cone in the presence of high TiO_2 loading amounts and the possible agglomeration of the nanoparticles (Gebru and Das, 2017; Zhang et al., 2021b).

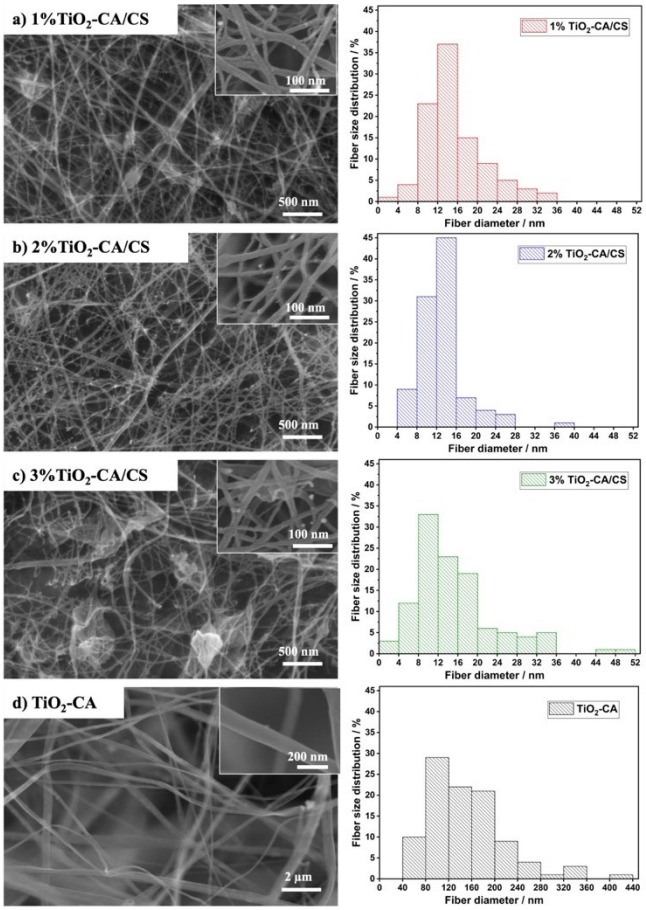

Figure 6.2. SEM images and fiber diameter distributions of (a) 1%TiO_2-CA/CS, (b) 2%TiO_2-CA/CS, (c) 3%TiO_2-CA/CS, and (d) TiO_2-CA electrospun fibers.

6.4.2. Mechanical properties of TiO_2-CA/CS fibrous membranes

As shown in Figure 6.3, the tensile strength of 1%TiO_2-CA/CS, 2%TiO_2-CA/CS, and 3%TiO_2-CA/CS were 19.02±0.91, 21.84±0.85, and 13.02±1.01, respectively. The addition of TiO_2 nanoparticles into the CA/CS matrix remarkably improved the tensile strength (Zhang et al.,

2021a). It could be explained by the transfer and diversion of force from the CA/CS fibers to the nanoparticles, and the stable interface between TiO_2 and the CA/CS matrix (Habiba et al., 2019; Kochkina & Butikova, 2019). The significantly higher tensile strength of the 2%TiO_2-CA/CS sample corresponded to its homogeneous fibrous structure and well dispersed TiO_2 nanoparticles, which resulted in better stress distribution and energy absorption (Feng et al., 2019; Zhang et al., 2021a). All the TiO_2-CA/CS membranes showed higher tensile strength than that of the TiO_2-CA sample (2.19±0.17 MPa). It can be attributed to the hydrogen bonding interactions between the amine groups of CS and the acetyl groups of CA that contributed to the retardation of loading stress (Han et al., 2019). However, the introduction of TiO2 had a negative impact on the strain of the TiO2-CA/CS membranes. With the increase of the TiO_2 contents from 1 wt% to 3 wt%, the elongation at break of the membranes reduced considerably from 1.61±0.11 % to 0.98±0.07 %, because the TiO_2 nanoparticles restrained the matrix flexibility and mobility. Similar phenomena were reported in TiO_2-reinforced starch-based nanocomposite films (Oleyaei et al., 2016).

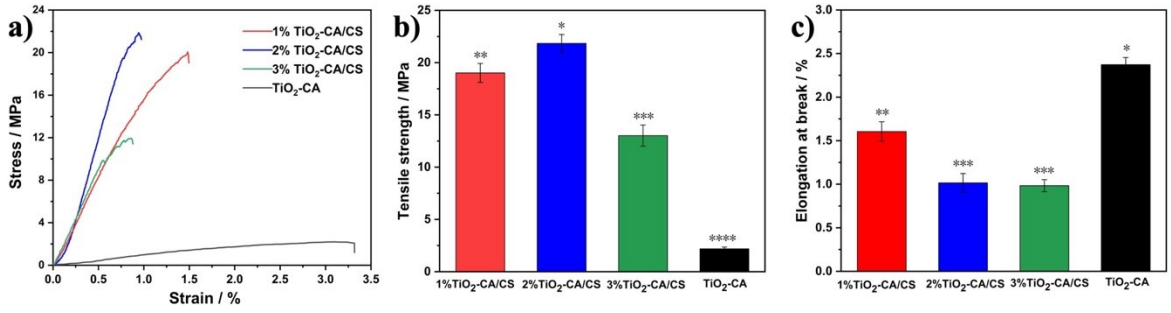

Figure 6.3. Mechanical properties of the electrospun fibrous membranes: (a) stress-strain curves, (b) tensile strength, and (c) elongation at break. Different asterisks on the top of each column represent significant differences ($p < 0.05$).

6.5. Removal of HA

6.5.1. Effect of pH

The effect of initial solution pH on HA removal using electrospun TiO_2-CA/CS membranes was investigated within a pH range of 4 to 12. Experiments conducted at pH<4 were excluded due to the coagulation and precipitation of HA (Abate and Masini, 2003; Brigante et al., 2007; Zhang et al., 2021a). As depicted in Figure 6.4, the synergistic removal efficiency of HA using TiO_2-CA/CS was pH-dependent and increased at lower pH values. The p*Ka* values of HA and the primary amine of CS were around 4.0 and 6.5, respectively, and the point of zero charge (pzc) value of TiO_2 falls within a pH range of 6.0 to 7.5 (Laird and Koskinen, 2008; Mohammed et al., 2017; Paz, 2006). Therefore, at pH=4, electrostatic attraction occurred between the deprotonated carboxylic groups of HA and the positively charged CS and TiO_2 nanoparticles, contributing to the superior removal efficiency towards HA. Meanwhile, the nonpolar methyl groups of CA interacted with the hydrophobic moieties of HA through hydrophobic interaction, and the positive charges of TiO_2 were favorable for transferring photo-generated electrons to the surface of TiO_2 and discouraging the recombination of photoelectrons and photoholes, leading to the prolonged generation of ROS (Xue et al., 2011). It was worth noting that the 2%TiO_2-CA/CS sample showed the highest removal efficiency towards HA at all pH levels, while the TiO_2-CA fibers were the least efficient. It confirmed that the strong adsorption of HA onto the surface of the electrospun fibers was highly conducive to the photocatalytic process (Krasian et al., 2019).

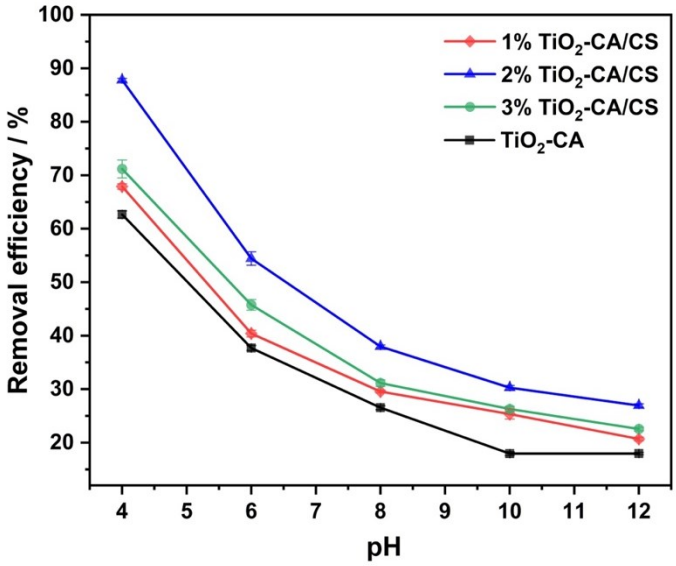

Figure 6.4. Effect of pH on the removal of HA using electrospun TiO_2-CA/CS and TiO_2-CA fibrous membranes (dosage: 0.3 g/L; initial concentration of HA solution: 30 ppm; volume: 20 mL; and irradiation time: 180 min)

6.5.2. Effect of irradiation time

The removal efficiencies of various TiO_2-incorporated fibrous composites under UV irradiation or in the dark as a function of treatment time are illustrated in Figure 6.5 (a). The synergistic effect of adsorption and photocatalysis was evaluated by comparing with the photocatalysis under UV irradiation without the adsorptive sites of CS and the adsorption of TiO_2-CA/CS fibers in dark conditions. All samples exhibited rapid removal of HA within the first 30 min, implying tremendously available adsorptive sites. The adsorption process usually occurs faster than the photocatalytic oxidation (Liu et al., 2014). As the adsorption process continued, the active sites became increasingly occupied, and the removal efficiencies of the samples in the dark reached the equilibrium after approximately 60 min, which was in accordance with our previous report (Zhang et al., 2021a). The TiO_2-CA membrane adsorbed HA through the hydrophobic interaction between

HA and CA and surface complexation of TiO_2 and HA (Sun and Lee, 2012). However, its removal efficiency in the dark was the lowest because of the absence of CS. It was noteworthy that 1%-3% TiO_2-CA/CS fibrous membranes demonstrated continuous removal of HA from the aqueous solution under UV irradiation, and the removal efficiencies were approximately 1.5 times higher than those achieved by adsorption solely within 180 min. Moreover, the removal efficiency of TiO_2-CA with UV irradiation was also lower than those of the 1%-3% TiO_2-CA/CS membranes, demonstrating the remarkable synergistic effect of the adsorption process and photocatalytic activity towards the removal of HA. The 2% TiO_2-CA/CS sample exhibited the highest efficiency due to the uniform fibrous structure, which facilitated the adsorption and degradation of HA. Table 6.2 summarizes several TiO_2-incorporated photocatalysts for HA removal, and the fibrous TiO_2-CA/CS membranes reported here showed a comparable removal efficiency at a lower dosage of 0.3 g/L.

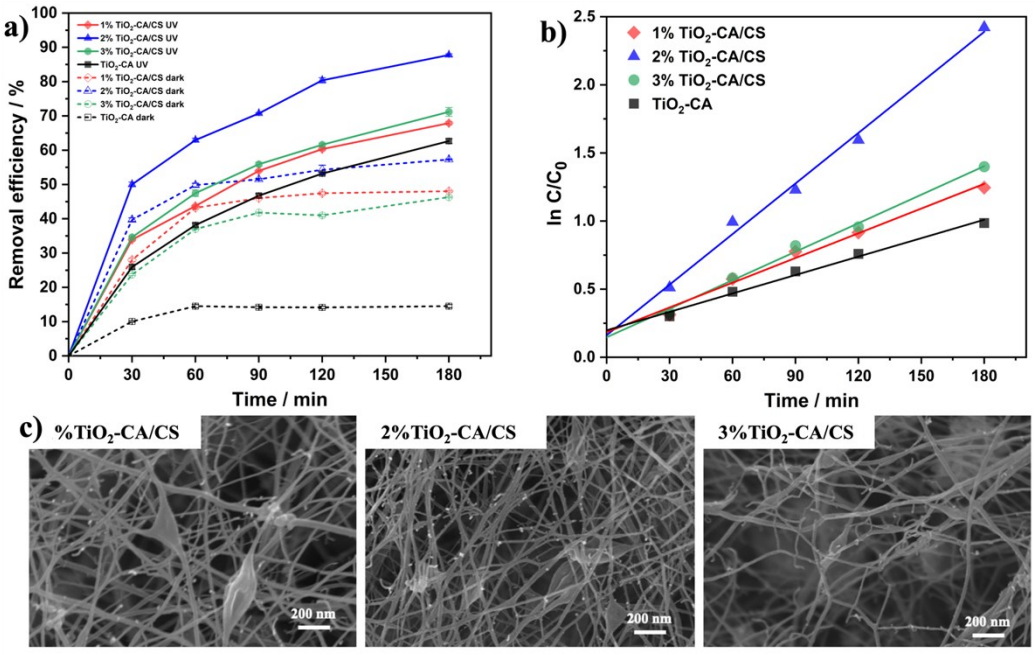

Figure 6.5. (a) Removal efficiency of TiO_2-incorporated fibers with various compositions under UV irradiation or in dark, (b) kinetics of HA removal using TiO_2-incorporated fibers (pH: 4.0; dosage: 0.3 g/L;

initial concentration of HA solution: 30 ppm; volume: 20 mL), and (c) SEM images of TiO_2-CA/CS fibers after 180 min UV irradiation.

Table 6.2. List of previously reported TiO_2 based photocatalysts for HA removal.

Photocatalysts	Dosage (g/L)	Removal efficiency (%)	Time (min)	References
Molybdenum-doped TiO_2 nanoparticles	2	83	200	(Abedi et al., 2022)
Reduced graphene oxide- TiO_2 nanocomposites	1.2	88.7	180	(Zhou et al., 2019)
Fe-doped TiO_2 nanoparticles	0.4	74	60	(Kamani et al., 2021)
Fe-doped TiO_2@Fe_3O_4	0.4	100	60	(Moein et al., 2020)
N-doped TiO_2 nanotubes/graphene composite film	1	92.3	120	(Wang et al., 2022)
TiO_2-coated ceramic foam		83	720	(Mori et al., 2013)
This study	0.3	87.7	180	

6.5.3. Kinetics of HA removal

To examine and compare the removal rates of HA using various TiO_2-incorporated fibrous composites, the experimental data were fitted into the Langmuir-Hinshelwood kinetic model, which is the most commonly used kinetic expression of the heterogenous catalytic processes (Kumar et al., 2008). The kinetics and fitted parameters are shown in Figure 6.5 (b) and listed in Table 6.3, respectively. The obtained square correlation coefficients (R^2) for all the samples were above 0.96, suggesting that the removal of HA using TiO_2-incorporated fibrous membranes was well fitted by the Langmuir-Hinshelwood kinetic model and relied on the synergistic adsorption upon the fibers and oxidation of HA by TiO_2 in the matrix. The 2%TiO_2-CA/CS sample exhibited an noticeably higher constant rate, whereas TiO_2-CA had the lowest constant rate, which further confirmed the superior removal performance of 2%TiO_2-CA/CS and the success of the synergistic

strategy. The morphologies of the fibrous composites after 180 min UV irradiation are shown in Figure 6.5 (c). It was evident that no significant changes in the structural integrity and fibrous morphologies were observed. It demonstrated the stability of the electrospun CA/CS fibers, and the fibrous structure was important for the continuous removal of contaminants and the recovery of TiO_2 nanoparticles (Li et al., 2022).

Table 6.3. Summary of fitted parameters of HA removal using the Langmuir-Hinshelwood kinetic model.

Samples	k_r (mg/ (L min))	R^2
1%TiO_2-CA/CS	0.027	0.975
2%TiO_2-CA/CS	0.051	0.992
3%TiO_2-CA/CS	0.029	0.988
TiO_2-CA	0.021	0.961

6.6. Conclusions

The hypothesis has been confirmed that, by one-step electrospinning, the TiO_2-CA/CS fibrous membranes could extend the removal of HA from the aqueous solution via synergistic effects of adsorption and photodegradation. The removal efficiency of HA varied at different pH values, TiO_2 loading amounts, and fiber compositions. Due to the ultrafine fibrous morphology, homogeneity, and uniform distribution of TiO_2 catalysts, the 2%TiO_2-CA/CS fibrous membrane exhibited the highest tensile strength and removal efficiency towards HA. With a low fiber dosage of 0.3 g/L, a removal ratio of 87.7% was achieved under UV irradiation after 180 min, while the sample in the dark could only remove 54.2% of HA and the adsorption reached the equilibrium after 60 min. Hence, this work presents a promising strategy for developing high-performance adsorbents for wastewater treatment.

6.7. References

Abate G, Masini JC (2003) Influence of pH and ionic strength on removal processes of a sedimentary humic acid in a suspension of vermiculite. Colloids Surf. A: Physicochem Eng Asp 226:25-34. https://doi.org/https://doi.org/10.1016/S0927-7757(03)00418-7

Abedi K, Shahmoradi B, Wantala K, Suwannaruang T, Amini N, Maleki A, Lee SM, Shivaraju HP (2022) Immobilized Mo:TiO_2 nanoparticles for humic acid removal in an aqueous medium using solar spectrum. J Mater Sci: Mater Electron 33:16777-16788. https://doi.org/10.1007/s10854-022-08542-w

Bi L, Chen Z, Li L, Kang J, Zhao S, Wang B, Yan P, Li Y, Zhang X, Shen J (2021) Selective adsorption and enhanced photodegradation of diclofenac in water by molecularly imprinted TiO_2. J Hazard Mater 407:124759. https://doi.org/10.1016/j.jhazmat.2020.124759

Birben NC, Uyguner-Demirel CS, Kavurmaci SS, Gürkan YY, Turkten N, Cinar Z, Bekbolet M (2017) Application of Fe-doped TiO_2 specimens for the solar photocatalytic degradation of humic acid. Catal Today 281:78-84. https://doi.org/https://doi.org/10.1016/j.cattod.2016.06.020

Brigante M, Zanini G, Avena M (2007) On the dissolution kinetics of humic acid particles: Effects of pH, temperature and Ca^{2+} concentration. Colloids Surf A: Physicochem Eng Asp 294: 64-70. https://doi.org/https://doi.org/10.1016/j.colsurfa.2006.07.045

Erhayem M, Sohn M (2014) Stability studies for titanium dioxide nanoparticles upon adsorption of Suwannee River humic and fulvic acids and natural organic matter. Sci Total Environ 468-469:249-257. https://doi.org/https://doi.org/10.1016/j.scitotenv.2013.08.038

Feng S, Zhang F, Ahmed S, Liu Y (2019) Physico-Mechanical and Antibacterial Properties of PLA/TiO_2 Composite Materials Synthesized via Electrospinning and Solution Casting Processes. Coatings 9:525. https://doi.org/10.3390/coatings9080525

Gebru KA, Das C (2017) Removal of Pb (II) and Cu (II) ions from wastewater using composite electrospun cellulose acetate/titanium oxide (TiO_2) adsorbent. J Water Process Eng 16:1-13. https://doi.org/https://doi.org/10.1016/j.jwpe.2016.11.008

Gopi S, Pius A, Kargl R, Kleinschek KS, Thomas S (2019) Fabrication of cellulose acetate/chitosan blend films as efficient adsorbent for anionic water pollutants. Polymer Bulletin 76:1557-1571. https://doi.org/10.1007/s00289-018-2467-y

Habiba U, Lee JJL, Joo TC, Ang BC, Afifi AM (2019) Degradation of methyl orange and congo red by using chitosan/polyvinyl alcohol/TiO_2 electrospun nanofibrous membrane. Int J Biol Macromol 131:821-827. https://doi.org/https://doi.org/10.1016/j.ijbiomac.2019.03.132

Han X, Ye Y, Lam F, Pu J, Jiang F (2019) Hydrogen-bonding-induced assembly of aligned cellulose nanofibers into ultrastrong and tough bulk materials. J Mater Chem 7:27023-27031. https://doi.org/10.1039/C9TA11118B

He X, Cheng L, Zhang X, Xiao Q, Zhang W, Lu C (2015) Tissue engineering scaffolds electrospun from cotton cellulose. Carbohydr Polym 115:485-493. https://doi.org/https://doi.org/10.1016/j.carbpol.2014.08.114

Joung S, Amemiya K, Murabayashi M, Itoh K (2006) Adsorbed species on TiO2 associated with the photocatalytic oxidation of trichloroethylene under UV. J Photochem Photobiol A: Chem 184:273-281. https://doi.org/10.1016/j.jphotochem.2006.04.040

Kamani H, Ashrafi SD, Jahantiq A, Norabadi E, Dashti Zadeh M (2021) Catalytic degradation of humic acid using Fe–doped TiO_2 - ultrasound hybrid system from aqueous solution. Int J Environ Anal Chem 103:8017-8031. https://doi.org/10.1080/03067319.2021.1979535

Khorsandi H, Bina B, Khorsandi J (2015) Evaluation of UV/TiO_2 Photo-Catalytic Process for Removing Humic Compounds from Water. Pol J Environ Stud 24:1063-1068

Kiennork S, Nakhowong R, Chueachot R, Tipparach U (2015) Preparation and Characterization of Electrospun TiO_2 Nanofibers via Electrospinning. Integr Ferroelectr 165:131-137. https://doi.org/10.1080/10584587.2015.1063915

Kochkina NE, Butikova OA (2019) Effect of fibrous TiO_2 filler on the structural, mechanical, barrier and optical characteristics of biodegradable maize starch/PVA composite films. Int J Biol Macromol 139:431-439. https://doi.org/https://doi.org/10.1016/j.ijbiomac.2019.07.213

Krasian T, Punyodom W, Worajittiphon P (2019) A hybrid of 2D materials (MoS_2 and WS_2) as an effective performance enhancer for poly(lactic acid) fibrous mats in oil adsorption and oil/water separation. Chem Eng J 369:563-575. https://doi.org/https://doi.org/10.1016/j.cej.2019.03.092

Kumar KV, Porkodi K, Rocha F (2008) Langmuir–Hinshelwood kinetics – A theoretical study. *Catal Commun 9*:82-84. https://doi.org/https://doi.org/10.1016/j.catcom.2007.05.019

Laird DA, Koskinen WC (2008) Chapter 21 - Triazine Soil Interactions. In LeBaron HM, McFarland JE, Burnside OC (eds) The Triazine Herbicides, 1st edn. Elsevier, Amsterdem, pp. 275-299. https://doi.org/https://doi.org/10.1016/B978-044451167-6.50024-6

Li W, Zhang H, Chen W, Yang L, Wu H, Mao N (2022) The effects of cotton cellulose on both energy band gap of g-C_3N_4–TiO_2 nanoparticles and enhanced photocatalytic properties of cotton-g-C_3N_4–TiO_2 composites. Cellulose 29:193-212. https://doi.org/10.1007/s10570-021-04318-3

Liao AA, Spitzer M, Motheo AJ, Bertazzoli R (2008) Electrocombustion of humic acid and removal of algae from aqueous solutions. J Appl Electrochem 38:721-727. https://doi.org/10.1007/s10800-008-9502-x

Liao J, Lin S, Pan N, Li D, Li S, Li J (2012) Free-standing open-ended TiO2 nanotube membranes and their promising through-hole applications. Chem Eng J 211–212:343-352. https://doi.org/10.1016/j.cej.2012.09.070

Liu H, Hu C, Zhao H, Qu J (2009) Coagulation of humic acid by PACl with high content of Al13: The role of aluminum speciation. Sep Purif Tech 70:225-230. https://doi.org/10.1016/j.seppur.2009.09.020

Liu S, Lim M, Amal R (2014) TiO_2-coated natural zeolite: Rapid humic acid adsorption and effective photocatalytic regeneration. Chem Eng Sci 105:46-52. https://doi.org/https://doi.org/10.1016/j.ces.2013.10.041

Lv T, Pan L, Liu X, Lu T, Zhu G, Sun Z (2011) Enhanced photocatalytic degradation of methylene blue by ZnO-reduced graphene oxide composite synthesized via microwave-assisted reaction. J Alloys Compd 509:10086-10091. https://doi.org/https://doi.org/10.1016/j.jallcom.2011.08.045

Marinho BA, Cristóvão RO, Boaventura RAR, Vilar VJP (2019) As(III) and Cr(VI) oxyanion removal from water by advanced oxidation/reduction processes—a review. Environ Sci Pollut Res 26:2203-2227. https://doi.org/10.1007/s11356-018-3595-5

Marinho BA, de Souza SMAGU, de Souza AAU, Hotza D (2021) Electrospun TiO_2 nanofibers for water and wastewater treatment: a review. J Mater Sci 56:5428-5448. https://doi.org/10.1007/s10853-020-05610-6

Moein H, Nabi Bidhendi G, Mehrdadi N, Kamani H (2020) Efficiency of Photocatalytic Degradation of Humic Acid Using Magnetic Nanoparticles (Fe-doped TiO_2@Fe_3O_4) in Aqueous Solutions. Health Scope 9:e102577. https://doi.org/10.5812/jhealthscope.102577

Mohammed MA, Syeda JTM, Wasan KM, Wasan EK (2017) An Overview of Chitosan Nanoparticles and Its Application in Non-Parenteral Drug Delivery. Pharmaceutics 9:53 https://doi.org/10.3390/pharmaceutics9040053

Monisha S, Selvasekarapandian S, Mathavan T, Milton Franklin Benial A, Manoharan S, Karthikeyan S (2016) Preparation and characterization of biopolymer electrolyte based on cellulose acetate for potential applications in energy storage devices. J Mater Sci: Mater Electron 27:9314-9324. https://doi.org/10.1007/s10854-016-4971-x

Mori M, Sugita T, Mase A, Funatogawa T, Kikuchi M, Aizawa K, Kato S, Saito Y, Ito T, Itabashi H (2013) Photodecomposition of humic acid and natural organic matter in swamp water using a TiO_2-coated ceramic foam filter: Potential for the formation of disinfection byproducts. Chemosphere 90:1359-1365. https://doi.org/https://doi.org/10.1016/j.chemosphere.2012.07.056

Nidheesh PV, Singh TSA (2017) Arsenic removal by electrocoagulation process: Recent trends and removal mechanism. Chemosphere 181:418-432. https://doi.org/https://doi.org/10.1016/j.chemosphere.2017.04.082

Oleyaei SA, Almasi H, Ghanbarzadeh B, Moayedi AA (2016) Synergistic reinforcing effect of TiO_2 and montmorillonite on potato starch nanocomposite films: Thermal, mechanical and barrier properties. Carbohydr Polym 152:253-262. https://doi.org/https://doi.org/10.1016/j.carbpol.2016.07.040

Paz Y (2006) Preferential photodegradation – why and how? Comptes Rendus Chimie 9:774-787. https://doi.org/https://doi.org/10.1016/j.crci.2005.03.032

Qiu Z, Wang M, Zhang T, Yang D, Qiu F (2020) In-situ fabrication of dynamic and recyclable TiO2 coated bacterial cellulose membranes as an efficient hybrid absorbent for tellurium extraction. Cellulose 27:4591–4608. https://doi.org/10.1007/s10570-020-03096-8

Rahman MM, Huang D, Ewulonu CM, Wang C, Kuga S, Wu M, Huang Y (2021) Preparation of multifunctional cellulosic fabric based on graphene/TiO_2 nanocoating. Cellulose 28:1153-1165. https://doi.org/10.1007/s10570-020-03558-z

Rao G, Zhang Q, Zhao H, Chen J, Li Y (2016) Novel titanium dioxide/iron (III) oxide/graphene oxide photocatalytic membrane for enhanced humic acid removal from water. Chem Eng J 302:633-640. https://doi.org/https://doi.org/10.1016/j.cej.2016.05.095

Roy M, Saha R (2021) 6 - Dyes and their removal technologies from wastewater: A critical review. In Bhattacharyya S, Mondal NK, Platos J, Snášel V, Krömer P (Eds), Intelligent Environmental Data Monitoring for Pollution Management, Academic Press, pp. 127-160. https://doi.org/https://doi.org/10.1016/B978-0-12-819671-7.00006-3

Sasaki T, Goto R, Saito T, Kobayashi T, Ikuji T, Sugiyama Y (2018) Gamma-ray irradiation impact of humic substances on apparent formation constants with Cu(II). J Nucl Sci Technol 55:1299-1308. https://doi.org/10.1080/00223131.2018.1503573

Selling, G. W., Woods, K. K., and Biswas, A. (2011). Electrospinning formaldehyde-crosslinked zein solutions. *Polymer International*, *60*(4), 537-542. https://doi.org/https://doi.org/10.1002/pi.3009

Sharaf SM, Al-Mofty SED, El-Sayed ESM, Omar A, Abo Dena AS, El-Sherbiny IM (2021) Deacetylated cellulose acetate nanofibrous dressing loaded with chitosan/propolis nanoparticles for the effective treatment of burn wounds. Int J Biol Macromol 193:2029-2037. https://doi.org/https://doi.org/10.1016/j.ijbiomac.2021.11.034

Sudoh R, Islam MDS, Sazawa K, Okazaki T, Hata N, Taguchi S, Kuramitz H (2015) Removal of dissolved humic acid from water by coagulation method using polyaluminum chloride (PAC) with calcium carbonate as neutralizer and coagulant aid. J Environ Chem Eng 3:770-774. https://doi.org/10.1016/j.jece.2015.04.007

Sun DD, Lee PF (2012) TiO_2 microsphere for the removal of humic acid from water: Complex surface adsorption mechanisms. Sep Purif Techol 91:30-37. https://doi.org/https://doi.org/10.1016/j.seppur.2011.08.035

Szymański K, Morawski AW, Mozia S (2016) Humic acids removal in a photocatalytic membrane reactor with a ceramic UF membrane. Chem Eng J 305:19-27. https://doi.org/10.1016/j.cej.2015.10.024

Tsiourvas D, Tsetsekou A, Arkas M, Diplas S, Mastrogianni E (2011) Covalent attachment of a bioactive hyperbranched polymeric layer to titanium surface for the biomimetic growth of

calcium phosphates. J Mater Sci: Mater Med 22:85-96. https://doi.org/10.1007/s10856-010-4181-7

Tung TX, Xu D, Zhang Y, Zhou Q, Wu Z (2019) Removing Humic Acid from Aqueous Solution Using Titanium Dioxide: A Review. Pol J Environ 28:529-542. https://doi.org/10.15244/pjoes/85196

Wang A, Chen W, Geng N, Lan X, Liu M, Wu X (2022) Novel Electrochemical Preparation of N-Doped TiO_2/Graphene for Enhanced Stability and Photocatalysis Degradation of Humic Acid. Sustainability 14:10614. https://doi.org/10.3390/su141710614

Wang X, Wu Z, Wang Y, Wang W, Wang X, Bu Y, Zhao J (2013) Adsorption–photodegradation of humic acid in water by using ZnO coupled TiO_2/bamboo charcoal under visible light irradiation. J Hazard Mater 262:16-24. https://doi.org/https://doi.org/10.1016/j.jhazmat.2013.08.037

Wang Y, Yang J, Du R, Chen L (2017) Transition Metal Ions Enable the Transition from Electrospun Prolamin Protein Fibers to Nitrogen-Doped Freestanding Carbon Films for Flexible Supercapacitors. ACS Appl Mater Interfaces 9:23731-23740. https://doi.org/10.1021/acsami.7b05159

World Health Organization (WHO). Drinking water challenges. https://www.who.int/news-room/fact-sheets/detail/drinking-water. Accessed 21 May 2022

Xu C, Cui A, Xu Y, Fu X (2013) Graphene oxide–TiO_2 composite filtration membranes and their potential application for water purification. Carbon 62:465-471. https://doi.org/https://doi.org/10.1016/j.carbon.2013.06.035

Xue G, Liu H, Chen Q, Hills C, Tyrer M, Innocent F (2011) Synergy between surface adsorption and photocatalysis during degradation of humic acid on TiO_2/activated carbon composites. J Hazard Mater, 186:765-772. https://doi.org/https://doi.org/10.1016/j.jhazmat.2010.11.063

Yadav M, Gupta R, Sharma RK (2019) Chapter 14 - Green and Sustainable Pathways for Wastewater Purification. In S. Ahuja (Ed), Advances in Water Purification Techniques. Elsevier, pp. 355-383. https://doi.org/https://doi.org/10.1016/B978-0-12-814790-0.00014-4

Zhang X, Du AJ, Lee P, Sun DD, Leckie JO (2008a) Grafted multifunctional titanium dioxide nanotube membrane: Separation and photodegradation of aquatic pollutant. Appl Catal B: Environ 84:262-267. https://doi.org/10.1016/j.apcatb.2008.04.009

Zhang X, Du AJ, Lee P, Sun DD, Leckie JO (2008b) TiO_2 nanowire membrane for concurrent filtration and photocatalytic oxidation of humic acid in water. J Memb Sci 313:44-51. https://doi.org/https://doi.org/10.1016/j.memsci.2007.12.045

Zhang Y, Wang F, Wang Y (2021a) Electrospun Cellulose Acetate/Chitosan Fibers for Humic Acid Removal: Construction Guided by Intermolecular Interaction Study. ACS Appl Polym Mater 3:5022-5029. https://doi.org/10.1021/acsapm.1c00778

Zhang Y, Wang F, Wang Y (2021b) Recent developments of electrospun nanofibrous materials as novel adsorbents for water treatment. Mater Today Commun, 27:102272. https://doi.org/https://doi.org/10.1016/j.mtcomm.2021.102272

Zhou X, Zhou S, Ma F, Xu Y (2019) Synergistic effects and kinetics of rGO-modified TiO_2 nanocomposite on adsorption and photocatalytic degradation of humic acid. J Environ Manag 235:293-302. https://doi.org/https://doi.org/10.1016/j.jenvman.2019.01.026

Connecting Statement to Chapter 7

The synergistic performance of photooxidation and adsorption achieved by TiO_2-CA/CS fibrous membranes was demonstrated in Chapter 6, which extended the saturation point of CA/CS adsorbents and realized continuous removal of HA. So far, we have explored several approaches to functionalize electrospun CA fibrous membranes. Considering the ultra-fine fiber structure and large surface area, we intended to assemble the electrospun CA fibers into 3D fibrous aerogels for oils/organic solvent removal in Chapter 7.

Chapter 7. Construction of three-dimensional aerogels from electrospun cellulose fibers as highly efficient and reusable oil absorbents

7.1. Abstract

The escalating environmental impact of oil pollution has necessitated the development of efficient and sustainable absorbent materials. This study presents a strategy to prepare 3D interconnected porous structure from 2D electrospun cellulose acetate (CA) fibrous membranes, allowing better phase permeation and storage for oil retention. Specifically, bottom-up assembly of electrospun fibers was achieved through homogenizing fiber dispersion in water and covalently crosslinking, followed by a silanization process to improve the hydrophobicity of the fiber surface. The interconnected 3D networks, high porosity, hydrophobicity, and mechanical robustness of the aerogels were confirmed by scanning electron microscopy (SEM), Fourier transform infrared (FT-IR) spectroscopy, water contact angle (WCA), and compression tests. All the aerogels exhibited multiscale morphological structures composed of major pores (up to 20 μm), minor pores (up to 1 μm), and semi-micron scaled fibers as the building blocks, and were capable of absorbing diversified oils and organic solvents owing to their three-dimensional interconnected porous structures (porosity >93.5%). In particular, Aerogel 1-1 exhibited exceptional oil absorption capacities (up to 37.82 g/g) and superior reusability as evidenced by the minimal changes in its absorption capacity and compressive strength after 20 absorption-compression cycles. Therefore, this work highlights the potential of the electrospun cellulose fiber-constructed aerogels for efficient oil pollution remediation and industrial wastewater treatment.

Keywords: electrospinning, cellulose fibers, aerogel, oil absorption, reusable

7.2. Introduction

The rapid growth of industrialization and civilization, coupled with large-scale oil production, has inevitably led to oil/organic solvent pollution from household sewage, industrial discharge, and transportation-related spills [1, 2]. This issue has escalated into a global concern, impacting both

the ecosystems and urban dwellings, creating a substantial need for efficient, economical, and environmentally friendly remediation methods. Absorbent materials have piqued the interest and been considered as an effective approach for pollution control regarding the following aspects: 1. Their convenience stemmed from the straightforward applications without the need for complex infrastructures; 2. They embed and trap contaminants rather than transferring them to another medium or generating secondary pollutions and by-products; 3. They can be recycled for further use by simple methods, which makes them a cost-effective and sustainable option in long-term pollution management strategies.

Electrospun fibers have been extensively fabricated and investigated for applications in wastewater treatment, attributed to their large surface-to-volume ratio, highly porous structure, good interconnectivity, and structural stability [3-7]. Our previous study demonstrated the high performance of electrospun cellulose acetate (CA)-based adsorbents for organic acid removal [8]. However, the oil absorption capacity of electrospun fibrous membranes is compromised by their intrinsic lamellar deposition structures [9, 10], where the fibers pack together and lead to a shortage of space in the depth direction. Notably, three-dimensional aerogel absorbents possess intriguing properties, such as spacious storage room, low density, high porosity, high specific surface area, and flexibility, which underscore their potential for effective oil absorption. Up to date, the developed aerogels can be generally categorized into three groups: inorganic aerogels, synthetic polymer-based aerogels, and natural polymeric aerogels [11]. Inorganic aerogels, such as carbon nanotube/graphene sponges and silica aerogel [12, 13, 14, 15], are featured with low density and good thermal stability, but are often hindered by high production costs, complicated preparation processes, and poor mechanical properties. Synthetic polymer aerogels, such as polyurethane- and polydimethylsiloxane-based sponges [16, 17], have exhibited good mechanical properties and

reusability, but lack of biocompatibility to the environment. Natural polymer-based aerogels (cellulose, chitosan, lignin, etc.) are recognized as low-cost, renewable, and biodegradable matrices and have been widely explored for the control of oil pollution [18-20]. These aerogels were usually prepared by the sol-gel transition that yielded thick cellular walls. Alternatively, electrospun fibrous aerogels have shown tremendous potential in highly efficient oil absorption owing to the open hierarchical structure and extremely low-energy surface. Recently, Jiang et al. [21] developed polyacrylonitrile/polydimethylsiloxane nanofibrous aerogels from electrospun fibers with outstanding oil adsorption capacity and mechanical resilience, while Tian et al. [22] fabricated cellulose acetate-based electrospun nanofiber aerogels for efficient removal of drug residues and oil contaminations from wastewater. Moreover, pH-responsive hydrogels were constructed using cellulose acetate-based core-shell fibers and exhibited high oil/water separation efficiency [23]. However, the utilization of electrospun cellulose fibers has been seldom reported.

Herein, we hypothesize that electrospun cellulose fibers are promising building blocks for the construction of highly efficient and reusable oil absorbents. In this study, electrospun CA fibers were hydrolyzed, dispersed, and crosslinked to create three-dimensional aerogels, which were hydrophobically modified for oil/organic solvent absorption. The chemical and morphological structure and mechanical properties of the fibrous aerogels were systematically investigated. The absorption experiments were carried out with various oils and organic solvents as the models, followed by the evaluation of the aerogel recyclability regarding the retention of compressive strength and absorption capacity.

7.3. Experimental section

7.3.1. Materials

The cellulose acetate (CA) tow (molecular weight 75-95 kDa, acetyl content of 39.95 wt %, degree of substitution 2.47) utilized for manufacturing cigarette filters was kindly provided by Celanese Corporation (Irving, US). Acetic acid (CH_3COOH, glacial), sodium hydroxide (NaOH, ACS reagent grade), ethanol (anhydrous), methyltrimethoxysilane (MTMS, 97%), potassium carbonate (K_2CO_3, 98%), silicone oil, pump oil, toluene (99.5%), hexanes (98.5%), and chloroform (99.8%) were purchased from Fisher Scientific (Mississauga, ON, Canada). Epichlorohydrin (Epc, >99%) was purchased from Sigma-Aldrich (Oakville, ON, Canada). All chemicals were used as received and without further purification. Deionized water was used throughout the experimental procedures.

7.3.2. Fabrication of electrospun cellulose fiber assembled hydrogels

Electrospun CA fibers were prepared by dissolving 12 wt% of CA tow in acetic acid and stirring for 48 h at room temperature. Electrospinning parameters were optimized in the preliminary experiment to allow the steady deposition of fibers on the collector. Specifically, the homogeneous CA solution was pumped and ejected from a stainless-steel needle (diameter 0.6 mm) at a rate of 1.3 mL h^{-1}, and the optimized voltage and nozzle-to-collector distance were 30 kV and 13 cm, respectively. The obtained electrospun CA membrane was vacuum dried in a desiccator at room temperature for 24 h to remove the residual trace acetic acid. The deacetylation of CA followed the method reported by Abdellah et al. [24], which reduced the degree of acetylation from 39.3% to 2.8% in 60 minutes. Specifically, CA fibers were carried out by immersing the electrospun CA membrane in 70 mL of 0.05 M NaOH/EtOH solution and stirring for 1 h at room temperature.

Alkaline hydrolysis was ceased by washing the obtained cellulose (CL) fibrous membrane with distilled water until the pH level was neutral. The CL fibrous membrane was then dispersed in deionized water with a ratio of 7 wt% using a Vitamix blender (E310, Vitamix Corporation, Cleveland, OH, USA) for 30 min. The CL fiber suspension was poured into a 10 mL beaker, followed by the adjustment of the suspension pH to 10 using 0.2 M NaOH solution. Desired volumes of Epc were added into the CL fiber suspensions and reacted at 70 ℃ for 3 h to allow the formation of the three-dimensional fibrous hydrogels. The hydrogels were washed in a water bath and coded as Hydrogel 1-0.5, Hydrogel 1-0.75, and Hydrogel 1-1, corresponding to a CL/Epc ratio of 1-0.5, 1-0.75, and 1-1, respectively.

7.3.3. Fabrication of hydrophobically modified aerogels

The hydrogels were frozen with liquid nitrogen followed by lyophilization. According to Gong et al. [25], the thermal chemical vapor deposition (CVD) treatment with uniform coating and high deposition rate was employed to improve the hydrophobicity of the CL fibrous aerogels. The saturated K_2CO_3 solution (10 mL) was prepared in an open vial and placed in a desiccator together with the aerogels to reach 43% relative humidity. MTMS (10 mL) was added into another open vial and placed in the same desiccator that was then tightly sealed. The hydrophobic modification was carried out by placing the desiccator in a drying oven at 60 ℃ for five days. The modified aerogels were kept in the fume hood to remove reactant residuals and by-products and coded as Aerogel 1-0.5, Aerogel 1-0.75, and Aerogel 1-1. The schematic illustration of the fibrous aerogel preparation is presented in Figure 7.1.

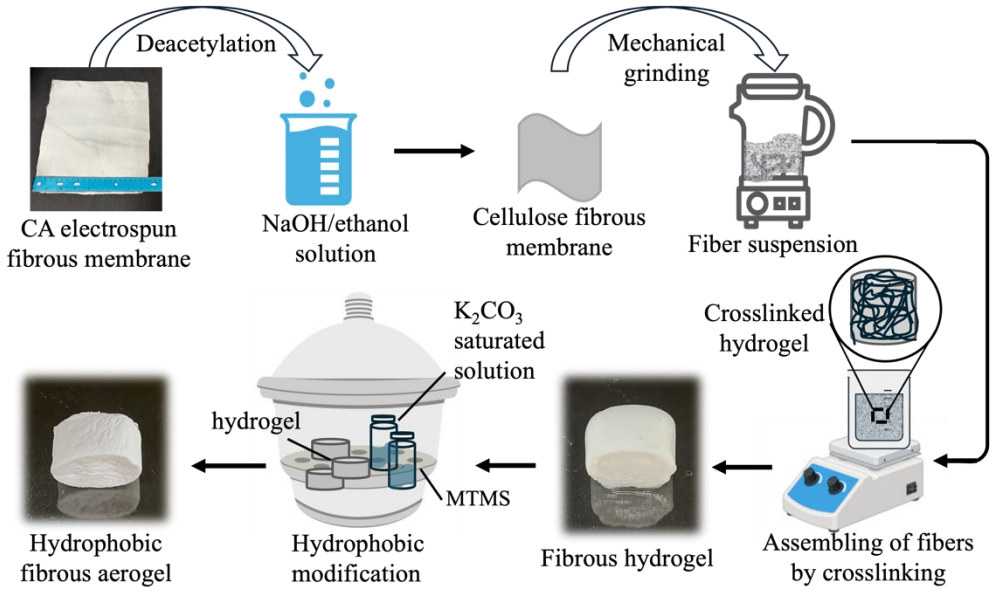

Figure 7.1. Schematic illustration of the preparation of hydrophobically modified fibrous aerogels.

7.3.4. Characterization

7.3.4.1. Fourier Transform Infrared (FT-IR) Spectroscopy

The Varian Excalibur 3100 FT-IR spectrometer (Varian, Melbourne, Australia) equipped with an attenuated total reflectance accessory (Specac, Orpington, UK) was utilized to analyze the chemical structure of the electrospun fibers and hydrophobic fibrous aerogels. Each FT-IR spectrum was recorded in transmittance mode, averaging 64 scans with a resolution of 4 cm^{-1}.

7.3.4.2. Morphological properties

Scanning electron microscopy (SEM) images of the electrospun fibers and aerogels were taken on a Hitachi TM1000 SEM (Hitachi, Ltd, Tokyo, Japan) operated at an acceleration voltage of 15 kV. All samples were coated with 4 nm of platinum/gold layers using a Leica EM ACE200 sputter-coater (Leica Microsystems, Wetzlar, Germany) prior to the observation.

7.3.4.3. Water contact angle (WCA)

The wettability of the as-prepared aerogels was analyzed by WCA measurements at room temperature using a contact angle goniometer (OCA 20, DataPhysics Instruments Corp., Filderstadt, Germany). A droplet of deionized water (4 μL) was deposited by a syringe on the surface/cross-section of the samples, followed by image capture and analysis. The WCA measurement was given by the goniometer according to the shape of the drop, and the average of the values taken at three different locations with five replicates for each sample was calculated as the contact angle.

7.3.4.4. Silane content

The silane content of the aerogels was determined by the gravimetric method according to Yu et al [26]. The weights of the aerogel before (W_0) and after CVD treatment (W_t) were recorded, and the silane content was calculated using the following equation:

$$Silane\ content\ (mg\ g^{-1}) = (W_t - W_0)/W_0 \tag{7-1}$$

7.3.4.5. Density and porosity

The dimension and mass of the aerogels were measured by a vernier caliper and an analytical balance with 0.01 mm and 0.1 mg readabilities, respectively, for calculating the apparent density (ρ, mg/cm3) of the aerogels. For calculating the porosity (P) of the aerogels, the small amounts of Epc and MTMS added in the crosslinking and hydrophobic modification were neglected. The equation as follows was used:

$$P\ (\%) = \left(1 - \frac{\rho_A}{\rho_C}\right) \times 100 \tag{7-2}$$

where ρ_A is the apparent density of the as-prepared aerogels, and ρ_C is the bulk density of cellulose which is taken as 1.6 g/cm^3 [27].

7.3.4.6. Mechanical properties

The compressive mechanical properties of the as-prepared hydrogels and aerogels were performed using an ADMET eXpert 7601 testing machine (ADMET, Norwood, MA, USA) equipped with a 250 lb load cell at room temperature. The samples were compressed to 70% of their original heights at a crosshead velocity of 2 mm min^{-1}, and the compressive stress-strain curves were recorded accordingly. The dimensions of each sample were measured using a vernier caliper with 0.01 mm readability, and the compressive strength (σ) of the cylindrical sample was obtained by dividing the maximum force by its cross-sectional area. The compression test for each sample was repeated for at least three times.

7.3.5. Oil/organic solvent absorption capacity

The absorption capacity of the as-prepared aerogels for oils and organic solvents, including pump oil, silicone oil, canola oil, chloroform, hexane, and toluene, was investigated using the following method. The aerogels were immersed in the different oils/organic solvents for 10 minutes at room temperature. The saturated aerogels were then taken out and allowed to drain for 2 minutes. The absorption capacity (Q) of each aerogel was calculated according to Eq. (7-3):

$$Q\ (g\ g^{-1}) = \frac{m_w - m_d}{m_d} \tag{7-3}$$

where m_w is the mass of the aerogel after oil/solvent absorption, and m_d is the mass of the original dry sample.

7.3.6. Recyclability

The cyclic compression method was applied to evaluate the recyclability of the aerogels as an oil absorbent. Specifically, each sample was immersed in the pump oil for 10 minutes, and then either

tightly compressed to 70% or loosely compressed to 50% of the original height to release the oil. The compressed aerogels were immediately immersed in the pump oil again to proceed with the cycles. This absorption-compression cyclic process was repeated 6 times for tight compression and 20 times for loose compression, and the compressive stress-strain curves during the cycles were plotted. The weights of the aerogels before and after oil absorption were recorded to determine the absorption capacity (using Eq. 7-3). Three trials for each sample were conducted to obtain the average values and standard deviations.

7.3.7. Statistical analysis

All statistical analyses of the results were performed using SPSS software Statistical (version 27, IBM, Armonk, NY, USA) with a $p < 0.05$ considered to be significant. Statistical interpretations of the results were investigated via analysis of variance (ANOVA) followed by multiple comparison tests of the individual means using Duncan's multiple range test at a confidence level of 95%. Experimental results were expressed as the mean of at least three batches ± standard deviation.

7.4. Results and discussion

7.4.1. Structures and properties of cellulose fibrous aerogels

FT-IR spectroscopy was performed to analyze alterations in the chemical structures of the samples during the preparation and modification. As depicted in Figure 7.2, the spectra of electrospun CA fibers displayed three distinct peaks, corresponding to the vibrations of C=O, $-CH_3$, and C-O at 1750, 1372, and 1224 cm^{-1}, respectively [28]. In comparison, these three characteristic peaks became very weak in the spectrum of the deacetylated CA fibers, while a noticeable and intensified

red shift of the peak at 3330 cm^{-1} existed corresponding to the vibration of hydroxyl groups, indicating the successful conversion of CA fibers into CL fibers [29]. The spectra of the three fibrous aerogels treated with different crosslinker contents exhibited analogous patterns. Compared to the CL fibers, the absorption band at 3330 cm^{-1} shifted to higher wavenumbers due to the formation of crosslinked networks between the hydroxyl groups of CL and the epoxide groups of Epc [30]. Additionally, the intensified vibrations of C-O-C at 1060 cm^{-1} and C-H from -CH_2 at 2840-2928 cm^{-1} were observed on the spectra of the aerogels, attributed to the introduction of crosslinkers containing abundant -CH_2- groups into the matrix [31, 32]. Two new peaks emerged on the spectra of the aerogels after the hydrophobic modification, representing the asymmetric stretching of C-Si from C-Si-O at 1270 cm^{-1} and the vibration of Si-O-Si at 770 cm^{-1} [33]. It therefore confirmed the covalent attachment of silicone on the as-prepared aerogels. Notably, the Aerogel 1-1 sample exhibited a pronounced blue shift of the absorption peak representing hydroxyl groups to 3430 cm^{-1}, which could be explained by the introduction of better crosslinking or silanization effects, or a combination of both.

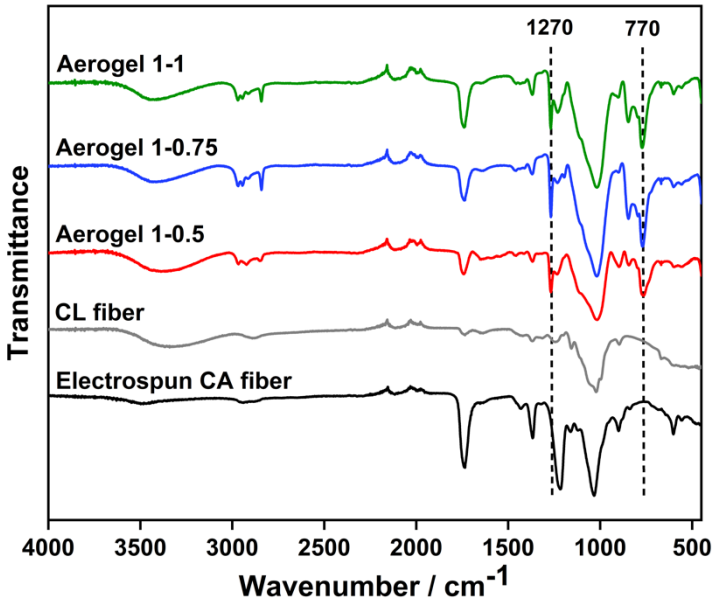

Figure 7.2. FT-IR spectra of the electrospun fibers and fibrous aerogels with various crosslinker contents.

The morphologies of the electrospun fibers and the fibrous hydrogels and aerogels were investigated by SEM (shown in Figure 7.3). The CL fibers, which were subjected to the deacetylation process, retained their structural integrity and were interwoven and crosslinked to form the fibrous hydrogels with isotropic three-dimensional networks and various pore sizes. The silanization of the aerogels had minimal impact on the porous structures as observed in Figure 7.3a, but it was noteworthy that the pore sizes of the aerogels reduced significantly from approximately 20 μm to 10 μm with an increase in crosslinker contents. This phenomenon could be explained by the propensity for CL fiber aggregation through hydrogen bonding in the presence of a low crosslinker amount. Conversely, an increased crosslinker content consumed more hydroxyl groups and resulted in better separation of the fibers. This phenomenon was also reported by Bai and Li in the preparation of porous CL beads with Epc [34]. A multi-scale morphology of the as-prepared aerogel is demonstrated in Figure 7.3b. The formation of major pores (10 to 20 μm) was driven by

the phase separation between solvent crystals and the gel matrices, where ice crystals condensed among the crosslinked CL fibers and left behind the porous structure upon the ice crystal sublimation [35]. The cell walls of the minor pores (0.5 to 1 μm) were generated through the CL fiber entanglement and self-assembly. Acting as the building blocks, semi-micron scaled CL fibers played a role in joining adjacent walls, thereby facilitating the formation of the interconnected networks [36]. This porous structure of the as-prepared aerogels would highly facilitate the rapid mass transfer in the oil absorption applications.

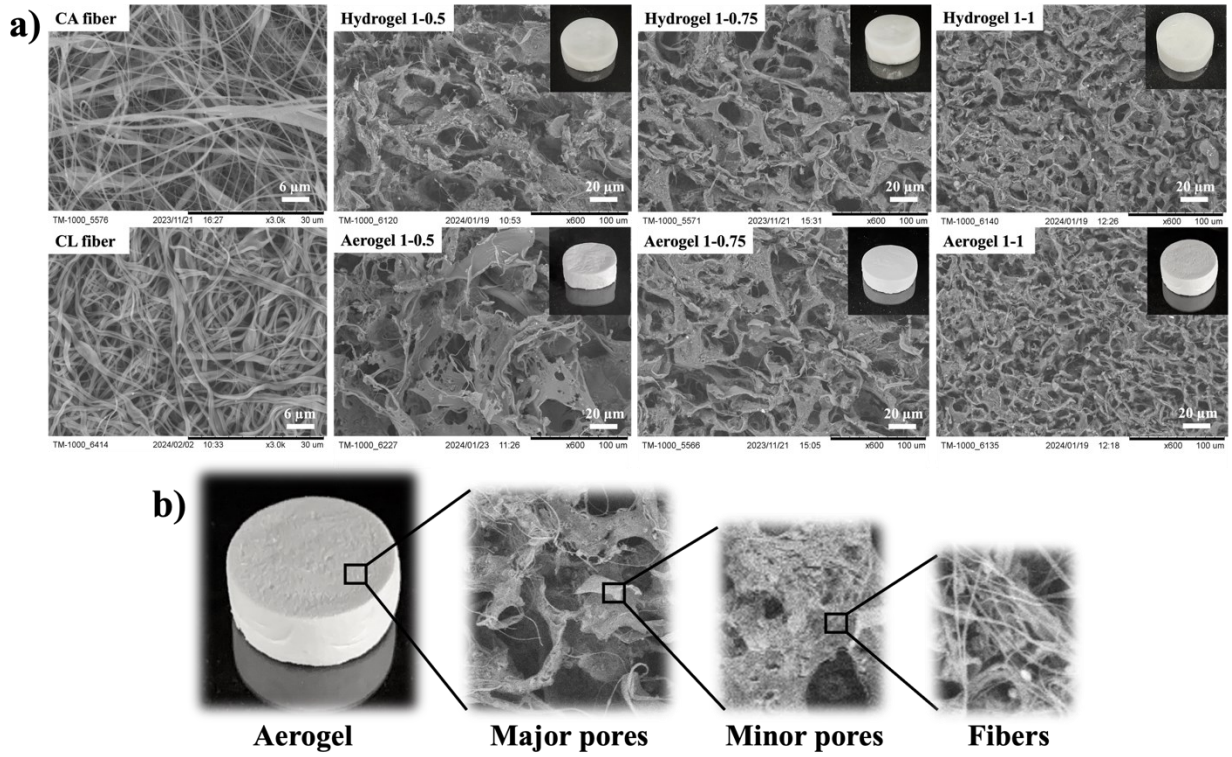

Figure 7.3. (a) SEM images of electrospun fibers and fibrous hydrogels and aerogels with various crosslinker contents. The insets are the photographs of the hydrogels and aerogels, and (b) the scaling down morphological structures of the aerogels.

The highly interconnected porous structure of the fibrous aerogels was also reflected in their low density and high porosity (Table 7.1). The average density and porosity of the fibrous aerogels

with respect to the increased crosslinker contents changed from 102.87±3.13 to 75.22±1.40 mg/cm^3 and from 93.57±0.20% to 95.30±0.09%, respectively. This might be attributed to the better separated CL fibers that could well support the three-dimensional network. Especially, the Aerogel 1-1 sample exhibited a notably higher silane content compared to other samples. It could be attributed to its uniform pore distribution and greater surface area, which facilitated the vapor permeation and organosilane deposition [37].

Table 7.1. Densities, porosities, and silane contents of the hydrophobically modified aerogels.

Samples	CL/Epc ratio (w/v)	Density (mg/cm^3)	Porosity (%)	Silane content (mg/g)
Aerogel 1-0.5	1-0.5	102.87±3.13 ^{a}	93.57±0.20 ^{c}	86.53±4.53 ^{c}
Aerogel 1-0.75	1-0.75	90.84±6.89 ^{b}	94.32±0.43 ^{b}	93.38±1.32 ^{b}
Aerogel 1-1	1-1	75.22±1.40 ^{c}	95.30±0.09 ^{a}	108.01±4.33 ^{a}

The mechanical robustness is an essential consideration in the development of efficient oil absorbents. Therefore, the compressive stress (σ) of the fibrous hydrogels and aerogels as a function of strain (ε) in air was studied. As shown in Figure 7.4a, all samples experienced an initial linear Hookean regime at relatively low compressive strain (ε < 45%), signifying the elastic buckling of the fibers and deformation of the pores. Subsequently, a gradual densification regime was observed under higher compressive strain (ε > 45%), corresponding to the densification of cellular pores [18, 38]. All cylindrical fibrous samples could be compressed to over 70% of their original heights without cracking, revealing desirable flexibility and stability. It was noted that the chemical crosslinking played a more important role in the compressive strength of the aerogels [39], and the compressive modulus of Aerogel 1-1 achieved 0.77±0.02 MPa, which was evidently superior to those of many previously reported CL aerogels [18, 40].

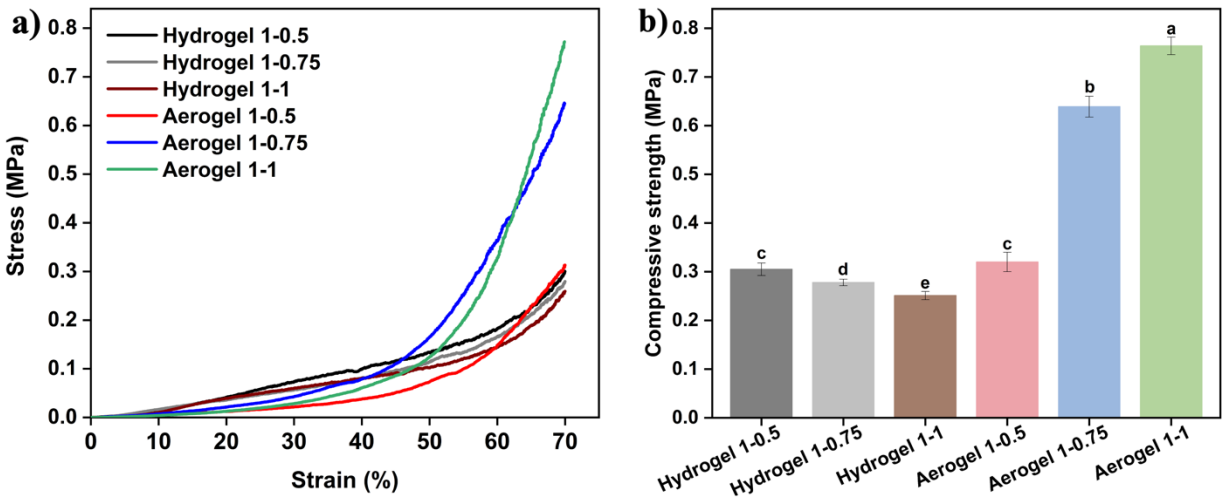

Figure 7.4. Mechanical properties of the fibrous hydrogels and aerogels: (a) Stress-strain curves, and (b) compressive strengths. Different letters on the top of each column represent significant differences ($p < 0.05$).

The WCA measurements of the fibrous aerogels were assessed to reflect their wettability and stability, which is a crucial indicator for the delivery of high-performance oil absorption. The fibrous aerogels showed high WCA of 131.4±0.8°, 125.7±1.3°, and 125.5±1.8° for Aerogel 1-1, Aerogel 1-0.75, and Aerogel 1-0.5, respectively (Figure 7.5a). Other than the surfaces, the fibrous aerogels also exhibited high WCA on the interior cross-sections with no significant differences, implying the thorough exposure of the aerogels to organosilane through the CVD method. Notably, Aerogel 1-1 exhibited the highest WCA owing to its superior silane content [41]. As shown in Figure 5b, a water droplet could stand on the surface of the aerogel with a full spherical shape for 5 minutes, whereas the chloroform droplet spread on the surface and was readily absorbed by the aerogel.

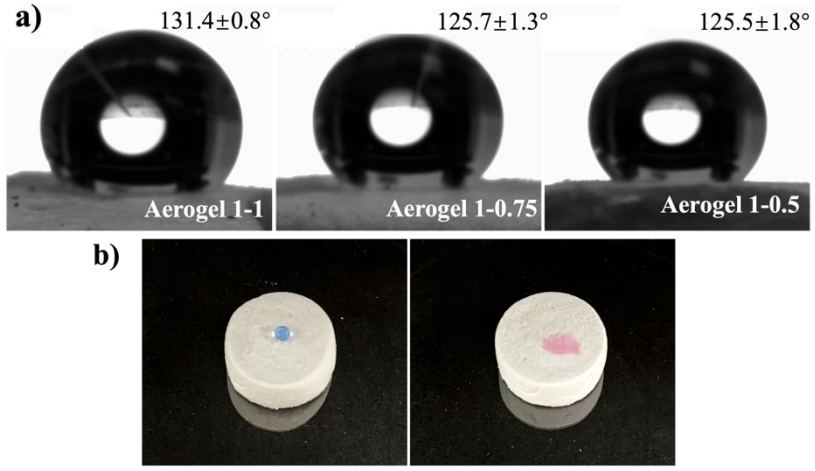

Figure 7.5. (a) Water contact angles of aerogels with various crosslinker contents, and (b) the photos of blue-colored water and red-colored chloroform on the surface of Aerogel 1-1.

7.4.2. Oil/Organic solvent absorption

The absorption capability of the fibrous aerogels was assessed by removing oils and organic solvents with various densities. Several common pollutants found in industrial discharge and daily life were utilized as representative absorbates, including chloroform, hexane, toluene, pump oil, silicone oil, and canola oil. The as-prepared aerogels demonstrated superior absorption capacity towards all these oils and organic solvents within the range of 24.40 to 37.82 g/g (Figure 7.6a), depending on the chemical structure, viscosity, density, and surface tension of the oils and organic solvents [18, 42]. It was evident that Aerogel 1-1 exhibited the highest absorption capacity towards diversified oils and organic solvents; for example, it reached an average absorption capacity of 37.82 g/g towards chloroform within 10 minutes (Figure 7.6b), which was significantly higher than those of Aerogel 1-0.5 and Aerogel 1-0.75 (33.13 and 35.12 g/g). The absorption mechanism of the fibrous aerogels mainly relied on the hydrophobic surface of the fibers that repelled water but strongly attracted non-polar oil molecules. This process was followed by the mass transfer of

oils and organic solvents into the three-dimensional porous networks of the aerogels through liquid diffusion and pore filling powered by capillary force [43]. Therefore, the high absorption capacity of Aerogel 1-1 was due to (1) the intensified capillary force from fibers-oil interactions; (2) better retention of oils/organic solvents within a sufficient amount of major/minor pores; and (3) higher silane contents deposited on the surface of CL fiber, requiring minimal surface energy for the oil/organic solvent absorption [44-46]. Conversely, the aerogels with lower porosities had less oil storage capacity, while the large pore size of the Aerogel 1-0.5 sample resulted in the weaker capillary force and negatively impacted the absorption of oils and organic solvents. As shown in Figure 7.6c, Aerogel 1-1 demonstrated fast and complete pump oil removal from water within 10 minutes (7.91 g pump oil in 0.26 g aerogel). The fibrous aerogel floated on the water surface after the absorption, facilitating the recovery of the absorbents. The absorption capacity of Aerogel 1-1 towards various oils and organic solvents was higher or comparable to those of previously reported materials: cyanuric chloride-attached nanocrystalline cellulose siloxane aerogel (~16 g/g) [44], MTMS-treated cellulose nanocrystal/poly(vinyl)alcohol aerogel (21.2-32.7 g/g) [25], polymeric epoxidized soybean oil-grafted cellulose aerogel (27 g/g of toluene and 28 g/g of pump oil) [47], sodium alginate/graphene oxide/silicon oxide aerogel (17.92 g/g of hexane) [48], silane functionalized polyvinyl-alcohol formaldehyde sponges (4-14 g/g) [49], and reduced graphene oxide/carbon nanotube-decorated polydimethylsiloxane sponge (2.4-7.3 g/g) [12].

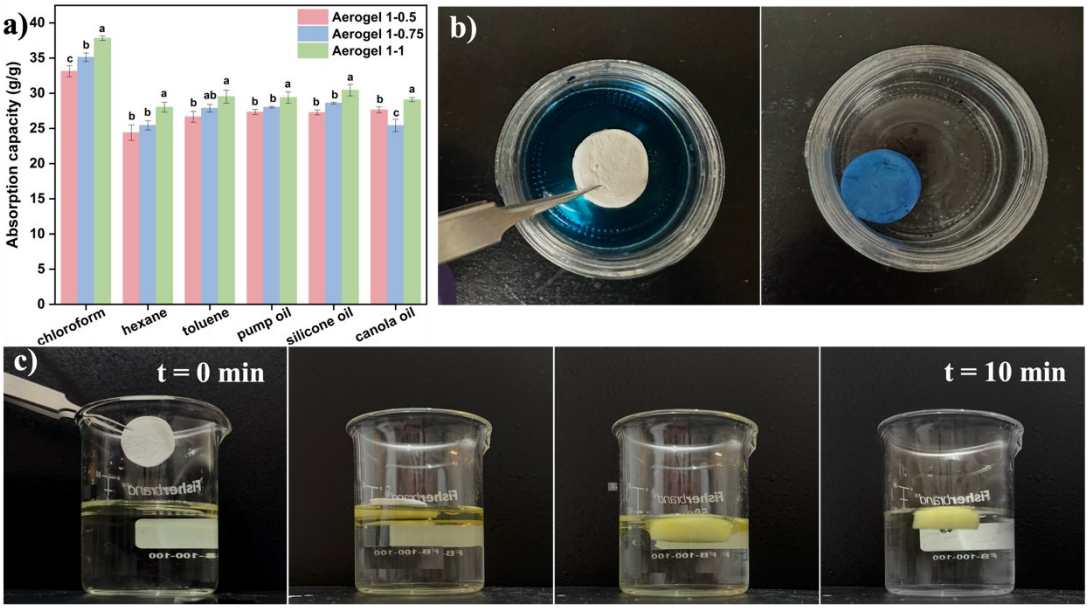

Figure 7.6. (a) Absorption capacity of aerogels with different crosslinker contents towards various oils and organic solvents, (b) uptake of blue-colored chloroform in Aerogel 1-1, and (c) removal of pump oil from water with Aerogel 1-1. Different letters on the top of each column represent significant differences ($p < 0.05$).

7.4.3. Reusability

Due to the high flexibility and porosity, the fibrous aerogels could be even compressed to 70% of their original heights and reused, but a compression of 50% was enough to release most of the absorbates. Pump oil was selected as the illustrative medium and the absorption-compression process was repeated to study the changes in the compressive strength and absorption capacity. As shown in Figure 7.7, in general, the absorption capacity and compressive strength of the aerogels slightly decreased after tight compressions. It might be due to the occurrence of irreversible pore collapse during the excessive compression process, and similar phenomenon was also reported by Mulyadi et al. in the investigation of styrene/acrylic monomer-modified cellulose nanofibril aerogels [50]. Notably, all the aerogels still preserved more than 85% of their original absorption

capacities (compression time=0) after six tight compression cycles, and no visible damage was observed, signifying their compressibility and durability. Aerogel 1-1 achieved superior retention of compressive strength (0.71 MPa) and absorption capacity (27.26 g/g of pump oil) as well as the rapid shape recovery during the six tight compression cycles. The reusability of the current fibrous aerogels was better than those of the traditional cellulose aerogels and electrospun membrane absorbents. For instance, cellulose aerogels made from wastepaper remained the absorption capacity towards heptane of less than 55% after five cycles [51], while the microcrystalline cellulose aerogel prepared through the sol-gel route preserved less than 80% of its original machine oil absorption capacity following five cycles [52]. At the same time, the reusability of electropsun membrane absorbents for the removal of mineral oil and motor oil was lower than 78.5% and 10% of their original absorption capacities after five cycles, respectively [53,54]. Aerogel 1-1 was then selected to further investigate its resilience and durability through 20 loose compression cycles for the removal of pump oil. It was worth noting that Aerogel 1-1 demonstrated outstanding retention of both absorption capacity and compressive strength after 20 cycles, showing no significant differences from the original values (Figure 7d). This result indicated the potential for the reuse of the fibrous aerogels, but future studies are still needed to further improve the elasticity of the three-dimensional fibrous networks.

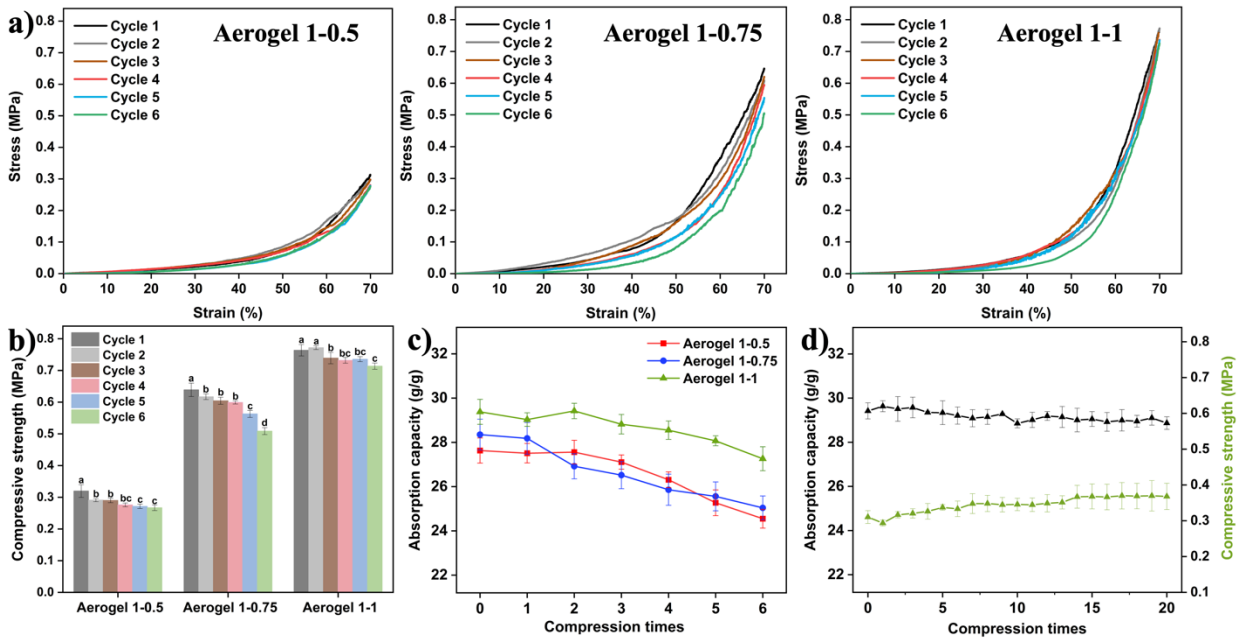

Figure 7.7. Reusability of the aerogels to remove pump oil for six tight absorption-compression cycles: (a) stress-strain curves of the aerogels with various crosslinker contents, (b) compressive strengths of the aerogels after each cycle, (c) the absorption capacities of the aerogels after each cycle, and (d) reusability of Aerogel 1-1 to remove pump oil for twenty loose absorption-compression cycles. Different letters on the top of each column represent significant differences ($p < 0.05$).

7.5. Conclusions

The hypothesis has been confirmed that the electrospun CL fibers were promising building blocks for constructing three-dimensional interconnected networks as highly efficient and reusable absorbents for oil removal. The fibrous aerogels exhibited high porosity (>93.5%), hydrophobicity (WCA >125.5 °), and compressive strength (up to 0.77 MPa). In particular, when the ratio of CL and Epc was 1:1, the hydrophobically modified aerogel possessed the outstanding mechanical properties, high absorption capacities towards multiple oils and organic solvents, and excellent reusability. All the aerogels could be reused by a simple compression and retain more than 85% of their original absorption capacities even after six tight absorption-compression cycles, highlighting

their durability and practicability. Therefore, this work demonstrates a strategy to build high-performance three-dimensional functional structures for oil spill cleanup and industrial effluent treatment.

7.6. References

[1] Y. Su, T. Fan, W. Cui, Y. Li, S. Ramakrishna and Y. Long, *Advanced Electrospun Nanofibrous Materials for Efficient Oil/Water Separation.* Advanced Fiber Materials. **4** (2022): p. 938-958. https://doi.org/10.1007/s42765-022-00158-3.

[2] G. J. Dunderdale, C. Urata, T. Sato, M. W. England and A. Hozumi, *Continuous, High-Speed, and Efficient Oil/Water Separation using Meshes with Antagonistic Wetting Properties.* ACS Applied Materials & Interfaces. **7** (2015): p. 18915-18919. https://doi.org/10.1021/acsami.5b06207.

[3] J. Ge, J. Zhang, F. Wang, Z. Li, J. Yu and B. Ding, *Superhydrophilic and underwater superoleophobic nanofibrous membrane with hierarchical structured skin for effective oil-in-water emulsion separation.* Journal of Materials Chemistry A. **5** (2017): p. 497-502. http://dx.doi.org/10.1039/C6TA07652A.

[4] M. Khamforoush, O. Pirouzram and T. Hatami, *The evaluation of thin film composite membrane composed of an electrospun polyacrylonitrile nanofibrous mid-layer for separating oil–water mixture.* Desalination. **359** (2015): p. 14-21. https://doi.org/10.1016/j.desal.2014.12.016.

[5] N. H. Ismail, W. N. W. Salleh, A. F. Ismail, H. Hasbullah, N. Yusof, F. Aziz and J. Jaafar, *Hydrophilic polymer-based membrane for oily wastewater treatment: A review.* Separation and Purification Technology, **233** (2020): p. 116007. https://doi.org/10.1016/j.seppur.2019.116007.

[6] D. Wang and J. Wang, *Electrospinning Polyvinyl alcohol/silica-based nanofiber as highly efficient adsorbent for simultaneous and sequential removal of Bisphenol A and Cu(II) from water.* Chemical Engineering Journal. **314** (2017): p. 714-726. https://doi.org/10.1016/j.cej.2016.12.037.

[7] N. Olaru, N. Anghel, P. Pascariu and G. Ailiesei, *Synthesis and testing of cellulose acetate nicotinate as adsorbent for rhodamine B dye.* Journal of Applied Polymer Science. **136** (2019): p. 47772. https://doi.org/10.1002/app.47772.

[8] Y. Zhang, F. Wang and Y. Wang, *Electrospun Cellulose Acetate/Chitosan Fibers for Humic Acid Removal: Construction Guided by Intermolecular Interaction Study.* ACS Applied Polymer Materials. **3** (2021): p. 5022-5029. https://doi.org/10.1021/acsapm.1c00778.

[9] Y. Si, L. Wang, X. Wang, N. Tang, J. Yu and B. Ding, *Ultrahigh-Water-Content, Superelastic, and Shape-Memory Nanofiber-Assembled Hydrogels Exhibiting Pressure-Responsive Conductivity.* Advanced Materials. **29** (2017): p. 1700339. https://doi.org/10.1002/adma.201700339.

[10] Y. Shen, D. Li, L. Wang, Y. Zhou, F. Liu, H. Wu, et al., *Superelastic Polyimide Nanofiber-Based Aerogels Modified with Silicone Nanofilaments for Ultrafast Oil/Water Separation.* ACS Applied Materials & Interfaces. **13** (2021): p. 20489-20500. https://doi.org/10.1021/acsami.1c01136.

[11] S, Sabir, *Approach of Cost-Effective Adsorbents for Oil Removal from Oily Water.* Critical Reviews in Environmental Science and Technology. **45** (2015): p. 1916-1945. https://doi.org/10.1080/10643389.2014.1001143.

[12] W. Zhan, S. Yu, L. Gao, F. Wang, X. Fu, G. Sui and X. Yang, *Bioinspired Assembly of Carbon Nanotube into Graphene Aerogel with "Cabbagelike" Hierarchical Porous Structure for Highly*

Efficient Organic Pollutants Cleanup. ACS Applied Materials & Interfaces. **10** (2018): p. 1093-1103. https://doi.org/10.1021/acsami.7b15322.

[13] L. Li, T. Hu, H. Sun, J. Zhang and A. Wang, *Pressure-Sensitive and Conductive Carbon Aerogels from Poplars Catkins for Selective Oil Absorption and Oil/Water Separation*. ACS Applied Materials & Interfaces. **9** (2017): p. 18001-18007. https://doi.org/10.1021/acsami.7b04687

[14] G. Hayase, K. Kanamori, G. Hasegawa, A. Maeno, H. Kaji and K. Nakanishi, *A Superamphiphobic Macroporous Silicone Monolith with Marshmallow-like Flexibility.* Angewandte Chemie International Edition. **52** (2013): p. 10788-10791. https://doi.org/10.1002/anie.201304169

[15] P. B. Sarawade, J.-K. Kim, A. Hilonga, D. V. Quang and H. T. Kim, *Synthesis of hydrophilic and hydrophobic xerogels with superior properties using sodium silicate.* Microporous and Mesoporous Materials. **139** (2011): p. 138-147. https://doi.org/10.1016/j.micromeso.2010.10.030.

[16] A. Li, H.-X. Sun, D.-Z. Tan, W.-J. Fan, S.-H. Wen, X.-J. Qing, et al., *Superhydrophobic conjugated microporous polymers for separation and adsorption.* Energy & Environmental Science. **4** (2011): p. 2062-2065. http://dx.doi.org/10.1039/C1EE01092A.

[17] S.-J. Choi, T.-H. Kwon, H. Im, D.-I. Moon, D. J. Baek, M.-L. Seol, et al., *A Polydimethylsiloxane (PDMS) Sponge for the Selective Absorption of Oil from Water.* ACS Applied Materials & Interfaces. **3** (2011): p. 4552-4556. https://doi.org/10.1021/am201352w.

[18] M. Dilamian and B. Noroozi, *Rice straw agri-waste for water pollutant adsorption: Relevant mesoporous super hydrophobic cellulose aerogel.* Carbohydrate Polymers. **251** (2021): p. 117016. https://doi.org/10.1016/j.carbpol.2020.117016.

[19] M. Cao, Y. Hu, W. Cheng, S. Huan, T. Bai, Z. Niu, et al., *Lignin-based multi-scale cellular aerogels assembled from co-electrospun nanofibers for oil/water separation and energy storage.* Chemical Engineering Journal. **436** (2022): p. 135233. https://doi.org/10.1016/j.cej.2022.135233.

[20] Y. Su, T. Fan, W. Cui, Y. Li, S. Ramakrishna and Y. Long, *Recyclable and biodegradable superhydrophobic and superoleophilic chitosan sponge for the effective removal of oily pollutants from water.* Chemical Engineering Journal. **330** (2017): p. 423-432. https://doi.org/10.1007/s42765-022-00158-3.

[21] G. Jiang, J. Ge, Y. Jia, X. Ye, L. Jin, J. Zhang, et al., *Coaxial electrospun nanofibrous aerogels for effective removal of oils and separation of water-in-oil emulsions.* Separation and Purification Technology. **270** (2021): p. 118740. https://doi.org/10.1016/j.seppur.2021.118740.

[22] G. Tian, C. Duan, W. Lu, X. Liu, B. Zhao, Z. Meng, Q. Wang, and S. Nie, *Cellulose acetate-based electrospun nanofiber aerogel with excellent resilience and hydrophobicity for efficient removal of drug residues and oil contaminations from wastewater*. Carbohydrate Polymers. **329** (2024): p. 121794. https://doi.org/10.1016/j.carbpol.2024.121794.

[23] L. Zang, J. Ma, D. Lv, Q. Liu, W. Jiao and P. Wang, *A core–shell fiber-constructed pH-responsive nanofibrous hydrogel membrane for efficient oil/water separation*. Journal of Materials Chemistry A. **5** (2017): p. 19398-19405. http://dx.doi.org/10.1039/C7TA05148D

[24] M. H. Abdellah, C. Oviedo and G. Szekely, *Controlling the degree of acetylation in cellulose-based nanofiltration membranes for enhanced solvent resistance*. Journal of Membrane Science. **687** (2023): p. 122040. https://doi.org/10.1016/j.memsci.2023.122040.

[25] X. Gong, Y. Wang, H. Zeng, M. Betti and L. Chen, *Highly Porous, Hydrophobic, and Compressible Cellulose Nanocrystals/Poly(vinyl alcohol) Aerogels as Recyclable Absorbents for*

Oil–Water Separation. ACS Sustainable Chemistry & Engineering. **7** (2019): p. 11118-11128. https://doi.org/10.1021/acssuschemeng.9b00066.

[26] L. Yu, Z. Zhang, H. Tang and J. Zhou, *Fabrication of hydrophobic cellulosic materials via gas–solid silylation reaction for oil/water separation.* Cellulose. **26** (2019): p. 4021-4037. https://doi.org/10.1007/s10570-019-02355-7.

[27] W. E. Lee, *Cellular solids, structure and properties: MST.* Materials Science and Technology. **16** (2000): p. 233.

[28] S. M. Sharaf, S. E.-D. Al-Mofty, E.-S. M. El-Sayed, A. Omar, A. S. Abo Dena and I. M. El-Sherbiny, *Deacetylated cellulose acetate nanofibrous dressing loaded with chitosan/propolis nanoparticles for the effective treatment of burn wounds.* International Journal of Biological Macromolecules. **193** (2021): p. 2029-2037. https://doi.org/10.1016/j.ijbiomac.2021.11.034.

[29] C. Liu and R. Bai, *Preparation of chitosan/cellulose acetate blend hollow fibres for adsorptive performance.* Journal of Membrane Science. **267** (2005): p. 68-77. https://doi.org/10.1016/j.memsci.2005.06.001.

[30] Y. Seki, A. Altinisik, B. Demircioğlu and C. Tetik, *Carboxymethylcellulose (CMC)–hydroxyethylcellulose (HEC) based hydrogels: synthesis and characterization.* Cellulose. **21** (2014): p. 1689-1698. https://doi.org/10.1007/s10570-014-0204-8.

[31] M. S. Islam, M. N. Alam and T. G. M. van de Ven, *Sustainable cellulose-based hydrogel for dewatering of orange juice.* Cellulose. **27** (2020): p. 7637-7648. https://doi.org/10.1007/s10570-020-03295-3.

[32] Y. Zhao, M. He, L. Zhao, S. Wang, Y. Li, L. Gan, et al., *Epichlorohydrin-Cross-linked Hydroxyethyl Cellulose/Soy Protein Isolate Composite Films as Biocompatible and Biodegradable*

Implants for Tissue Engineering. ACS Applied Materials & Interfaces. **8** (2016): p. 2781-2795. https://doi.org/10.1021/acsami.5b11152.

[33] B. Duan, H. Gao, M. He and L. Zhang, *Hydrophobic Modification on Surface of Chitin Sponges for Highly Effective Separation of Oil.* ACS Applied Materials & Interfaces. **6** (2014): p. 19933-19942. https://doi.org/10.1021/am505414y.

[34] Y. Bai and Y. Li, *Preparation and characterization of crosslinked porous cellulose beads.* Carbohydrate Polymers. **64** (2006): p. 402-407. https://doi.org/10.1016/j.carbpol.2005.12.009.

[35] M. Mariano, N. El Kissi and A. Dufresne, *Cellulose nanocrystals and related nanocomposites: Review of some properties and challenges.* Journal of Polymer Science Part B: Polymer Physics. **52** (2014): p. 791-806. https://doi.org/10.1002/polb.23490.

[36] J. Sun, Y. Liu, Z. Wu, M. Xu, L. E, C. Ma, et al., *Compressible, anisotropic lamellar cellulose-based carbon aerogels enhanced by carbon dots for superior energy storage and water deionization.* Carbohydrate Polymers. **252** (2021): p. 117209. https://doi.org/10.1016/j.carbpol.2020.117209.

[37] I. A. Udoetok, R. M. Dimmick, L. D. Wilson and J. V. Headley, *Adsorption properties of cross-linked cellulose-epichlorohydrin polymers in aqueous solution.* Carbohydrate Polymers. **136** (2016): p. 329-340. https://doi.org/10.1016/j.carbpol.2015.09.032.

[38] M. Wang, X. Li, W. Hua, L. Deng, P. Li, T. Zhang and X. Wang, *Superelastic three-dimensional nanofiber-reconfigured spongy hydrogels with superior adsorption of lanthanide ions and photoluminescence.* Chemical Engineering Journal. **348** (2018): p. 95-108. https://doi.org/10.1016/j.cej.2018.04.135.

[39] T. Huber, S. Feast, S. Dimartino, W. Cen and C. Fee *Analysis of the Effect of Processing Conditions on Physical Properties of Thermally Set Cellulose Hydrogels*. Materials. **12** (2019), p.

1066.https://doi.org/10.3390/ma12071066.

[40] X. Qin, A. Lu and L. Zhang, *Gelation behavior of cellulose in NaOH/urea aqueous system via cross-linking.* Cellulose. **20** (2013): p. 1669-1677. https://doi.org/10.1007/s10570-013-9961-z.

[41] L. O. Mota and I. Gimenez, *Cellulose-based materials crosslinked with epichlorohydrin: A mini review.* Rev. Virtual Quím. **15** (2023): p. 159-170. https://doi.org/10.21577/1984-6835.20220071.

[42] T. Xu, Z. Wang, Y. Ding, W. Xu, W. Wu, Z. Zhu and H. Fong, *Ultralight electrospun cellulose sponge with super-high capacity on absorption of organic compounds.* Carbohydrate Polymers. **179** (2018): p. 164-172. https://doi.org/10.1016/j.carbpol.2017.09.086m

[43] R. S. Rengasamy, D. Das and C. Praba Karan, *Study of oil sorption behavior of filled and structured fiber assemblies made from polypropylene, kapok and milkweed fibers.* Journal of Hazardous Materials. **186** (2011): p. 526-532. https://doi.org/10.1016/j.jhazmat.2010.11.031.

[44] Y. Zhang, M. Yin, X. Lin, X. Ren, T.-S. Huang and I. S. Kim, *Functional nanocomposite aerogels based on nanocrystalline cellulose for selective oil/water separation and antibacterial applications.* Chemical Engineering Journal. **371** (2019): p. 306-313. https://doi.org/10.1016/j.cej.2019.04.075.

[45] B. Tansel and B. Pascual, *Removal of emulsified fuel oils from brackish and pond water by dissolved air flotation with and without polyelectrolyte use: Pilot-scale investigation for estuarine and near shore applications.* Chemosphere. **85** (2011): p. 1182-1186. https://doi.org/10.1016/j.chemosphere.2011.07.006.

[46] N. T. Cervin, C. Aulin, P. T. Larsson and L. Wågberg, *Ultra porous nanocellulose aerogels as separation medium for mixtures of oil/water liquids.* Cellulose. **19** (2012): p. 401-410. https://doi.org/10.1007/s10570-011-9629-5.

[47] X. Xu, F. Dong, X. Yang, H. Liu, L. Guo, Y. Qian, et al., *Preparation and Characterization of Cellulose Grafted with Epoxidized Soybean Oil Aerogels for Oil-Absorbing Materials.* Journal of Agricultural and Food Chemistry. **67** (2019): p.637-643. https://doi.org/10.1021/acs.jafc.8b05161.

[48] Y. Yang, X. Chen, Y. Li, Z. Yin and M. Bao, *Construction of a Superhydrophobic Sodium Alginate Aerogel for Efficient Oil Absorption and Emulsion Separation.* Langmuir. **37** (2021): p. 882-893. https://doi.org/10.1021/acs.langmuir.0c03229.

[49] B. Wang, X. Yang, D. Sha, K. Shi, J. Xu and X. Ji, *Silane Functionalized Polyvinyl-Alcohol Formaldehyde Sponges on Fast Oil Absorption.* ACS Applied Polymer Materials. **2** (2020): p. 5309-5317. https://doi.org/10.1021/acsapm.0c01052.

[50] A. Mulyadi, Z. Zhang and Y. Deng, *Fluorine-Free Oil Absorbents Made from Cellulose Nanofibril Aerogels.* ACS Applied Materials & Interfaces. **8** (2016): p. 2732-2740. https://doi.org/10.1021/acsami.5b10985.

[51] H. Bi, X. Huang, X. Wu, X. Cao, C. Tan, Z. Yin, et al., *Carbon Microbelt Aerogel Prepared by Waste Paper: An Efficient and Recyclable Sorbent for Oils and Organic Solvents*. Small. **10** (2014): p. 3544-2550. https://doi.org/10.1002/smll.201303413.

[52] Y. Zhao, K. Zhong, W. Liu, S. Cui, Y. Zhong and S. Jiang, *Preparation and oil adsorption properties of hydrophobic microcrystalline cellulose aerogel*. Cellulose. **27** (2020): p. 7663-7675. https://doi.org/10.1007/s10570-020-03309-0.

[53] S. Mantripragada, S. Gbewonyo, D. Deng and L. Zhang, *Oil absorption capability of electrospun carbon nanofibrous membranes having porous and hollow nanostructures*. Materials Letters. **262** (2020): p. 127069. https://doi.org/10.1016/j.matlet.2019.127069.

[54] H. T. Kahraman, A. Yar, A. Avcı and E. Pehlivan. *Preparation of nanoclay incorporated*

PAN fibers by electrospinning technique and its application for oil and organic solvent absorption. Separation Science and Technology. **53** (2018): p. 303-311. https://doi.org/10.1080/01496395.2017.1384018.

Chapter 8. Comprehensive Discussion

The circular economy is a novel production and consumption model that promotes sustainable growth over time. Its aim is to optimize resources, reduce raw material consumption, and recycle or repurpose wastes. The three basic principles of the circular economy are to reduce, reuse, and recycle (Osman et al., 2019). By following these principles, we brought up this thesis study to functionalize CA and other biomass wastes and residues into value-added products using electrospinning technique. Notably, the CA tow we used in the study is the raw material of cigarette filter, CS was extracted from crab shell, and CNCs were derived from textile wastes.

Electrospinning piqued our interest due to its important role as one of the appropriate strategies in adsorption for wastewater treatment. Electrospinning is a facile and efficient method for preparing fibers with various diameters, which have large specific surface area, good interconnectivity, and structural stability. Meanwhile owing to the random arrangement of fibers prepared by electrospinning, a large number of isotropic pores evenly distribute among fibers. These characteristics make electrospun fibers useful in a wide range of applications, including filtration & adsorption materials (Xue et al., 2019).

Chapter 2 highlighted the attractive features of cellulose as the most abundant natural polymer which exhibited excellent biocompatibility, biodegradability, and non-toxicity. These characteristics make it and its derivatives ideal for creating sustainable and environmentally friendly multifunctional materials. In Chapter 3, from the comprehensive literature review, the latest progress in electrospun nanofibers including their construction methods and conditions, various available raw materials, and applications in the removal of various aqueous pollutants (organic dye solutions, heavy metals, phenolic compounds, pesticides, antibiotics, natural organic matters, and so on) were summarized and discussed, which were followed by the conclusion and prospects associated with future opportunities and challenges in this active research area. It was

highlighted in Chapter 2 and 3 that CA was a widely applied polymeric matrices in a variety of applications. Compared to the poor solubility of cellulose (CL), CA has greatly improved solubility in many solvents and can form continuous and controllable fibers, so it is one of the most used CL derivatives for the production of electrospun nanofibers (Olaru et al., 2019; Liu et al., 2020; Chen et al., 2020). Additionally, the review also discussed CS as the most abundant natural amino polysaccharide derived by the deacetylation of chitin for effectively adsorbing heavy metals and organic compounds through its active hydroxyl and amine groups, offering extensive chelating groups and strength to nanofibers (Haider & Park, 2009). It was revealed that CA was generally employed as matrix material due to its limited adsorption capacity, while CS tends to be swollen in aqueous media. Therefore, CA and CS could compensate each other by constructing the CA/CS composites through electrospinning technique. To our knowledge, the composites of CA and CS derived from biomass wastes via electrospinning for adsorption was not well-explored. Based on the above considerations, the main objective of this thesis is to develop electrospun CA-based fibrous structures for water treatment.

In Chapter 4, we aimed to first develop an effective fibrous adsorbent derived from CA and CS through electrospinning technique. HA was involved as an illustrative contaminant for evaluating the performance of the as-prepared CA/CS fibrous adsorbents. HA is a complex mixture of organic acids that contains abundant carboxyl and phenolate groups. It is formed through the biodegradation of dead organic matter and is a principal component of humic substances (Xie et al., 2020). These substances are the major organic constituents of soil (humus), peat, and coal. It is also a significant component of many upland streams, dystrophic lakes, and ocean water. However, its presence in the waterways poses a potential risk to the aqua environment and water treatment process, which is often neglected. In natural waterbodies, HA can affect the quality of

water in several ways: they can influence the pH, color, and odor of water, interact with toxic metals and pollutants to either mobilize or immobilize them, and affect the biological availability of nutrients. In water treatment, HA can pose challenges by reacting with chlorine during disinfection processes to form disinfection byproducts, such as trihalomethanes and haloacetic acids, which are potential health hazards.

In our previous study, the intermolecular forces of HA interacting with self-assembled monolayers (SAM, such as OH-SAMs, CH_3-SAMs, NH_2-SAMs, and COOH-SAMs) in various aqueous environments were quantitatively probed (Xie et al., 2020). The average adhesion energy followed the trend as NH_2-SAMs (~3.11 mJ/m^2) > CH_3-SAMs (~2.03 mJ/m^2) > OH-SAMs (~1.38 mJ/m^2) > COOH-SAMs (~0.52 mJ/m^2), indicating the significant role of electrostatic attraction in contributing to the HA adhesion, followed by hydrophobic interaction and hydrogen bonding. With these useful implications, CS and CA featured with abundant amino and methyl groups respectively, were employed to fabricate electrospun adsorbents for HA removal from aqueous solutions with promising efficiency.

The findings in Chapter 4 indicated that: 1. Hydrogen bonds were formed between amine groups of CS and acetyl/hydroxyl groups of CA, providing intact and reliable CA/CS fibrous matrix with good stability for applications in aqueous environments; 2. Uniform and continuous fibrous structures composed of semimicron-scaled fibers were obtained, which enabled large surface area and interconnected porous structures for facilitating the adsorption process; 3. Besides the roles of functional groups of CS and CA, the fiber morphologies could also significantly affect the adsorption capacities. The CA/CS 1:1 fibers showed a maximum adsorption capacity of 184.72 mg/g within 60 minutes, which was higher than those of CA/CS 3:1 and 1:3 adsorbents at all pH levels. Bead-free and homogeneous fibers resulted in a large surface area and subsequent high

adsorption capacity. 4. The electrostatic and hydrophobic interactions between the deprotonated carboxylic groups of HA and protonated amino groups of CS and the hydrophobic moieties of HA and CH_3^- groups of CA led to the adsorption of HA on the electrospun CA/CS fibers. It indicated that it is feasible to use intermolecular interaction mechanisms to guide the design of highly efficient adsorbents.

As the CA/CS fibrous adsorbents were showing effective control of HA in aqueous solutions, it was further explored in Chapter 5 regarding the improvement of CA/CS fiber properties and subsequent enhancement of removal efficiency toward HA. The adsorption mechanism heavily relies on the active sites present on the surface of the adsorbent (Pavithra et al., 2021). These sites are specific locations where adsorbate molecules attach to the adsorbent surface. The number and nature of these active sites play a pivotal role in determining the adsorption capacity and efficiency of the adsorbent material. The active sites should be readily accessible to the adsorbate molecules to initiate better interactions between the adsorbate molecules and the active sites of the adsorbents, consequently, leading to more efficient removal of contaminants. Additionally, the mechanical strength of the adsorbent plays a vital role in practical applications to maintain membrane integrity and ensure its durability. Therefore, we proposed a core-sheath structured CA/CS fiber by incorporating CNCs in the core as a natural reinforcing and load-bearing component while concentrating CS at the outer layer of the fibers to provide more accessible binding sites.

Co-axial electrospinning, an evolution of the conventional electrospinning technique, has been employed for the fabrication of core-sheath structured fibers. Specifically, polymer solutions are electrospun through two separate capillaries with a co-axial structure. The rapid fabrication process limits the interaction between polymer chains and inhibits the two entities from completely mixing after solidification. Therefore, it is easy to separately adjust the sheath and core components of the

fibers in a co-axial electrospinning setup to achieve the desired functionalities. The applications of co-electrospinning in the fabrication of membrane adsorbents have been rarely reported. Additionally, the additives can change the rheological behavior of CA solutions and affect the electrospinning process. Therefore, an optimization process, involving solution viscosity, polymer concentrations, applied voltage, tip-to-collector distance, and feeding rates of core and sheath solutions, was necessary to achieve the co-axial electrospinning of core-sheath structured fibers in Chapter 5.

The core-sheath fibers with different CA/CS ratios in the outer layer of the fibers as well as various CNCs concentrations in the core of the fibers were successfully fabricated through co-axial electrospinning after the optimizations of parameters. All the CA/CS-CNCs fibers exhibited nano-scaled diameters, which was highly desirable. It was found that the viscosities of electrospun solutions increased perceptibly as the CNC content rose, inducing the formation of convex- and concave-shaped fibers. Besides the morphological changes, the addition of CNCs considerably improved the tensile strength of the CA/CS fibers. On the one hand, it was because of that the stress could be transferred and diverted from CS/CA fabrics to the rigid CNCs, and on the other hand, the interaction between CNCs and the fiber matrix also contributed to the resistance of loading forces. In the results of adsorption studies, with lower mass proportions of CS incorporated in the core-sheath fibers, the maximum adsorption capacity reached by using the core-sheath structured fibers had no significant difference from that of the uniaxial fibers. It indicated a highly improved removal efficiency achieved by using core-sheath structured fibers, which could be attributed to the rational design in the fabrication of electrospun adsorbents. Therefore, it was concluded that a core-sheath structured fiber with improved mechanical strength and removal efficiency was successfully fabricated through co-axial electrospinning.

In the previous chapters, we explored and discussed adsorption extensively as a promising method for removing contaminants from aqueous environments attributed to its simple operation and cost-effectiveness. However, the process of adsorption has limitations that can affect its application and efficiency. One of the main limitations of the adsorption process is the finite number of active sites available on the adsorbent's surface. When these sites are fully occupied, the adsorbent becomes saturated and loses the capacity to capture more adsorbate molecules. Regeneration is thus required for further utilization of adsorbent materials, which is costly and time-consuming, and can compromise adsorbent effectiveness.

Photocatalytic oxidation is an effective alternative treatment for the destruction of pollutants in aqueous systems. Its oxidation mechanism of hydroxyl radicals achieves complete mineralization of the target compound, making it a major advantage. Among the various photocatalysts explored, titanium dioxide (TiO_2) stands out as a frontrunner due to its exceptional photocatalytic activity, stability, and non-toxicity (Birben et al., 2017). The basic process of photocatalytic reactions is initiated by the absorption of illumination with energy equal to or greater than the band gap of the TiO_2 semiconductor surface. Subsequently, redox reactions can occur between the valence band hole, which strongly oxidizes, and the conduction band electron, which strongly reduces, and the adsorbed species.

Although TiO_2 is considered one of the most popular photocatalysts, it still has limitations. When in powder form, TiO_2 is not only prone to agglomeration but also difficult to recycle, requiring complicated separation methods. Therefore, the system's economic viability is instantly increased in terms of the post-treatment issues. Alternatively, the catalyst can be attached to suitable solid support without the need for separation from the effluent streams. When a photocatalytic membrane is used, most of the slurry drawbacks may be avoided (Tung et al., 2019). Additionally,

the nature of photocatalysis as a surface-oriented process is a fundamental aspect that underpins its mechanism and efficiency. In photocatalytic processes, the reactions predominantly occur at the surface of the photocatalyst (Batzill, 2011). Therefore, the coupling of membrane adsorbent and nanoparticle catalyst can enhance the overall efficiency of the treatment process. Adsorption can concentrate pollutants on the adsorbent's surface, making them more accessible to photocatalytic degradation. On the other hand, photocatalytic processes can regenerate the adsorbent surface by degrading adsorbed pollutants, thereby extending the adsorbent's lifespan, and reducing the need for frequent replacement or regeneration.

In Chapter 6, the successful incorporation of TiO_2 in the CA/CS fibers was confirmed from the new peak introduced representing the vibration of Ti-O-Ti in FT-IR spectra. We also conducted the elemental analysis and SEM observation and revealed a uniform distribution of TiO_2 nanoparticles in the CA/CS fibers. Moreover, the intensity of the characteristic peaks of CA and CS persisted following the introduction of TiO_2, suggesting that the incorporation of TiO_2 nanoparticles did not impact the structures of CA and CS and was through physical enclosing. All the TiO_2-impregnated samples exhibited the ultrafine and continuous fibers with nano-scaled diameters. The deposition of TiO_2 nanoparticles became more concentrated as its contents rose from 1 to 2 wt%, but the distribution of TiO_2 appeared to be looser when the amount of TiO_2 was 3 wt%. This phenomenon might be attributed to (1) the enfoldment of TiO_2 nanoparticles inside the beady-shaped fibers as a result of the perceptibly increased viscosity of 3%TiO_2-CA/CS electrospun solution; (2) loading a higher amount of TiO_2 nanoparticles caused an unstable Taylor cone at the tip of needle and instability of fluid, leading to an impact on the deposition of TiO_2 nanoparticles on the electrospun fibers (Gebru and Das, 2017). It could be concluded that 2%TiO_2-CA/CS fibers exhibited not only a more uniform and less beady morphological structure but also better incorporation of TiO_2

nanoparticles in the fibers. The removal effects of HA using TiO_2-incorporated fibrous composites under different reaction conditions (dark or UV illumination) as a function of treatment time were studied. The 2%TiO_2-CA/CS fibers exhibited the highest removal efficiency under UV illumination compared to those of the 2%TiO_2-CA fibers under illumination and 2%TiO_2-CA/CS fibers in the dark. This indicated the remarkable synergistic effects of the adsorption process and photocatalytic activity, contributing to the continuous removal of HA. The mechanism involved the initial attraction of contaminants on the surface of the fibers, and then the mineralization of HA occurred through the interaction of excited electrons and the hole with water, hydroxide radical (•OH), or oxygen in redox reactions. Therefore, the (•OH) radicals were formed through two reactions: 1. the valence band holes reacting with adsorbed water molecules; and/or 2. reactions between the TiO_2 nanoparticles and the valence band holes. The reactive radical hydroxyl (•OH) can hydroxylate aromatic compounds of HA, leading to successive oxidation, addition, and ring opening. The resultant intermediates undergo further carboxylation to produce carbon dioxide and water. In summary, the molecular structures of HA can be broken down or rearranged by the photocatalysis process (Tung et al., 2019). Notably, the morphologies of the fibrous composites after 180 UV irradiations were examined, and it was evident that no significant changes in the structural integrity and fibrous morphologies were observed.

The outcomes of Chapter 6 have demonstrated the synergic effect of photooxidation and adsorption on the extended lifespan for HA removal. So far, we have explored the rational design of 2D electrospun fibrous membranes derived from CA. To further investigate the potential of electrospun fibers, 3D cylindrical fibrous aerogels were fabricated for oil/organic solvent absorption in Chapter 7. The research rationale behind this study is that electrospun membranes have porous structure and large surface area but limited internal space for liquid storage and

retention. We hypothesized that the assembling of electrospun fibers into 3D bulk aerogels could combine the features of fibrous membrane and 3D structure, resulting in facile and efficient oil/water separation and superior oil absorption capacity. The electropsun CA membranes were hydrolyzed to obtain the CL fibers with abundant active hydroxyl groups for crosslinking, while a silanization process was followed to improve the hydrophobicity of the CL fibrous aerogels. The results showed the successful formation of crosslinked networks between the hydroxyl groups of CL and epoxide groups of epichlorohydrin (Epc). A hydrophobic silicone layer covalently attached to the surface of CL fibers, which was confirmed by the occurrence of new peaks representing C-Si and Si-O-Si vibrations in FTIR spectra. A hierarchical morphology of the fibrous aerogels was observed scaling down from the cylindrical aerogel (~2 cm in diameter), the major pores (~10 μm in diameter), the minor pores (~1 μm in diameter), and the fibers (~300 nm in diameter). This highly interconnected structure benefited the rapid mass transfer and oil storage. The fibrous aerogels exhibited fast oil absorption (within 10 minutes), high adsorption capacities towards diversified oils and organic solvents (up to 37.82g/g of chloroform), and high compressive strength (up to 0.77 MPa). Notably, it achieved superior retention of compressive strength and absorption capacity as well as rapid shape recovery after the six cycles of absorption-compression. It was concluded that the developed fibrous aerogels are a promising candidate for addressing oil pollution with good reusability and sustainability.

Chapter 9. General Conclusion and Future Research Recommendations

9.1. General Conclusions

Electrospun fibers have been recognized as one of the appropriate strategies in adsorption due to their highly porous structure, large specific surface area, and good structural stability. Up to date, numerous natural and synthetic polymers have been fabricated into ultrafine fibrous mats successfully via the electrospinning technique. It was highlighted in the literature review that CA has been widely applied as polymeric matrices for aqueous contaminant removal. Additionally, compared to the poor solubility of CL, CA can be dissolved in many solvents for electrospinning. CS is an abundant natural amino polysaccharide and can effectively adsorb heavy metals and organic compounds through its active hydroxyl and amine groups. By following the principles of circular economy, we brought up this thesis study to functionalize CA and other biomass wastes and residues into value-added products using electrospinning technique. Several general conclusions are summarized as follows:

1. We have successfully developed an effective fibrous adsorbent from CA and CS through electrospinning technique.
2. The electrospun CA/CS membranes possessed a uniform and continuous fibrous structure composed of semimicron-scaled fibers. These features provided the membranes with the large surface area and interconnected porous structure for efficient adsorption process.
3. The adsorption mechanisms of HA on electrospun CA/CS fibers mainly relied on the electrostatic attraction between the deprotonated carboxylic groups of HA and protonated amino groups of CS. Additionally, the hydrophobic moieties of HA could interact with CH_3^- groups of CA via hydrophobic attraction. It implied the feasibility of developing a functional material guided by the intermolecular interaction study.

4. The core-sheath structured CA/CS-CNCs fibers have been designed with CNCs in the core as a natural reinforcing component and CS in the sheath of the fibers for providing accessible binding sites, which significantly improved the mechanical strength and removal efficiency toward HA.
5. With lower mass proportions of CS incorporated, the core-sheath structured fibers reached a similar maximum adsorption capacity compared to the uniaxial fibers. It indicated the significance of the core-sheath structure and will contribute to the rational design of highly efficient adsorbents.
6. By incorporating TiO_2 into CA/CS membranes using the electrospinning method, the resultant fibrous membranes had a large surface area-to-volume ratio to facilitate the adsorption of pollutants and increase the contact probability of photoelectrons and photoholes with targeted contaminants.
7. The TiO_2-incorporated fibers had the postponed saturation point and could continuously remove HA by the synergistic effects of photooxidation and adsorption.
8. The fibrous aerogels were successfully developed from electrospun CA fibers, which are promising candidates for addressing oil pollution with good reusability.
9. The fibrous aerogels exhibited fast oil absorption, high absorption capacity towards diversified oils and organic solvents, high compressive strength, and good stability.

9.2. Future Research Recommendations

The significant findings in this study provided a foundation for future research on recycling low-value waste materials. It also contributed to the rational design of electrospun fibrous structures. Future research recommendations include:

1. Studies on novel solvent systems of CA to enable efficient production of CA electrospun fibers.
2. Further development of CA-based functional materials for targeting diversified aqueous contaminants.
3. Studies on the possibility of filler migration from the electrospun membranes and the migration pathways.
4. Exploration and improvement of CA-based electrospun adsorbents for real environmental conditions and complex wastewater samples.
5. Studies on the fate, stability, and degradability of electrospun materials in the natural aqueous environment.

General Reference List

Batzill., M. (2011). Fundamental aspects of surface engineering of transition metal oxide photocatalysts. *Energy Environ. Sci, 4(9), 3275-3286.* https://doi.org/10.1039/C1EE01577J

Beaumont, M., Jusner, P., Gierlinger, N., King, A. W. T., Potthast, A., Rojas, O. J., & Rosenau, T. (2021). Unique reactivity of nanoporous cellulosic materials mediated by surface-confined water. *Nat Commun*, *12*(1), 2513. https://doi.org/10.1038/s41467-021-22682-3

Birben, N. C., Uyguner-Demirel, C. S., Kavurmaci, S. S., Gürkan, Y. Y., Turkten, N., Cinar, Z., and Bekbolet, M. (2017). Application of Fe-doped TiO_2 specimens for the solar photocatalytic degradation of humic acid. *Catalysis Today*, *281*, 78-84. https://doi.org/https://doi.org/10.1016/j.cattod.2016.06.020

Chen, W., Ma, H., & Xing, B. (2020). Electrospinning of multifunctional cellulose acetate membrane and its adsorption properties for ionic dyes. *Int J Biol Macromol*. https://doi.org/10.1016/j.ijbiomac.2020.04.249

Gebru, K.A. & Das, C. (2017). Removal of Pb (II) and Cu (II) ions from wastewater using composite electrospun cellulose acetate/titanium oxide (TiO_2) adsorbent. *Journal of Water Process Engineering, 16: p. 1-13.* https://doi.org/10.1016/j.jwpe.2016.11.008

Haider, S., & Park, S.-Y. (2009). Preparation of the electrospun chitosan nanofibers and their applications to the adsorption of Cu(II) and Pb(II) ions from an aqueous solution. *Journal of Membrane Science, 328*(1), 90-96. doi:https://doi.org/10.1016/j.memsci.2008.11.046

Han, K. S., Lee, S., Kim, M., Park, P., Lee, M. H., & Nah, J. (2019). Electrically Activated Ultrathin PVDF‐TrFE Air Filter for High‐Efficiency PM1.0 Filtration. *Advanced Functional Materials*, *29*(37). https://doi.org/10.1002/adfm.201903633

Khodadadi, M., Al-Musawi, T. J., Kamranifar, M., Saghi, M. H., & Hossein Panahi, A. (2019). A comparative study of using barberry stem powder and ash as adsorbents for adsorption of humic acid. *Environmental Science and Pollution Research*, *26*(25), 26159-26169. https://doi.org/10.1007/s11356-019-05879-4

Klausen, J., Vikesland, P. J., Kohn, T., Burris, D. R., Ball, W. P., & Roberts, A. L. (2003). Longevity of Granular Iron in Groundwater Treatment Processes: Solution Composition Effects on Reduction of Organohalides and Nitroaromatic Compounds. *Environmental Science & Technology*, *37*(6), 1208-1218. https://doi.org/10.1021/es025965s

Lee, S., Franklin, S., Hassani, F. A., Yokota, T., Nayeem, M. O. G., Wang, Y., Leib, R., Cheng, G., Franklin, D. W., & Someya, T. (2020). Nanomesh pressure sensor for monitoring finger manipulation without sensory interference. *Science*, *370*(6519), 966. https://doi.org/10.1126/science.abc9735

Li, M. C., Wu, Q., Moon, R. J., Hubbe, M. A., & Bortner, M. J. (2021). Rheological Aspects of Cellulose Nanomaterials: Governing Factors and Emerging Applications. *Adv Mater*, *33*(21), e2006052. https://doi.org/10.1002/adma.202006052

Liu, K., Huang, Z., Dai, J., Jiang, Y., Yang, G., Liu, Y., Lin, C., Lv, Y., & Liu, M. (2020). Fabrication of amino-modified electrospun nanofibrous cellulose membrane and adsorption for typical organoarsenic contaminants: Behavior and mechanism. *Chemical Engineering Journal*, *382*. https://doi.org/10.1016/j.cej.2019.122775

Liu, S., Lim, M., & Amal, R. (2014). TiO2-coated natural zeolite: Rapid humic acid adsorption and effective photocatalytic regeneration. *Chemical Engineering Science*, *105*, 46-52. https://doi.org/https://doi.org/10.1016/j.ces.2013.10.041

O'Dea, R. M., Willie, J. A., & Epps, T. H. (2020). 100th Anniversary of Macromolecular Science Viewpoint: Polymers from Lignocellulosic Biomass. Current Challenges and Future Opportunities. *ACS Macro Letters*, *9*(4), 476-493. https://doi.org/10.1021/acsmacrolett.0c00024

Olaru, N., Anghel, N., Pascariu, P., & Ailiesei, G. (2019). Synthesis and testing of cellulose acetate nicotinate as adsorbent for rhodamine B dye. *Journal of Applied Polymer Science*, *136*(29), 47772. https://doi.org/https://doi.org/10.1002/app.47772

Osman, A.I., Abdelkader, A., Farrell, C., Rooney, D., & Morgan, K. Reusing, recycling and up-cycling of biomass: A review of practical and kinetic modelling approaches. *Fuel Process. Technol*. 2019, 192, 179–202. https://doi.org/10.1016/j.fuproc.2019.04.026

Pavithra, S., Thandapani, G., Sugashini, S., Sudha, P.N., Alkhamis, H.H., Alrefaei, A.F., & Almutairi, M.H. Batch adsorption studies on surface tailored chitosan/orange peel hydrogel composite for the removal of Cr(VI) and Cu(II) ions from synthetic wastewater. *Chemosphere* **2021**, *271*, 129415. https://doi.org/10.1016/j.chemosphere.2020.129415

Phan, D. N., Lee, H., Huang, B., Mukai, Y., & Kim, I. S. (2019). Fabrication of electrospun chitosan/cellulose nanofibers having adsorption property with enhanced mechanical property. *Cellulose, 26*(3), 1781-1793. doi:10.1007/s10570-018-2169-5

Schmitt, D., Saravia, F., Frimmel, F. H., & Schuessler, W. (2003). NOM-facilitated transport of metal ions in aquifers: importance of complex-dissociation kinetics and colloid formation. *Water Research*, *37*(15), 3541-3550. https://doi.org/https://doi.org/10.1016/S0043-1354(01)00525-5

Sun, X., Bai, L., Li, J., Huang, L., Sun, H., & Gao, X. (2021). Robust preparation of flexibly super-hydrophobic carbon fiber membrane by electrospinning for efficient oil-water separation in harsh environments. *Carbon*, *182*, 11-22. https://doi.org/10.1016/j.carbon.2021.05.047

Tung, T. X., Xu, D., Zhang, Y., Zhou, Q., and Wu, Z. (2019). Removing Humic Acid from Aqueous Solution Using Titanium Dioxide: A Review. *Polish Journal of Environmental Studies*, *28*(2), 529-542. https://doi.org/10.15244/pjoes/85196

Xia, Q., Chen, C., Yao, Y., Li, J., He, S., Zhou, Y., Li, T., Pan, X., Yao, Y., & Hu, L. (2021). A strong, biodegradable and recyclable lignocellulosic bioplastic. *Nature Sustainability*. https://doi.org/10.1038/s41893-021-00702-w

Xie, L., Lu, Q., Mao, X., Wang, J., Han, L., Hu, J., Lu, Q., Wang, Y., & Zeng, H. (2020). Probing the intermolecular interaction mechanisms between humic acid and different substrates with implications for its adsorption and removal in water treatment. *Water Research, 176, 115766.* https://doi.org/10.1016/j.watres.2020.115766

Yan, J., Wang, Y., Zhang, Y., Xia, S., Yu, J., & Ding, B. (2021). Direct Magnetic Reinforcement of Electrocatalytic ORR/OER with Electromagnetic Induction of Magnetic Catalysts. *Adv Mater*, *33*(5), e2007525. https://doi.org/10.1002/adma.202007525

Zhang, Y., Wang, F., & Wang, Y. (2021). Recent developments of electrospun nanofibrous materials as novel adsorbents for water treatment. *Materials Today Communications*, *27*, 102272. https://doi.org/https://doi.org/10.1016/j.mtcomm.2021.102272